Mesoproterozoic bimodal magmatism of southern Australia: assessing relative mantle input and implications for IOCG mineralisation prospectivity.

Thesis submitted in accordance with requirements of the University of Adelaide for an Honours Degree in Geology

Henry Charles Chalk
November 2014

MESOPROTEROZOIC BIMODAL MAGMATISM OF SOUTHERN AUSTRALIA: ASSESSING RELATIVE MANTLE INPUT AND IMPLICATIONS FOR IOCG MINERALISATION PROSPECTIVITY.

RUNNING TITLE: MESOPROTEROZOIC MANTLE INPUT IN SOUTHERN AUSTRALIA

ABSTRACT

Mesoproterozoic magmatism of the Gawler Craton and the Curnamona Province demonstrates regions of variable mantle input characteristics. Zircons from Hiltaba Suite granitoids and Gawler Range Volcanics, Gawler Craton, return ε_{Hf}(T) values ranging from +7.1 to -0.4, +2.0 to -7.4, and +0.2 to -5.3 from the western, central, and eastern Gawler Craton respectively. Ninnerie Supersuite granitoids and Benagerie Volcanic Suite, Curnamona Province, return ε_{Hf}(T) values ranging from +2.5 to -3.8. Mantle input modelling of the central/eastern Gawler Craton and the Curnamona Province returns similar mantle input fraction values ranging from 0.1 to 0.6, averaging 0.3, and 0.1 to 0.6, averaging 0.3, respectively. Hiltaba Suite magmatism of the western Gawler Craton is compositionally more juvenile than the central and eastern regions. The western Gawler Craton mantle input fractions range from 0.2 to 0.9 averaging 0.5, more elevated than the central/eastern regions of the Gawler Craton and the Curnamona province. The Benagerie Ridge region of the Curnamona Province displays similar bimodal *ca.* 1590 Ma magmatism, ε_{Hf}(T) values, mantle input characteristics, crustal preservation (exhumation) and regional iron oxide copper-gold alteration as the highly prospective Olympic IOCG Province, Gawler Craton.

KEYWORDS

Gawler Craton; Curnamona Province; Olympic IOCG Province; Benagerie Ridge; Mesoproterozoic; Lu-Hf; U/Pb geochronology; Hiltaba Suite; Ninnerie Supersuite; IOCG prospectivity

TABLE OF CONTENTS

List of Figures and Tables 4
1. Introduction 5
2. Geological Background 9
2.1. Regional Geology 9
2.1.1. Gawler Craton 9
2.1.2. Curnamona Province 10
2.2. Tectonic Setting and IOCG Mineralisation 13
3. Methods 14
3.1. Sample Preparation 14
3.2. U-Pb Geochronology 15
3.3. Lu-Hf Isotope Analysis 16
4. Results 17
4.1. U-Pb Geochronology and Lu-Hf Isotope Analysis 17
4.1.1 Gawler Craton Samples 21
4.1.2 Curnamona Province Samples 26
5. Discussion 30
5.1. Hf Isotopic Signature of ca. 1590 Ma Magmatism in the Gawler Craton and the Curnamona Province 31
5.2. Petrogenesis and Mantle Input of *ca.* 1590 Ma Magmatism 32
5.3. IOCG Prospectivity vs. Mantle Input – a One-dimensional Analysis 37
5.4. Chemistry and Crustal Architecture – an Integrated Approach to Prospectivity 38
6. Conclusions 41
Acknowledgments 42
References 42
Appendix A: Summary of Samples 47
Appendix B: Extended Analytical Methods 48
Appendix C: LA-ICP-MS Zircon U-Pb Geochronology Data 51
Appendix D: LA-MC-ICP-MS Zircon Lu-Hf Isotopic Data 61

LIST OF FIGURES

Figure 1. Regional geology map of the Gawler Craton and Curnamona Province 8
Figure 2. Geology map of the Crocker Well region 12
Figure 3. U-Pb concordia plots of the Gawler Craton 18
Figure 4. U-Pb concordia plots of the Curnamona Province 19
Figure 5. Zircon cathode luminescence images 20
Figure 6. ε_{Hf}(T) vs. age plots for Gawler Craton samples 22
Figure 7. ε_{Hf}(T) vs. age plots for Curnamona Province samples 27
Figure 8. Summary ε_{Hf}(T) vs. age plots for all data 29
Figure 9. ε_{Hf}(T) population density plots 30
Figure 10. Schematic of mantle input calculation 35
Figure 11. Mantle fraction histograms 36
Figure 12. South Australian Mesoproterozoic magmatic preservation 39

1. INTRODUCTION

Iron Oxide Copper Gold (IOCG) deposits represent an important current and future global source of copper, gold and uranium. South Australia hosts the giant Olympic Dam IOCG deposit, which is the world's fifth largest copper, third largest gold and single largest uranium deposit (Ehrig *et al.* 2012). Determining the factors influencing and controlling IOCG mineralisation has been the focus of much research (Hitzman *et al.* 1992; Porter 2000; Ferris *et al.* 2002; Porter 2002; Skirrow *et al.* 2002; Hunt *et al.* 2007; Groves *et al.* 2010; Hayward and Skirrow 2010; Porter 2010a; Williams *et al.* 2010). In general it is believed that early widespread sodic/calcic/potassic+magnetite/hematite alteration; clear temporal, but not close spatial association with batholithic complexes; proximal crustal scale structure; and reactive chemistry of mineralising fluids are essential components (Skirrow *et al.* 2002; Mark *et al.* 2006; Monteiro *et al.* 2008; Conor *et al.* 2010; Hayward and Skirrow 2010; Porter 2010a; Williams *et al.* 2010). This information is over-generalized as conditions vary between each deposit. It is often unclear what results in one terrain being highly mineralised while an analogous terrain is apparently barren. Within South Australia, the Olympic IOCG Province of the Gawler Craton, and the Benagerie Ridge region of the Curnamona Province (Fig. 1) provide an excellent case study of a highly prospective region with known mineralisation and a region perceived to be prospective.

The highly prospective Olympic IOCG Province in the Gawler Craton, South Australia, includes the giant Olympic Dam, and large Prominent Hill, Carrapateena, Wirrda Well and Hillside IOCG deposits (Fig. 1). The nearby Curnamona Province, on the South Australia-New South Wales border, hosts the smaller Kalkaroo and North Portia IOCG prospects in the Benagerie Ridge region (Fig. 1). Prior to Neoproterozoic formation of the Adelaide Geosyncline rift complex, the Olympic IOCG Province and the Benagerie Ridge are likely to have been contiguous. Both provinces share similar histories with an eastward migration of peralkaline volcanism and basin sedimentation of the Wallaroo Group (~1750 Ma) from the eastern Gawler Craton to the Willyama Supergroup (1720 to 1640 Ma) in the Curnamona Province (Conor 1995; Conor and Preiss 2008). Similarly, voluminous bimodal magmatism of the 1600 - 1575 Ma Gawler Range Volcanics (GRV) and Hiltaba Suite granitoids in the Gawler Craton is contemporaneous with magmatism of the 1600 - 1580 Ma Ninnerie Supersuite granites and Benagerie Volcanic Suite (BVS) in the Curnamona Province (Hand *et al.* 2008; Wade *et al.* 2012). IOCG alteration and mineralisation of the Olympic IOCG Province and the Benagerie Ridge corresponds with the onset of ca. 1590 Ma magmatism of the Hiltaba Suite and Ninnerie Supersuite (Daly *et al.* 1998; Budd *et al.* 2001; Skirrow *et al.* 2002; Burtt *et al.* 2004; Porter 2010b). Despite the similar geological histories and presence of ca. 1590 Ma magmatism in both regions, the Benagerie Ridge appears to be dramatically under-mineralised with respect to the world-class Olympic IOCG province.

The majority of IOCG deposits form in settings where broadly coeval magmatism was associated with crustal-scale pervasive alkali metasomatism (Williams *et al.* 2010), a setting common to the Olympic IOCG province and Benagerie Ridge. IOCG mineralisation is believed to form from the mixing of mantle-derived magmatic fluids with meteoric brines and/or reactive stratigraphy (Hayward and Skirrow 2010). Within the Olympic IOCG Province, a positive relationship is observed between mantle input of mineralising fluids and ore grade IOCG mineralisation. As documented by Nd, S and O isotopes, the giant Olympic Dam Cu-Au-Ag-U deposit has a distinct, enriched mantle input signature whereas nearby weakly mineralised prospects have less mantle input (Johnson and Cross 1995; Johnson and McCulloch 1995; Skirrow *et al.* 2007). This suggests the amount of mantle-derived input is an important factor in the development of significant ore grade IOCG mineralisation. Given the Benagerie Ridge illustrates regional IOCG alteration and mineralisation comparative to the Olympic IOCG Province but seems to lack large IOCG deposits, the possibility exists that there was insufficient mantle input into the Benagerie Ridge system to allow formation of large IOCG deposits. In order to assess the prospectivity of the Benagerie Ridge region an investigation of the relative mantle input into regional magmatism of the prospective Gawler Craton and the Curnamona Province is presented.

We present, U-Pb geochronology and lutetium-hafnium (Lu-Hf) isotope analysis of zircon from ca. 1590 Ma magmatic rocks of the Curnamona Province and Gawler Craton. Lu-Hf isotope data from the two regions is compared to allow characterization of the lithospheric mantle and relative mantle inputs into ca. 1590 Ma magmatism. A regional study of this kind has not previously been done in either the Gawler Craton or Curnamona Province. Assessment of relative mantle input in the magmatic suites subsequently allows for an evaluation of the prospectivity of the Benagerie Ridge region.

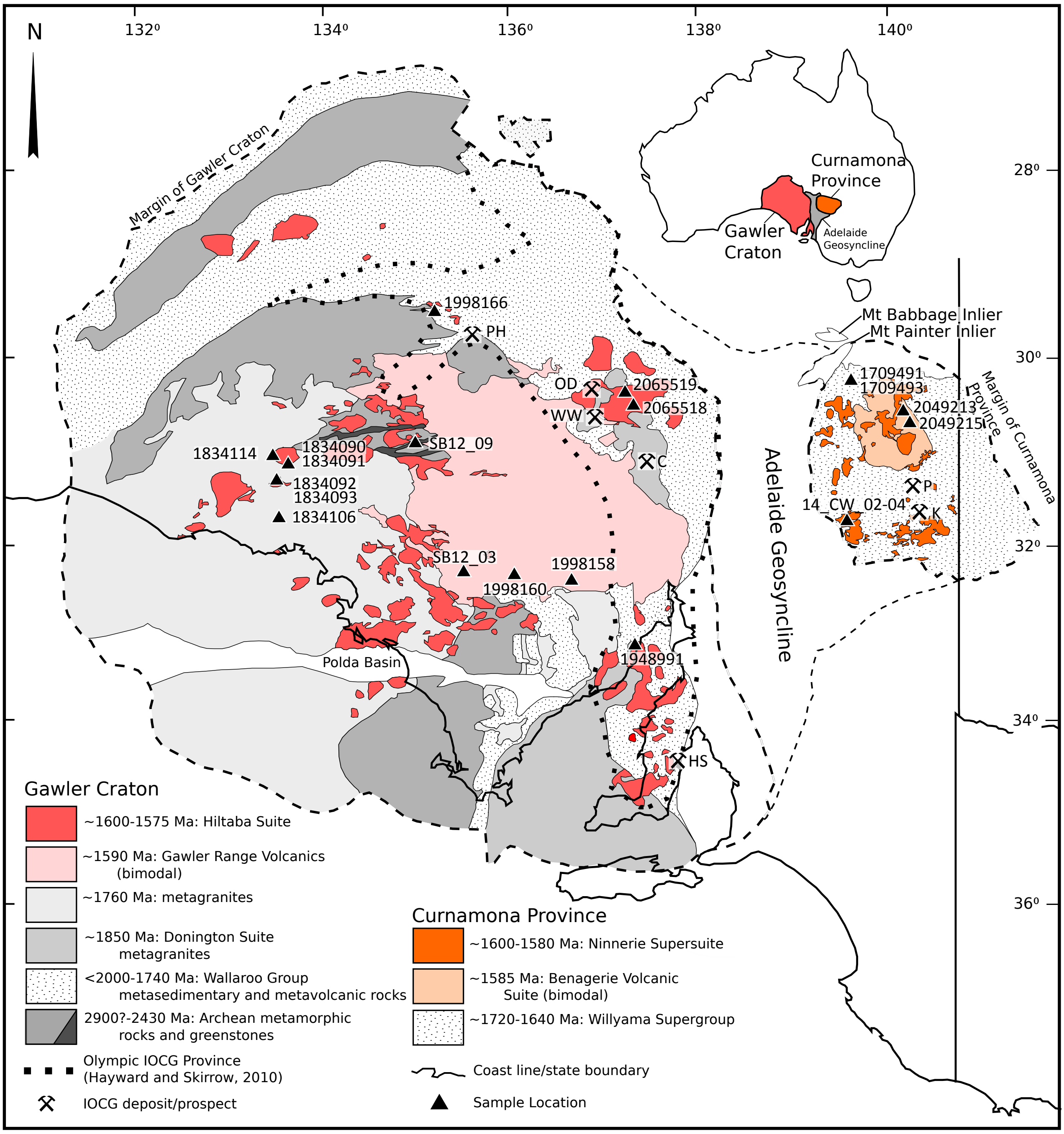

Figure 1. Location and simplified geology of the Gawler Craton and the Curnamona Province (pre- Neoproterozoic, and excluding the Mesoproterozoic Pandurra Formation), rock sample locations, and principal IOCG deposits/prospects in the Olympic IOCG Province and the Benagerie Ridge. IOCG deposit abbreviations from west to east: PH - Prominent Hill; OD - Olympic Dam; WW - Wirrda Well; C - Carrapateena; HS - Hillside; P - Portia; K - Kalkaroo. Sample number grid references and information is provided in Appendix A. Modified after Hayward and Skirrow (2010) and Wade (2012).

2. GEOLOGICAL BACKGROUND

2.1. Regional Geology

2.1.1 GAWLER CRATON

The Gawler Craton in Southern Australia is a large, late Archean to Mesoproterozoic crustal terrain (Hand *et al.* 2007). The oldest preserved rocks consist of late Archean (*ca*. 2560-2460 Ma) deformed and metamorphosed, magmatic and supacrustal rocks (McFarlane 2006). Donington Suite magmatism (*ca.* 1850 Ma) occurred across much of the eastern Gawler Craton, associated with a compressional tectonic setting (Hand *et al.* 2007). Post-Donington Suite intrusion, the eastern Gawler Craton underwent a period of extensive sediment deposition and peralkaline volcanism of the 1760-1740 Ma Wallaroo Group, prior to the 1730-1690 Ma Kimban Orogeny (Conor 1995; Daly *et al.* 1998; Cowley *et al.* 2003; Hand *et al.* 2007; Payne *et al.* 2008). The Kimban Orogeny included magmatism of the Middle Camp and Moody Suites and the post-tectonic *ca.* 1690-1670 Ma Tunkilla Suite (Teasdale 1997; Daly *et al.* 1998; Ferris and Schwarz 2004; Payne *et al.* 2006; Fanning *et al.* 2007). The effects of the Kimban Orogeny on the Gawler Craton include widespread formation of crustal-scale shear systems, granitic magmatism, and low- to high-grade metamorphism (Parker 1980; Hopper 2001; Vassallo and Wilson 2002; Betts *et al.* 2003; Payne *et al.* 2006; Hand *et al.* 2007; Payne *et al.* 2009). This was followed by the *ca.* 1618-1608 Ma intrusion of granitic to mafic St Peter Suite, which appears to volumetrically dominate the southwestern Gawler Craton (Swain *et al.* 2005; Fanning *et al.* 2007).

Early Mesoproterozoic tectonics of the Gawler Craton are dominated by the voluminous Gawler Range Volcanics (GRV) and Hiltaba Suite magmatism, with associated crustal anatexis represented by the peraluminous *ca.* 1590-1580 Ma Munjeela Suite (Payne 2008). The Hiltaba Suite consists predominately of highly fractionated granite to granodiorite, with a minor but widespread mafic component (Creaser 1996; Stewart and Foden 2003). Hiltaba Suite magmatism in the eastern Gawler Craton is temporally and spatially associated with regional-scale Fe and Na-Ca alteration and associated Cu-Au U-REE mineralization (Skirrow *et al.* 2002). The Hiltaba Suite plutons of the eastern Gawler Craton are strongly enriched in uranium (U), fluorine (F), barium (Ba), and light rare earth elements and show a negative europium anomaly with increasing silica content, suggesting crustal differentiation and/or contamination has occurred (Johnson and Cross 1995; Budd *et al.* 2001; Jagodzinski 2005; Budd 2006b; Budd 2006a; Zang *et al.* 2007). The GRV have a maximum preserved thickness of ~1.5 km and extend >25,000 km^2 across the central Gawler Craton (Blissett *et al.* 1993; Allen *et al.* 2003). The GRV consist of a dominantly felsic (dacite-rhyodacite-rhyolite) flat-lying upper portion and a compositionally diverse (basalt-andersite-dacite-rhyodacite-rhyolite) moderately to vertically dipping lower portion (Hand *et al.* 2007). Hiltaba Suite emplacement occurred in a crustal system undergoing high-grade metamorphism and widespread northwest-southeast contractional deformation (Hand *et al.* 2007). Deformation reactivated numerous crustal scale northeast–trending shear zones and north-west trending strike slip dilation structures, which together form suitable structural traps for 1590 to 1580 Ma mineralisation (Hand *et al.* 2007). Much of the central and western Gawler Craton has undergone subsequent uplift and erosion. However, Mesoproterozoic magmatism is well preserved along the eastern margin of the Gawler Craton.

2.1.2. CURNAMONA PROVINCE

The Curnamona Province is a Paleo- and Mesoproterozoic province located over the South Australia-New South Wales border. The oldest exposed rocks in the Curnamona Province are meta-sedimentary and meta-igneous rocks of the 1720-1640 Ma Willyama Supergroup (Conor and Preiss 2008). Meta-igneous rocks within the lower Willyama Supergroup are bimodal, dominated by felsic intrusives and volcanics, while the upper sequence is dominated by meta-sedimentary rocks (Robertson *et al.* 1998). In the southern Curnamona Province, the Willyama Supergroup underwent high temperature – low pressure metamorphism of the *ca.* 1610 to 1585 Ma Olarian Orogeny, culminating in widespread crustal anatexis at 1585 Ma (Ludwig and Cooper 1984; Forbes *et al.* 2005; Page *et al.* 2005; Rutherford *et al.* 2007). The effects of the Olarian Orogeny decrease northwards from upper amphibolite to greenschist facies metamorphism (Conor and Preiss 2008). During this period the Willyama Supergroup was intruded and unconformably overlain by the Ninnerie Supersuite, which is made up of the Bimbowrie Suite muscovite-biotite granites, the Crocker Well Suite sodic-muscovite-biotite and biotite only granites (Fig. 2), and the BVS (Wade 2011; Wade *et al.* 2012). The Crocker Well Suite, Olary Domain, has a significant mafic component as illustrated in the map of Fig. 2.

The Mt Painter Province at the northern margin of the Curnamona Province is composed of two basement inliers; the Mt Painter and Mt Babbage Inliers (Fig. 1). Basement rock is composed of metasedimentary rocks, *ca.* 1560 Ma granites and coeval *ca.* 1560 Ma mafic magmatism (Fraser and Neumann 2008; Kromkhun *et al.* 2013). The majority of the Ninnerie Supersuite granites appear to have been largely derived from partial melting of the Willyama Supergroup and lower crust, although the presence of more mafic metaluminous magmas indicates that there was some contribution from a mantle source (Barovich and Foden 2002). The BVS is peralkaline in character and dominated by felsic magmas with a subordinate mafic component. Rocks are generally porphyritic and range in composition from rhyolite to dacite, with minor basalt. Pervasive hydrothermal alteration (hematite, sericite, carbonate, K-feldspar, and albite) is common (Wade *et al.* 2012). The northern Curnamona Province and portions of the south are unconformably overlain by Neoproterozoic to Holocene sediments ranging up to >500 m in depth. The Benagerie Ridge is an area of relatively shallow, north south trending basement rocks in the upper-central portion of the Curnamona Province (Burtt *et al.* 2004; Wade *et al.* 2012).

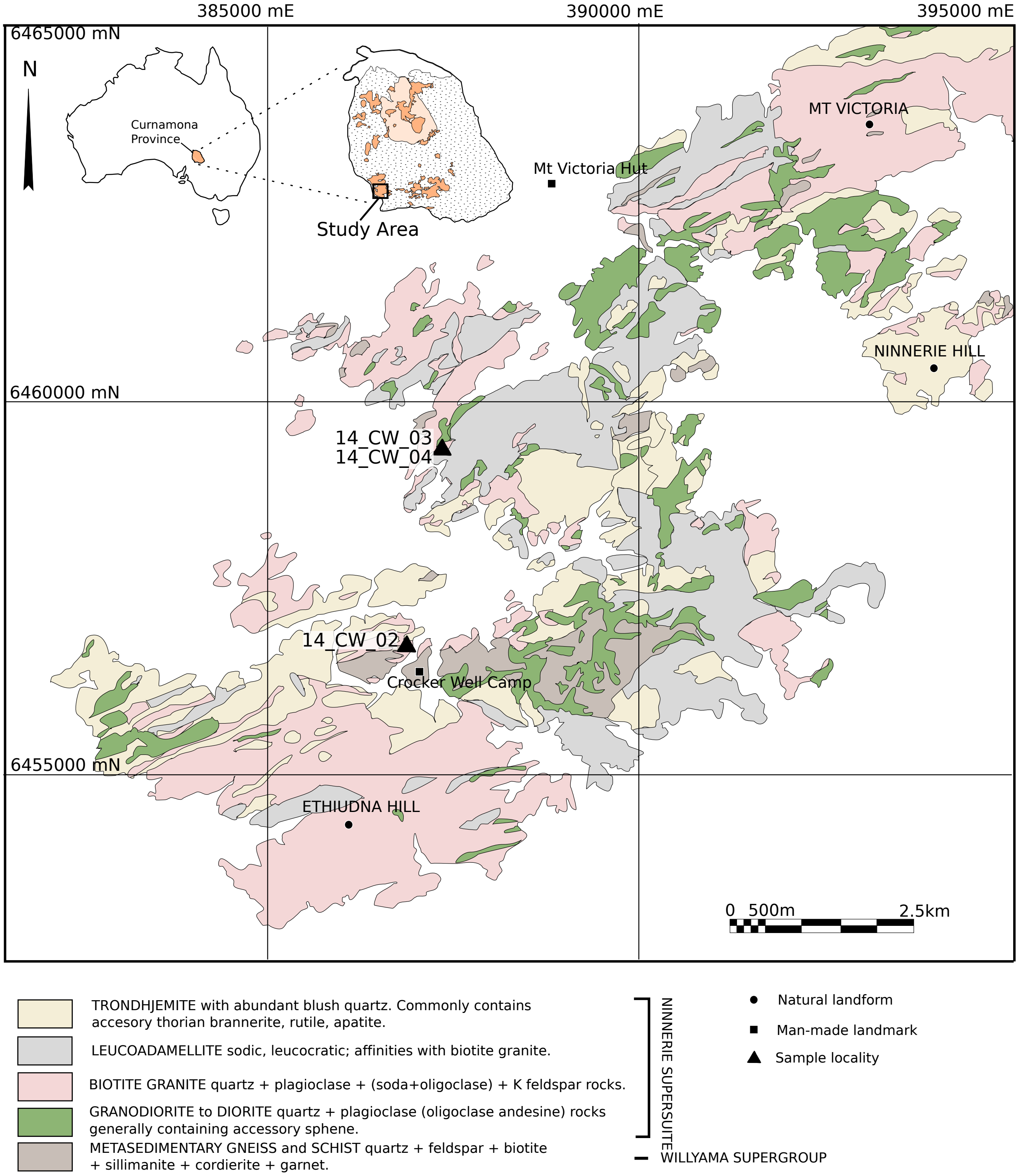

Figure 2. Location and geology map of the Crocker Well region of the Curnamona Province (pre-Neoproterozoic), including rock sample locations. Map shows the range of igneous lithologies including widespread mafic lithologies within the Crocker Well Suite of the Ninnerie Supersuite. Sample number grid references and descriptions provided in Appendix A. Modified after Laing (1995) and Wade (2012).

2.2. Tectonic Setting and IOCG Mineralisation

The Gawler Craton and the Curnamona Province both record an eastward migration of peralkaline volcanism from the eastern Gawler Craton *ca.* 1750 Ma Wallaroo Group, to the Curnamona Province *ca.* 1720 to 1640 Ma Willyama Supergroup (Conor 1995; Conor and Preiss 2008). These packages share similar sedimentary characteristics, including evidence for the presence of evaporites, which are significant brine sources during IOCG(U) deposit formation (Hunt *et al.* 2007; Conor *et al.* 2010). Following this, the Gawler Craton and Curnamona Province are said to represent part of an early Mesoproterozoic foreland basin (Hand *et al.* 2008). The foreland basin is said to have accommodated the voluminous bi-modal GRV (1600 to 1590 Ma) and Hiltaba Suite granitoids (1600 to 1575 Ma) in the west, and the equivalent BVS and Ninnerie Supersuite granites (1600 to 1580 Ma) in the Curnamona Province to the east (Hand *et al.* 2008). Regional scale IOCG alteration associated with ca. 1590 Ma magmatism of the Hiltaba Suite and Ninnerie Supersuite is evident in both terrains. Wide-scale alteration is evident in both regions; however, discovery of economic Cu-Au deposits is limited to the Gawler Craton.

IOCG mineralisation of the eastern Gawler Craton corresponds with the onset of ca. 1590 Ma magmatism of the Hiltaba Suite intrusives and the coeval GRV (Daly *et al.* 1998; Budd *et al.* 2001; Skirrow *et al.* 2002; Porter 2010b). Deposits in the Olympic IOCG Province show a strong spatial correlation with steeply-plunging intersection zones of regional east-northeast and second-order northwest trending faults (Hayward and Skirrow 2010). Works on mineralised systems commonly report mafic and ultramafic dykes coeval and within the mineralised system (Johnson and McCulloch 1995; Belperio *et al.* 2007; Hayward and Skirrow 2010). The Olympic Dam, Prominent Hill and Carrapateena Cu-Au deposits contain elevated concentrations of U, F, Ba and REE associated with hematic breccias and Cu-Au mineralisation (Reeve *et al.* 1990; Cross *et al.* 1993; Belperio *et al.* 2007; Hayward and Skirrow 2010). Mineralisation is likely the result of the mixing of enriched mantle-derived magmatic fluids with meteoric brines within or in close proximity of crustal scale fault structures (Ferris *et al.* 2002; Mark *et al.* 2006; Monteiro *et al.* 2008; Porter 2010a; Williams *et al.* 2010). IOCG mineralisation can form across a wide range of depths within the crust (> 12 to < 2 km), however high-grade Cu-Au mineralisation within the Olympic IOCG province formed at or very close to the paleo-surface, commonly exhibiting greenschist metamorphic facies (Jagodzinski 2005; Drummond *et al.* 2006; Belperio *et al.* 2007; Freeman and Tomkinson 2010; Porter 2010b; Williams *et al.* 2010).

3. METHODS

3.1. Sample Preparation

Samples in this study were collected from rock out crop and diamond drill core exhibiting minimal deformation, alteration and veining. Samples SB12_03, SB12_09, 1948991, 1998158, 1998160, 1998166, 2049213 and 2049215 were provided by Dr. Anthony Reid, Geological Survey of South Australia, DMITRE. Samples 2065518 and 2065519 were collected from the South Australian Government Glenside Core Library, Adelaide. Samples 14_CW_02, 14_CW_03 and 14_CW_04 were collected from the Olary region, Curnamona Province by the author. Zircon grains were separated using traditional hand panning and magnetic separation techniques and mounted in epoxy resin discs. Internal zircon structure was imaged using Back Scatter Electron and Cathode Luminescence detectors on a Phillips XL-40 SEM (see Appendix B for a detailed methodology).

3.2. U-Pb Geochronology

Zircon U-Pb geochronology was conducted at Adelaide Microscopy, University of Adelaide or Macquarie University. At Adelaide Microscopy, U-Pb isotopic analysis were performed using a New Wave 213nm Nd-YAG laser in a He ablation atmosphere, coupled to an Agilent 7500cx ICP-MS. A 50 s gas blank was analysed followed by 70 s of sample ablation analysis. The beam diameter at the sample surface was 30 or 40 μm depending on the available zircon grain size. At Macquarie University, U-Pb isotopic analysis were performed using a Photon Machines ArF laser in a He ablation atmosphere, coupled to a Agilent 7700 ICP-MS. Two pre-ablation shots are fired, followed by 30 sec of wash-out, 60 sec of background measurement and 120 sec of sample ablation analysis. The beam diameter at the sample surface was 40 μm.

At both facilities the isotopes measured were ^{204}Pb, ^{206}Pb, ^{207}Pb, ^{208}Pb, ^{232}Th and ^{238}U with 10, 15, 30, 10, 10 and 15 ms dwell times respectively. ^{235}U was calculated using a ^{238}U/^{235}U ratio of 137.88. Data were corrected for elemental fractionation and mass bias using 'Glitter' software (Griffin *et al.* 2004), with the primary zircon standard GJ-1 (normalisation data: ^{207}Pb/^{206}Pb = 608.3 Ma, ^{206}Pb/^{238}U = 600.7Ma and ^{207}Pb/^{235}U = 602.2 Ma, Jackson et al. 2004). Accuracy was monitored by repeat analysis of in-house standards; OG-1, Temora 2, Plesovice, Mud Tank and 91500. Instrument drift was also corrected for by standard bracketing every 15 unknown analyses and the application of a linear correction.
Reduced data was then exported into Microsoft Excel™ where subsequent conventional concordia and weighted average plots were generated using Isoplot 4.15 (Ludwig 2003). ^{207}Pb/^{206}Pb ages are primarily used in this study as the samples dated are older than *ca.* 1000 Ma and all uncertainties stated in data tables and alongside concordia diagrams are at the 1σ level.

U-Pb resultsfor the internal standards are as follows: GJ: weighted average $^{207}Pb/^{206}Pb$ age of 612 ± 6.7 Ma (n = 100, data below 90 % and above 105 % concordancy were not used in age calculations); 91500: weighted average $^{207}Pb/^{206}Pb$ age of 1066 ± 10 Ma (n = 52, data below 90 % and above 105 % concordancy were not used in age calculations); OG-1: weighted average $^{207}Pb/^{206}Pb$ age of 3462.9 ± 9.4 Ma (n = 17, data below 90 % and above 105 % concordancy not used in age calculations); Temora: weighted average $^{207}Pb/^{206}Pb$ age of 429 ± 22 Ma (n = 20, data below 80 % and above 110 % concordancy were not used in age calculations); Mudtank: weighted average $^{206}Pb/^{238}U$ age of 725 ± 5.6 Ma (n = 15, data below 90 % and above 105 % concordancy were not used in age calculations).

3.3. Lu-Hf Isotope Analysis

Lu–Hf isotopic analyses by LA-MC-ICP-MS were undertaken at the joint CSIRO-University of Adelaide facility, South Australia. Analyses were conducted on zircon samples analysed for U–Pb ages in this study. Analysis spots were placed as close as possible to concordant LA-ICP MS spot localities. Analytical methods for zircon Hf isotopic determination are detailed in Payne *et al.* (2013).

Analyses were conducted using a New Wave UP-193 Excimer laser (193 nm) attached to a Thermo-Scientific Neptune Multi Collector ICP-MS equipped with Faraday detectors and 10^{11} Ω amplifiers. The analyses were carried out in a helium atmosphere mixed upstream of the ablation cell with argon and nitrogen. A beam diameter of 50 µm, a 5 Hz repetition rate, and an intensity of approximately 6 J/cm^2 were used. Typical ablation times were 60–225 s involving a maximum of 15 measurement cycles, each consisting of ten 0.524 s integrations on ^{171}Yb, ^{173}Yb, ^{175}Lu, ^{176}Hf (+ Lu + Yb), ^{177}Hf, ^{178}Hf, ^{179}Hf and ^{180}Hf; one 0.524 s integration of REE ^{160}Gd, ^{163}Dy, ^{164}Dy, ^{165}Ho, ^{166}Er, ^{167}Er, ^{168}Er, ^{170}Yb and ^{171}Yb, and one 0.524 s integration of Hf oxides with masses ranging from 187 to 196 amu. This is inclusive of a 1.5 s idle time between subsequent mass changes and an off-peak baseline measurement. Oxide formation rates and REE-oxide interference in high REE zircon were monitored throughout the session. No oxide corrections were applied to the data collected during this study. Oxide formation rates were typically 0.02 – 0.03 %.

Data were normalised by an exponential mass bias correction using a stable ^{179}Hf/^{177}Hf ratio of 0.7325. Isobaric interferences on ^{176}Hf by Yb and Lu were corrected using the methods of Woodhead *et al.* (2004) with direct measurement of ^{171}Yb/^{173}Yb fractionation using the Yb isotopic values of Segal *et al.* (2003). Assuming the same mass bias behaviour as Yb, a correction for Lu isobaric interference on ^{176}Hf used a ^{176}Lu/^{175}Lu ratio of 0.02655 (Vervoort *et al.* 2004). Data were processed using software *Hf*TRAX v.3.2 (Payne *et al.* 2013). Instrument performance and stability was monitored by analysis of Plesovice (^{176}Hf/^{177}Hf = 0.282482 ± 0.000013, Slama *et al*. 2008) and Mudtank zircon (^{176}Hf/^{177}Hf = 0.282507 ± 0.000006, Woodhead and Hergt 2005) standards. In this study the average ^{176}Hf/^{177}Hf values are 0.282470 ± 0.000015 for Plesovice and 0.282506 ± 0.000015 for Mudtank.

4. RESULTS

4.1. U-Pb Geochronology and Lu-Hf Isotope Analysis

U-Pb geochronological analyses were done on 8 samples from the Gawler Craton and 5 samples from the Curnamona Province. Zircon grains elevated in ^{204}Pb (common Pb) and/or showing discordancy below 80 % or above 110 % were not used for age calculations. Weighted average ^{207}Pb/^{206}Pb and U-Pb concordia ages are presented in Figures 3 and 4, and a full table of results can be found in Appendix C. For all samples the ages presented are considered to be magmatic ages. This is based on zircon CL images showing oscillatory or magmatic style zoning in at least some of the zircons for each sample (Fig. 5).

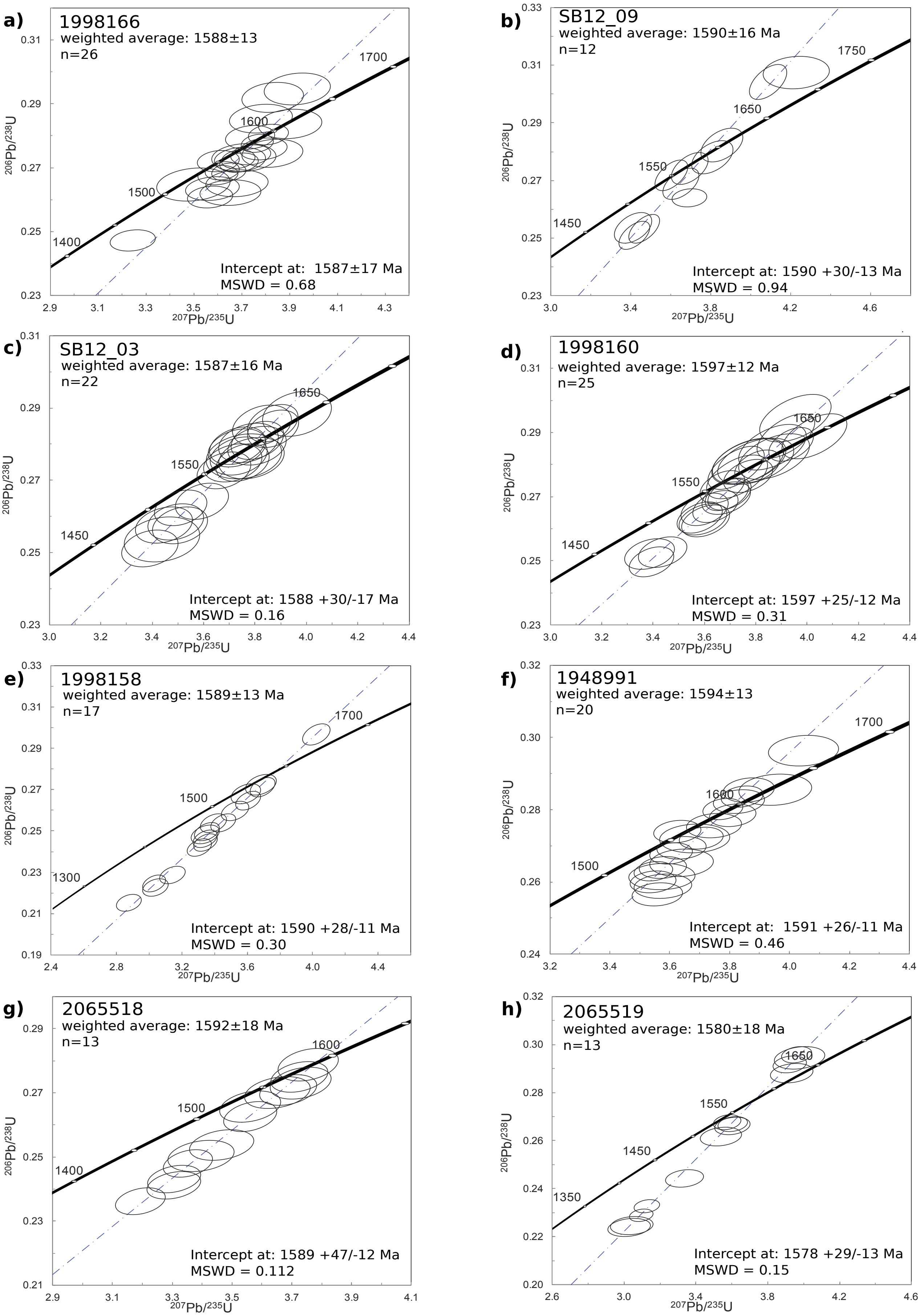

Figure 3. U/Pb concordia plots of all zircon grains used to calculate rock ages from the Gawler Craton. Weighted average $^{207}Pb/^{206}Pb$ and a concordia intercept age determinations for samples (a) 1998166 (Hiltaba Suite); (b) SB12_09 (Hiltaba Suite); (c) SB12_03 (GRV); (d) 1998160 (GRV); (e) 1998158 (GRV); (f) 1948991 (Hiltaba Suite); (g) 2065518 (GRV); (h) 2065519 (Hiltaba Suite). n = the number of analyses age determinations are based on.

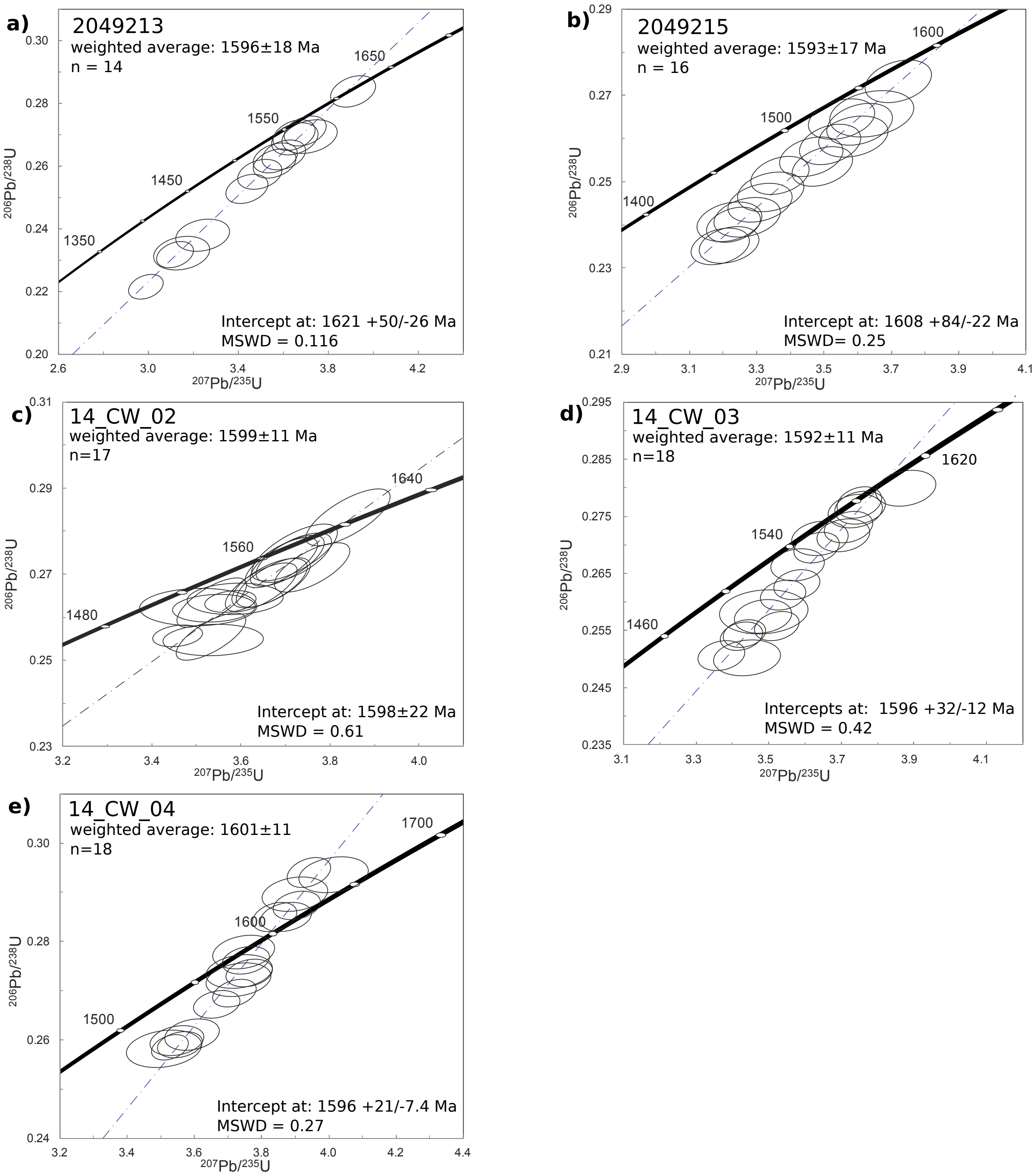

Figure 4. U/Pb concordia plots of all zircon grains used to determine rock ages from the Curnamona Province. Weighted average $^{207}Pb/^{206}Pb$ and concordia intercept age determinations for samples (a) 2049213 (BVS); (b) 2049215 (Bimbowrie Suite); (c) 14_CW_02 (Crocker Well Suite); (d) 14_CW_03 (Crocker Well Suite); (e) 14_CW_04 (Crocker Well Suite). n = the number of analyses age determinations are based on.

Lu-Hf isotopic analyses were undertaken on eight samples from the Gawler Craton and five from the Curnamona Province. Target zircons within each sample were the *ca*. 1590 grains. Data are presented comparatively in plots of $\varepsilon_{Hf}(T)$ versus $^{207}Pb/^{206}Pb$ age (Fig. 6−8) and by population density plots for the ε_{Hf}(T) values of each sample (Fig. 9). There is a general similarity in zircon Hf data from the Gawler Craton and Curnamona Province. Across the Gawler Craton the ε_{Hf}(T) values range from +2.0 to -7.4 with two outliers of -13.9, and within the Curnamona Province the values range from +2.5 to -3.8. ε_{Hf}(T) values of samples across the two regions are compared in Figure 7a & b and 9s & t, and Lu-Hf results from previous works are displayed in Figure 7c & d and 9v–y. A table of all results is presented in Appendix D.

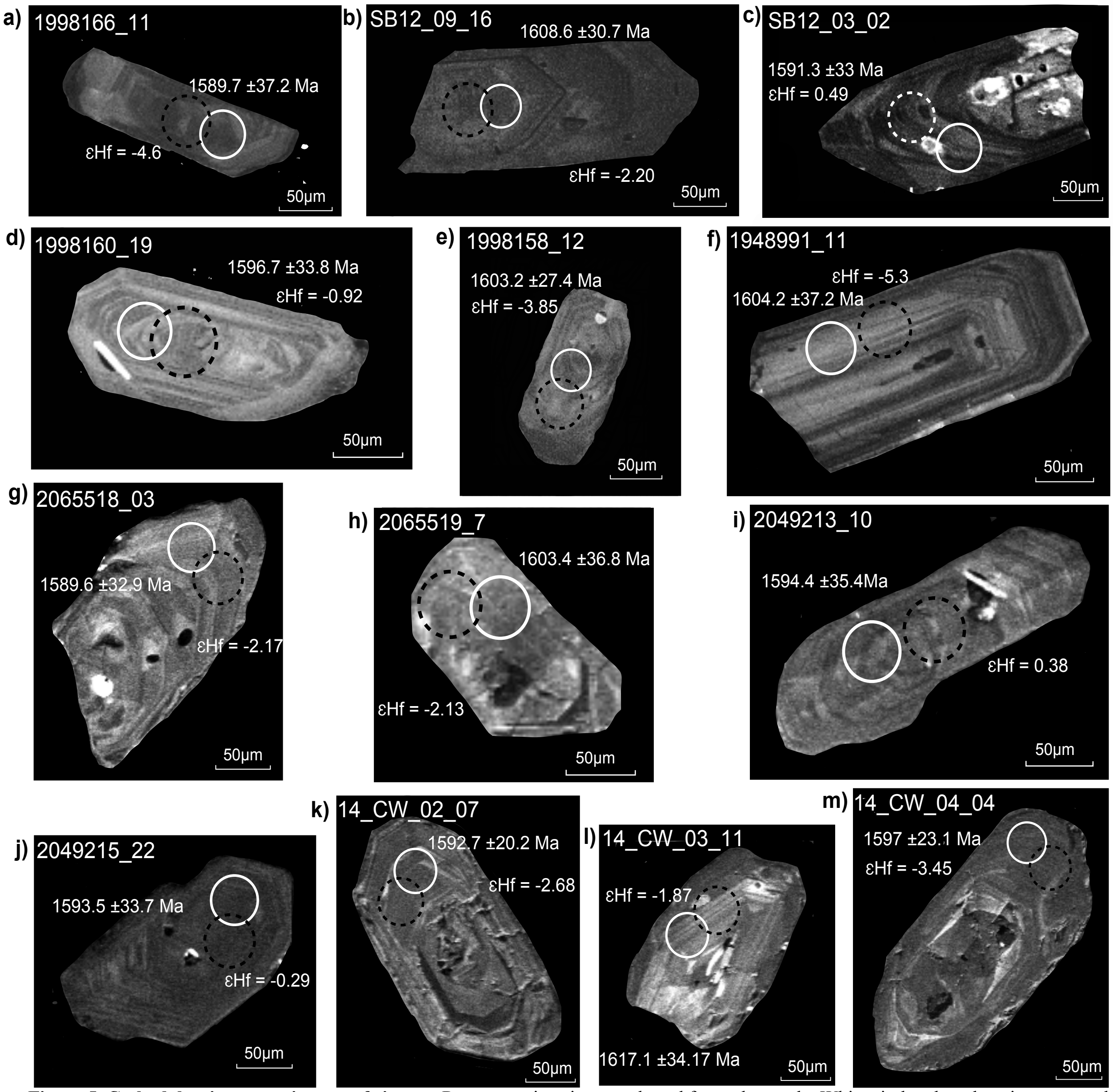

Figure 5. Cathodoluminescence images of zircons. Representative zircons selected for each sample. White circles show locations targeted by LA-ICP-MS analysis with weighted average $^{207}Pb/^{206}Pb$ ages shown. Black dotted circles show locations targeted by Hf-Lu analysis with corresponding εHf values shown. Areas within a zircon showing similar oscillatory zoning were targeted. Sample name at top of each image.

4.1.1 GAWLER CRATON SAMPLES

Sample 1998166 - Granite

Sample 1998166 is outcropping Hiltaba Suite granite located in the upper-central Gawler Craton area (Fig. 1). Zircon morphology is dominated by euhedral, elongate grains with aspect ratios from 2:1 to 4:1 and lengths of 70 to 300 µm. Under CL imaging grains are dull in colour with faint zoning, minimal dark inclusions and free of internal cracks (Fig. 5a). 30 analyses were completed. Zircons showing concordancy below 90 % were not used for age calculations. A group of 26 analyses define a weighted average $^{207}Pb/^{206}Pb$ age of 1588 ± 13 Ma (MSWD = 0.67) and an upper intercept age of 1588 ± 17 Ma (MSWD = 0.68; Fig. 3a). Hf-isotope analysis was undertaken on 22 U/Pb dated zircon grains and returned $\varepsilon_{Hf}(T)$ values ranging from -3.5 to -7.4 (Fig. 6a and 9e).

Sample SB12_09 - Granite

Sample SB12_09 is outcropping Hiltaba Suite granite located in the central Gawler Craton area (Fig. 1). Zircon morphology includes euhedral to subhedral elongate grains with aspect ratios varying from 2:1 to 3:1 and lengths of 30 to 200 µm. Under CL imaging grains are medium grey to black in colour, have rare oscillatory zoning, rare light coloured inherited cores, and scarce dark inclusions and internal cracks (Fig. 5b). 34 analyses were completed. Zircons showing concordancy below 90 % and above 110 % were not used for age calculations. A group of 12 analyses define a weighted average $^{207}Pb/^{206}Pb$ age of 1590 ± 16 Ma (MSWD = 1.12) and an upper intercept age of 1590 ± 18 Ma (MSWD = 0.94; Fig. 3b). Hf-isotope analysis was undertaken on 10 U/Pb dated zircon grains and returned $\varepsilon_{Hf}(T)$ values ranging from -0.5 to -4.1 with two outliers of -13.9 (Fig. 6b and 9f).

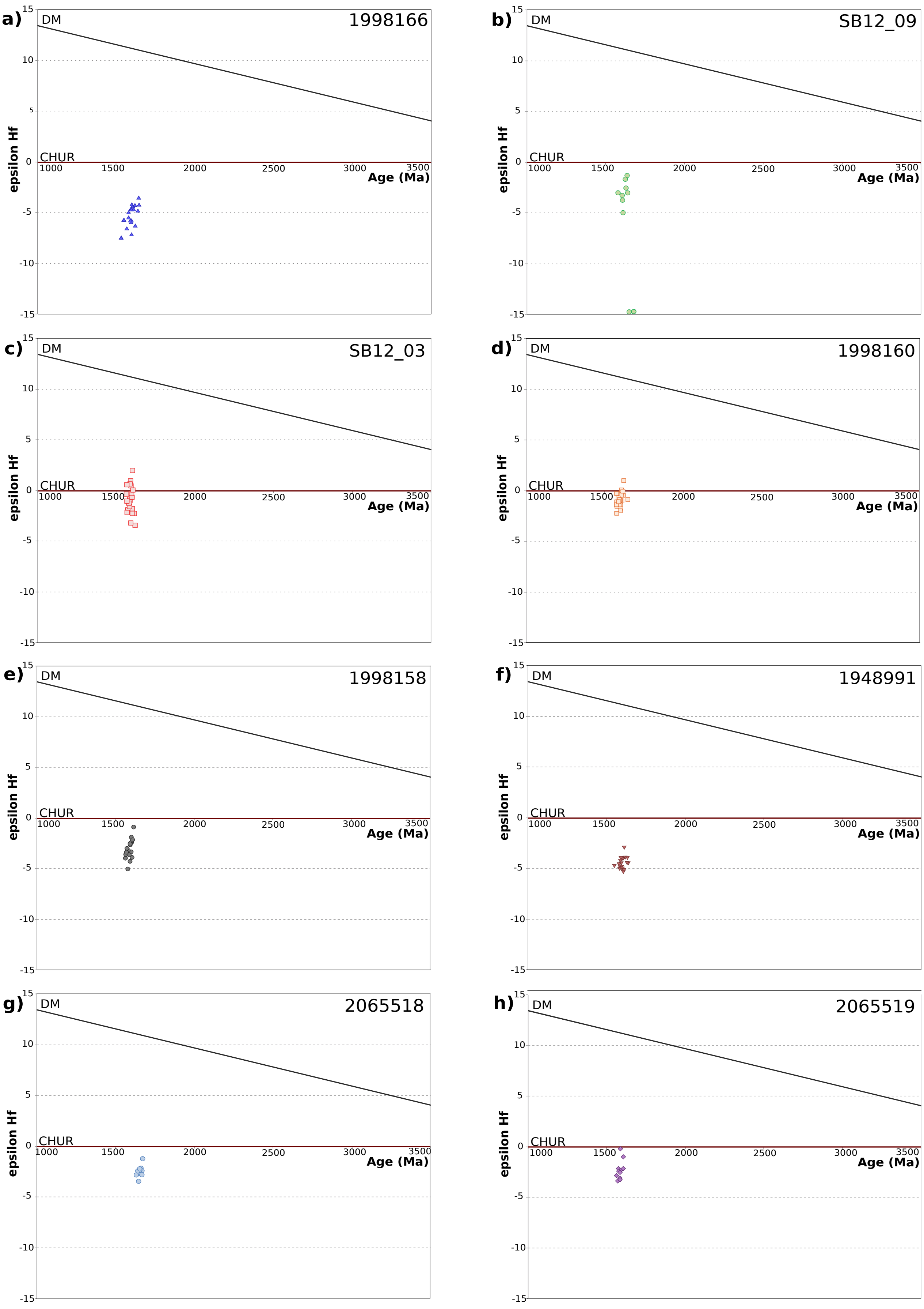

Figure 6. εHf vs age plots of Gawler Craton zircon data collected in this study. DM - depleted mantle, CHUR - chondritic uniform reservoir.

Sample SB12_03 - GRV

Sample SB12_03 is outcropping GRV located in the lower-central Gawler Craton area (Fig. 1). Zircon morphology includes euhedral to subhedral mostly elongate grains with aspect ratios and lengths from 1:1 to 3:1 and 50 to 400 μm respectively. Under CL imaging grains are heavily zoned with bands ranging in colour from dark grey to black and light grey to white. The majority of grains have mottled inherited cores, with oscillatory zoning surrounds. Dark inclusions within grains are common and internal cracks sporadic (Fig. 5c). 31 analyses were completed. Zircons showing concordancy below 90 % were not used for age calculations. A group of 22 analyses define a weighted average $^{207}Pb/^{206}Pb$ age of 1587 ± 16 Ma (MSWD = 0.16) and an upper intercept age of 1588 ± 19 Ma (MSWD = 0.16; Fig. 3c). Hf-isotope analysis was undertaken of 22 U/Pb dated zircon grains and returned $\varepsilon_{Hf}(T)$values ranging from +2.0 to -3.4 (Fig. 6c and 9g).

Sample 1998160 - Dacite

Sample 1998160 is outcropping Moonaree Dacite GRV located in the lower-central Gawler Craton area (Fig. 1). Zircon morphology includes euhedral to subhedral, sometimes elongate grains with aspect ratios of 1:1 to 4:1 and length 30 to 250 μm. Under CL imaging grains have medium grey and light grey zoning, and some host inclusion rich cores (Fig. 5d). 34 analyses were completed. Zircons showing concordancy below 90 % were not used for age calculations. A group of 25 analyses define a weighted average $^{207}Pb/^{206}Pb$ age of 1597 ± 12 Ma (MSWD = 0.31) and an upper intercept age of 1597 ± 16 Ma (MSWD = 0.31; Fig. 3d). Hf-isotope analysis was undertaken on 24 U/Pb dated zircon grains and returned $\varepsilon_{Hf}(T)$ values ranging from +1.0 to -2.2 (Fig. 6d and 9h).

Sample 1998158 - Rhyolite

Sample 1998158 is outcropping Eucaroo Rhyolite GRV located in the lower-central Gawler Craton area (Fig. 1). Zircon morphology includes euhedral to subhedral grains with aspect ratios varying from 1:1 to 4:1 and lengths of 30 to 250 µm. Under CL imaging, grains include irregular, faint, dark grey and medium grey zones. Inherited cores are uncommon and mottled. Light and dark coloured inclusions and internal cracks are common (Fig. 5e). 20 analyses were completed. Zircons showing concordancy below 80 % were not used for age calculations. A group of 17 analyses define a weighted average $^{207}Pb/^{206}Pb$ age of 1589 ± 13 Ma (MSWD = 0.29) and an upper intercept age of 1590 ± 22 Ma (MSWD = 0.30; Fig. 3e). Hf-isotope analysis was undertaken on 17 U/Pb dated zircon grains and returned $\varepsilon_{Hf}(T)$ values ranging from -0.9 to -5.0 (Fig. 6e and 9i).

Sample 1948991 – Granite

Sample 1948991 is medium-grained plagioclase+K-feldspar+biotite+quartz+ hornblende Hiltaba Suite granodiorite drill core from drill hole MRC007A (157-157.95 m), located in the lower-eastern Gawler Craton area (Fig. 1). Zircon morphology includes euhedral elongate grains with aspect ratios of 2:1 to 4:1 and lengths of 50 to 400 µm. Under CL imaging grains appear with zones varying in colour between dark grey and medium grey to light grey. Inherited cores are uncommon and appear mottled. Light and dark inclusions are uncommon and internal cracks common (Fig. 5f). 28 analyses were completed. Zircons showing concordancy below 90 % were not used for age calculations. A group of 20 analyses define a weighted average $^{207}Pb/^{206}Pb$ age of 1594 ± 13 Ma (MSWD = 0.46) and an upper intercept age of 1591 ± 15 Ma (MSWD = 0.46; Fig. 3f). Hf-isotope analysis was undertaken on 19 U/Pb dated zircon grains and returned $\varepsilon_{Hf}(T)$ values ranging from -2.9 to -5.3 (Fig. 6f and 9j).

Sample 2065518 - Rhyolite

Sample 2065518 is Fe-altered, fine-grained rhyodacite GRV drill core from drill hole RED 1 (392.1 to 393.1 m), located in the eastern Gawler Craton area (Fig. 1). Zircon morphology includes euhedral to subhedral grains with rare elongate grains. Aspect ratios range from 1:1 to 4:1 and lengths 70 to 300 μm. Under CL imaging grains are medium to light grey with either faint zoning or more commonly a mottled appearance. Inherited cores are uncommon, while dark inclusions and internal cracks are common (Fig. 5g). 19 analyses were completed. Zircons showing concordancy below 85% were not used for age calculations. A group of 13 analyses define a weighted average $^{207}Pb/^{206}Pb$ age of 1592 ± 18 Ma (MSWD = 0.107) and an upper intercept age of 1589 ± 31 Ma (MSWD = 0.112; Fig. 3g). Hf-isotope analysis was undertaken on 13 U/Pb dated zircon grains and returned $\varepsilon_{Hf}(T)$ values ranging from -1.0 to -3.2 (Fig. 6g and 9k).

Sample 2065519 - Granite

Sample 2065519 is fine to medium-grained quartz+K-feldspar+biotite Hiltaba Suite granite drill core from drill hole BLD 2 (841.4 to 842.2 m), located in the eastern Gawler Craton area (Fig. 1). Zircon morphology includes subhedral to anhedral grains with aspect ratios of 1:1 to 2:1 and lengths of 70 to 250 μm. Under CL imaging grains are light to medium grey and commonly mottled, with rare oscillatory zoning. Inherited cores are uncommon, while dark inclusions and internal cracks are common (Fig. 5h). 15 analyses were completed. Zircons showing concordancy below 80 % were not used for age calculations. A group of 13 analyses define a weighted average $^{207}Pb/^{206}Pb$ age of 1580 ± 18 Ma (MSWD = 0.14) and an upper intercept age of 1578 ± 21 Ma (MSWD = 0.15; Fig. 3h). Hf-isotope analysis was undertaken on 12 U/Pb dated zircon grains and returned $\varepsilon_{Hf}(T)$ values ranging from -0.2 to -3.4 (Fig. 6h and 9l).

4.1.2 CURNAMONA PROVINCE SAMPLES

Sample 2049213 - Rhyolite

Sample 2049213 is quartz-feldspar Fe-altered BVS rhyolite drill core from drill hole BRD013 (466 to 484 m) located in the upper-central Curnamona Province area (Fig. 1). Zircon morphology includes euhedral grains with aspect ratios of 2:1 to 4:1 and lengths of 100 to 450 μm. Under CL imaging grains have strong oscillatory zonation of medium to light grey. Dark inclusions and internal cracks are common within grains (Fig 5i). 21 analyses were completed. Zircons showing concordancy below 80 % were not used for age calculations. A group of 14 analyses define a weighted average $^{207}Pb/^{206}Pb$ age of 1596 ± 18 Ma (MSWD = 0.16) and an upper intercept age of 1609 ± 34 Ma (MSWD = 0.083; Fig. 4a). Hf-isotope analysis was undertaken on 12 U/Pb dated zircon grains and returned $\varepsilon_{Hf}(T)$ values ranging from +0.4 to -2.4 (Fig. 7a and 9n).

Sample 2049215 - Microgranite

Sample 2049215 is quartz+feldspar+biotite Ninnerie Supersuite microgranite drill core from drill hole Cu-1 (435.55 to 439 m) located in the upper-central Curnamona Province area (Fig. 1). Zircon morphology includes euhedral to subhedral grains with aspect ratios of 1:1 to 3:1 and lengths of 80 to 250 μm. Under CL imaging zoning varies greatly, ranging from mottled appearance to oscillatory and light to dark grey in colour. Inherited cores are uncommon while dark and light inclusions are common (Fig. 5j). 27 analyses were completed. Zircons showing concordancy below 80 % were not used for age calculations. A group of 16 analyses define a weighted average $^{207}Pb/^{206}Pb$ age of 1593 ± 17 Ma (MSWD = 0.27) and an upper intercept age of 1608 ± 51 Ma (MSWD = 0.25; Fig. 4b). Hf-isotope analysis was undertaken on 16 U/Pb dated zircon grains and returned $\varepsilon_{Hf}(T)$ values ranging from +2.5 to -1.7 (Fig. 7b and 9o).

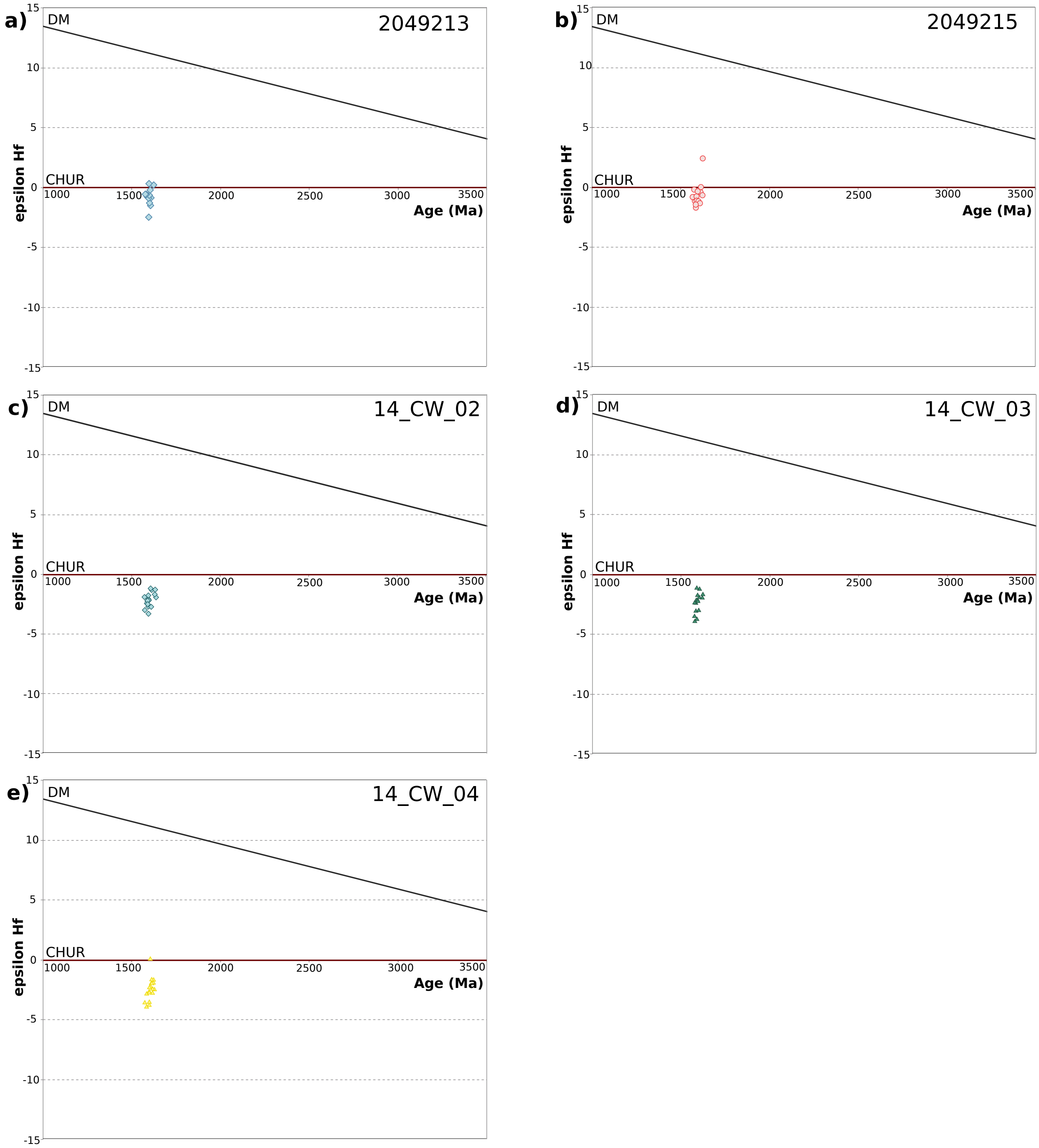

Figure 7. εHf vs age plots of Curnamona Province zircon data collected in this study. DM - depleted mantle, CHUR - chondritic uniform reservoir.

Sample 14_CW_02 - Granite

Sample 14_CW_02 is outcropping quartz+Kfeldspar+biotite Crocker Well Suite granite located in the lower-western Curnamona Province (Fig. 2). Zircon morphology includes euhedral to subhedral grains with aspect ratios of 1:1 to 3:1 and lengths of 100 to 500 μm.

Under CL imaging grains appear medium to light grey with irregular oscillatory zoning and rare grains with a mottled appearance. Inherited cores are frequent and highly mottled, while dark inclusions are very common and internal cracks common (Fig. 5k). 45 analyses were completed. Zircons showing concordancy below 90 % were not used for age calculations. A group of 17 analyses define a weighted average $^{207}Pb/^{206}Pb$ age of 1599 ± 11 Ma (MSWD = 0.57) and an upper intercept age of 1598 ± 22 Ma (MSWD = 0.61; Fig. 4c). Hf-isotope analysis was undertaken on 17 U/Pb dated zircon grains and returned $\varepsilon_{Hf}(T)$ values ranging from -1.2 to -3.3 (Fig. 7c and 9p).

Sample 14_CW_03 - Granodiorite

Sample 14_CW_03 is outcropping fine-grained quartz+Kfeldspar+biotite Crocker Well Suite granite located in the lower-western Curnamona Province (Fig. 2). Zircon morphology includes euhedral to anhedral grains with aspect ratios of 1:1 to 3:1 and lengths of 150 to 400 μm. Under CL imaging grains appear medium to very light grey with irregular zoning that is often mottled and rare grains with minimal to no zonation. Very light irregular patches within zircon grains are common. Dark inclusions are common and internal cracks uncommon (Fig. 5l). 20 analyses were completed. Zircons showing concordancy below 85 % were not used for age calculations. A group of 18 analyses define a weighted average $^{207}Pb/^{206}Pb$ age of 1592 ± 11 Ma (MSWD = 0.43) and an upper intercept age of 1596 ± 22 Ma (MSWD = 0.42; Fig. 4d). Hf-isotope analysis was undertaken on 16 U/Pb dated zircon grains and returned $\varepsilon_{Hf}(T)$ values ranging from -1.1 to -3.8 (Fig. 7d and 9q).

Sample 14_CW_04 – Deformed granodiorite

Sample 14_CW_04 is outcropping foliated coarse-grained Kfeldspar+biotite+quartz Crocker Well Suite granite located in the lower-western Curnamona Province (Fig. 2). Zircon morphology includes euhedral to subhedral grains with aspect ratios of 1:1 to 3:1 and lengths of 100 to 400 µm. Under CL imaging grains appear medium to light grey with irregular zoning including some with a mottled appearance. Dark inclusions and cracks are common within grains (Fig. 5m). 20 analyses were completed. Zircons showing concordancy below 90 % were not used for age calculations. A group of 18 analyses define a weighted average $^{207}Pb/^{206}Pb$ age of 1601 ± 11 Ma (MSWD = 0.45) and an upper intercept age of 1596 ± 11 Ma (MSWD = 0.27; Fig. 4e). Hf-isotope analysis was undertaken on 17 U/Pb dated zircon grains and returned $\varepsilon_{Hf}(T)$ values ranging from +0.2 to -3.8 (Fig. 7e and 9r).

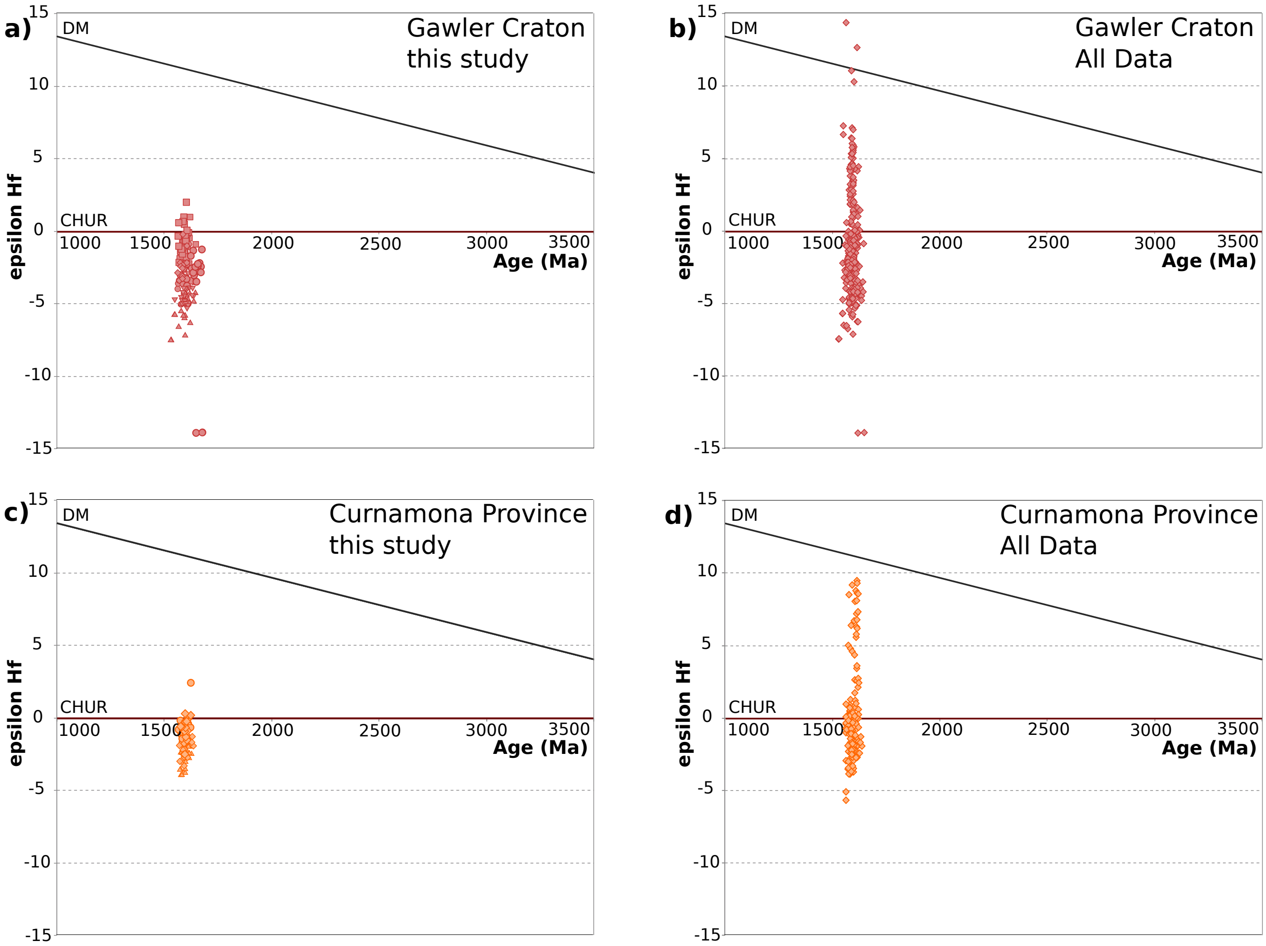

Figure 8. Summary εHf vs age plots of Gawler Craton and Curnamona. (a) All Gawler Craton zircon data collected in this study; (b) All Gawler Craton Hf data from previous studies; (c) All Curnamona Province zircon data collected in this study; (d) All Curnamona Province zircon from previous studies. DM - depleted mantle, CHUR - chondritic uniform reservoir. Data compiled in plots b) and d) sourced from Condie *et al.* (2005) and Belousova *et al.* (2009).

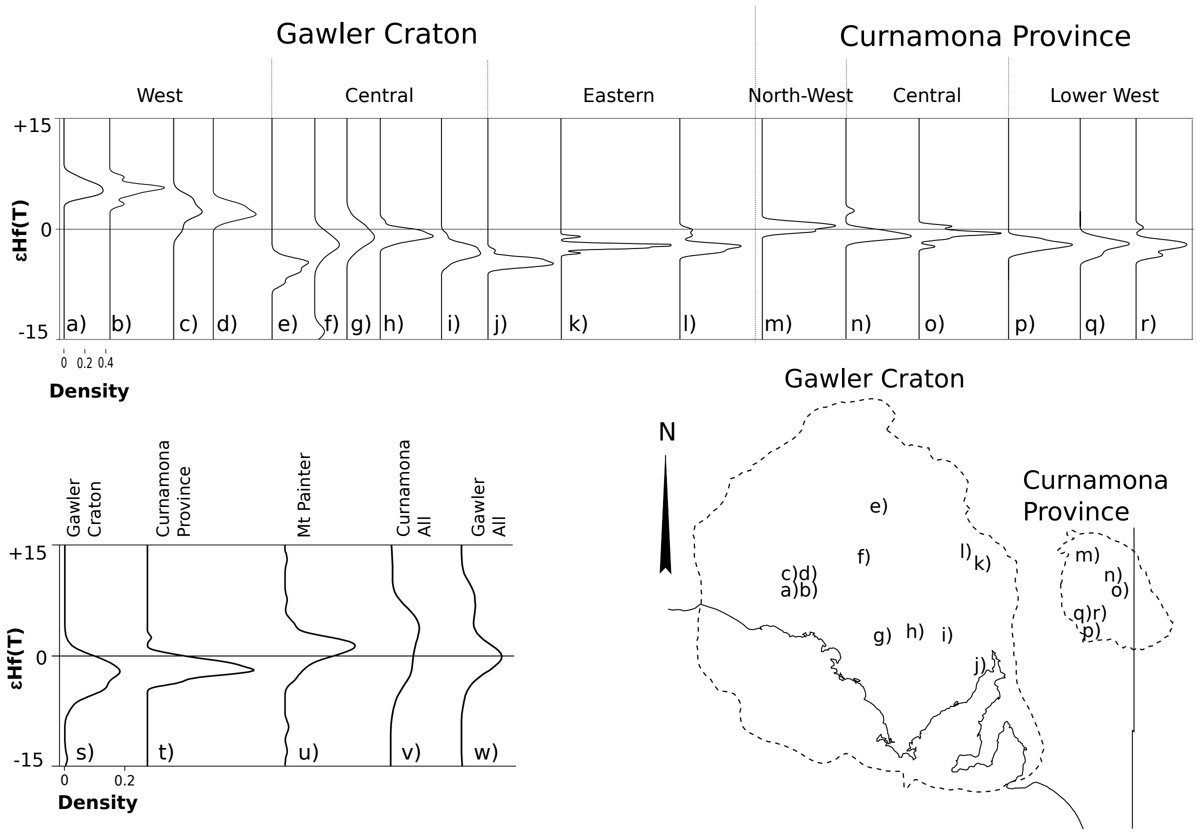

Figure 9. εHf population density plots of samples and collated eHf data from the Gawler Craton and Curnamona Province. The X-axis indicated the relative population density of a set of analyses; Y-axis represents εHf(T) values. Samples a) to r) have same X-axis scale (refer to a), and represent seperate sets of sample analyses . Samples s) to w) have same X-axis scale (refere to w), and represent collated data from the region. Sample numbers: a) 1834092; b) 1835093; c) 1834090; d) 1834090; e) 1998166; f) SB12_09; g) SB12_03; h) 1998160; i) 1998158; j) 1948991; k) 2065518; l) 2065519; m)1709493; n) 2049213; o) 2049215; p) 14_CW_02; q) 14_CW_03; r) 14_CW_04.Inset map gives approximate locations for each plot, more detailed locations presented in Figures 1 & 2 and Appendix A. Data for plots u) - w) sourced from Condie *et al.* (2005), Belousova *et al.* (2009) and Kromkhun *et al.* (2013).

5. DISCUSSION

Lu-Hf data collected on 13 samples in this study is augmented with unpublished Lu-Hf data from Dr. Anthony Reid, Geological Survey of South Australia, and Lu-Hf data from Kromkhun *et al.* (2013), to give data on a total of 21 samples of *ca.* 1590 Ma magmatism (Appendix 5). This data in combination with existing geochemical and Nd isotope data, allows for comparison of the bimodal Mesoproterozoic magmatism of the Gawler Craton and the Curnamona Province, and the implications for mineral prospectivity to be assessed.

5.1. Hf Isotopic Signature of *ca.* 1590 Ma Magmatism in the Gawler Craton and the Curnamona Province

Mesoproterozoic plutonic and volcanic samples analysed in this study from the Curnamona Province and the Gawler Craton exhibit both comparable and dissimilar ε_{Hf}(T) relationships (Fig. 9). Detrital zircon studies of Condie et al. (2005) and Belousova et al. (2009) report *ca.* 1590 Ma zircon Lu-Hf analysis within the Gawler Craton and Curnamona Province return ε_{Hf}(T) values ranging from -18.6 to +14.4 and -5.6 to +9.5 (-16.4 outlier) respectively. The Gawler Craton samples range to more positive and negative ε_{Hf}(T) values than those of the Curnamona Province when both magmatic and detrital *ca.* 1590 Ma zircons are included. Magmatic Lu-Hf isotope data can be broken up into three different populations based on geographical location and regional trends in ε_{Hf}(T) values. Magmatic ε_{Hf}(T) data of the western Gawler Craton (-0.4 to +7.1) is more positive than the central and eastern Gawler Craton (-7.4 to +2.0) which is slightly more negative than the Curnamona Province (-5.6 to +2.5). Differences between ε_{Hf}(T) values in the eastern and central Gawler Craton and the Curnamona Province are small and not distinguishable. In contrast, the western Gawler Craton magmatism has a relatively positive range of ε_{Hf}(T) values. This is consistent with the region generally exhibiting a different crustal composition to the remainder of the Gawler Craton. In the Western Gawler Craton, the *ca.* 1615 Ma St Peter Suite and *ca.* 1585 Ma Munjeela Suite are present. Nd isotope data of the St Peters Suite and Munjeela Suite give ε_{Nd}(T) values ranging from -0.2 to +7.5 and -3.1 (outlier) to +2.5 respectively (Payne 2008; Swain *et al.* 2008; Chalmers 2009), indicating juvenile crust existed in the western region during emplacement of the Hiltaba Suite. Hf isotope data from Mesoproterozoic magmatism of the Mt Painter Province indicates a relatively juvenile source at the northern margin of the Curnamona. This variation in crustal composition and architecture needs to be factored in when interpreting Hf and Nd isotope data to allow study of genetic differences in magma genesis across a terrain.

5.2. Petrogenesis and Mantle Input of ca. 1590 Ma Magmatism

Determining the relative roles of mantle- and crustally-derived melts in magmatic suite genesis is useful for assessing coeval magmatic rocks across different regions. For this study it is also important in subsequent investigation of possible influences on prospectivity. To identify mantle input in the Curnamona Province, central/eastern Gawler, and western Gawler Craton, two different methods were used.

The first basic method uses calculated average regional values for mantle and crustal composition (ε_{Hf}(T)) and concentration (Hf ppm) to calculate the fraction of mantle involved in the magma mixing process. Average input values for the crustal composition were calculated from Lu-Hf and Sm-Nd studies of Archean to Paleoproterozoic basement lithologies of the Gawler Craton and Paleoproterozoic rocks of the Curnamona Province (Turner *et al.* 1993; Creaser 1995; Fanning 1997; Schaefer 1999; Budd *et al.* 2001; Stewart and Foden 2003; Barovich and Hand 2008; Payne 2008; Swain *et al.* 2008; Dutch and Hand 2010; Fraser *et al.* 2010; Payne *et al.* 2010; Howard *et al.* 2011). ε_{Hf}(T) values were then back calculated to ε_{Hf}(1590) values representing crustal influences present during *ca.* 1590 Ma magmatism of the Gawler Craton and Curnamona Province. Average crustal ε_{Hf}(1590) values calculated for western Gawler Craton, central and eastern Gawler Craton, and the Curnamona Province are +0.1, -6.0 and -3.2 respectively.

Average input values for the mantle composition were calculated from Nd data of *ca.* 1590 Ma mafic and ultramafic magmatic rocks. The Nd data were calculated to ε_{Hf}(1590) values and an average composition was calculated for each region. Due to a lack of mafic data from the Curnamona Province these data were combined with data from the central and eastern Gawler Craton to provide a bulk average for both regions. Average mantle ε_{Hf}(1590) values calculated for western Gawler Craton, central and eastern Gawler Craton, and the Curnamona Province are +6.2 and +2 respectively (Stewart 1994; Johnson and McCulloch 1995; Stewart and Foden 2003; Fricke 2005; Chalmers 2009; Wade *et al.* 2012).

Variation of average crustal and mantle compositions between regions can be attributed to different crustal architecture and interpreted mantle composition across and between terrains. Most noticeably, the crust of the St Peters Suite region, western Gawler Craton, is more juvenile than crustal material of the central and eastern Gawler Craton. Calculated mantle fractions range from 0.24 to 0.85 averaging 0.53 in the western Gawler Craton; 0.06 to 0.56 averaging 0.34 in the central/eastern Gawler Craton; and 0.12 to 0.55 averaging 0.32 in the Curnamona Province. The mantle fraction calculated for granites and rhyolites of the different regions is very similar with the exception of two higher values in the western Gawler samples (Figure 11). These calculations suggest that in addition to the crust being more juvenile in the western Gawler Craton, there is also a higher mantle input into the Hiltaba Suite in this region, contributing to the positive $\varepsilon_{Hf}(T)$ values measured. The accuracy of this method is limited, as simple averaging cannot take into account crustal heterogeneity and non-Gaussian distributions of compositions. For example, the Gawler Craton contains more than one population of possible crustal influences (Archean and Paleoproterozoic). This produces a non-Gaussian distribution of crustal composition input values, rendering an average of the two non-representative.

The crustal and mantle melt compositions for a single location could be one of a range of different values, and as such a second model was used to better account for this. An analysis assigning a range of crustal and mantle compositions to a sample numerous times allow a histogram to be constructed showing the best range of mantle fraction that fits the data. The crustal and mantle datasets for each region are the same as those used in the first model, however averages are replaced by repetitive and random assignment of known compositional values in that region. Modelling involves the repetitive input of mantle and crustal compositional values, and sequential range of mantle fraction values into the magma mixing equation. Input data are randomly selected from a database of known crustal and interpreted mantle melt compositional values. The mantle fraction value that produces the best fit with the sample is recorded in a histogram. This process is repeated 100,000 times with each mantle fraction result placed in the histogram. This histogram presents the range and probability of all possible mantle fraction values for that particular sample in a region. Circumstances where the sample $\varepsilon_{Hf}(T)$ value is more positive than the mafic melt $\varepsilon_{Hf}(T)$ value or more negative than the crustal $\varepsilon_{Hf}(T)$ value can occur. The main cause of this is likely the presence of more evolved material deeper in the crust that is unable to be sampled and therefore accounted for in modelling. These results are represented as non-viable (Non-V) in the histogram.

A schematic of the process is presented in Figure 10. The results presented in histograms show a close relationship to results calculated in the first model. The second model however documents the range of and probability of possible mixing fractions that could be attained depending on the different crustal rocks and interpreted mantle composition seen in the region. A comparison of the two model outcomes is presented in Figure 11.

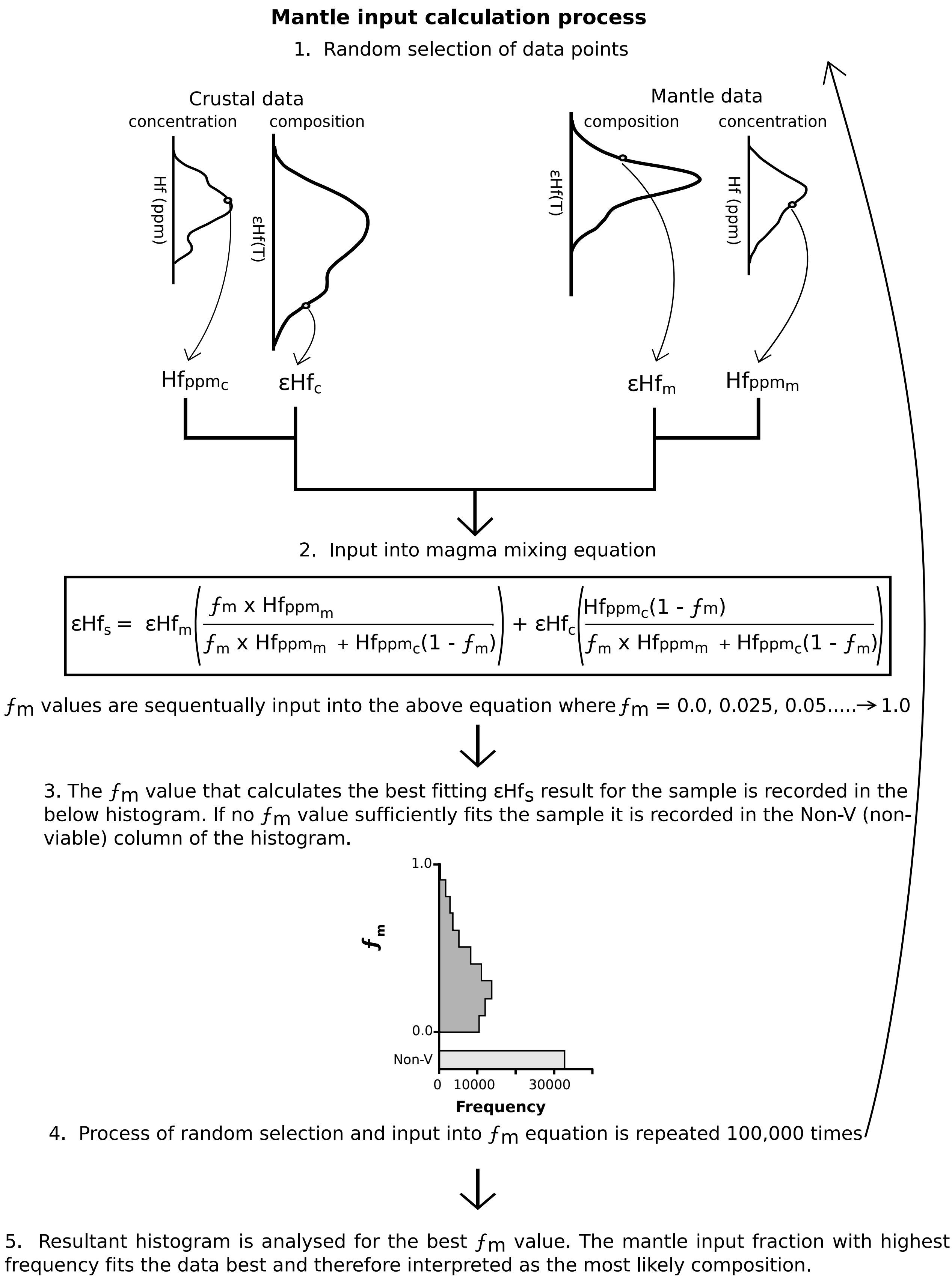

Figure 10. Schematic for calculating the mantle fraction using Hf isotope and geochemical data. Accuracy and validity of this method is dependant on a regional data base of crustal and mantle values containing all known source values. $ƒm$ = mantle fraction, Non-V = non-viable results, $εHfs$ = εHf value of sample being analysed. Code for calculation process written by Justin Payne and modified by author for use.

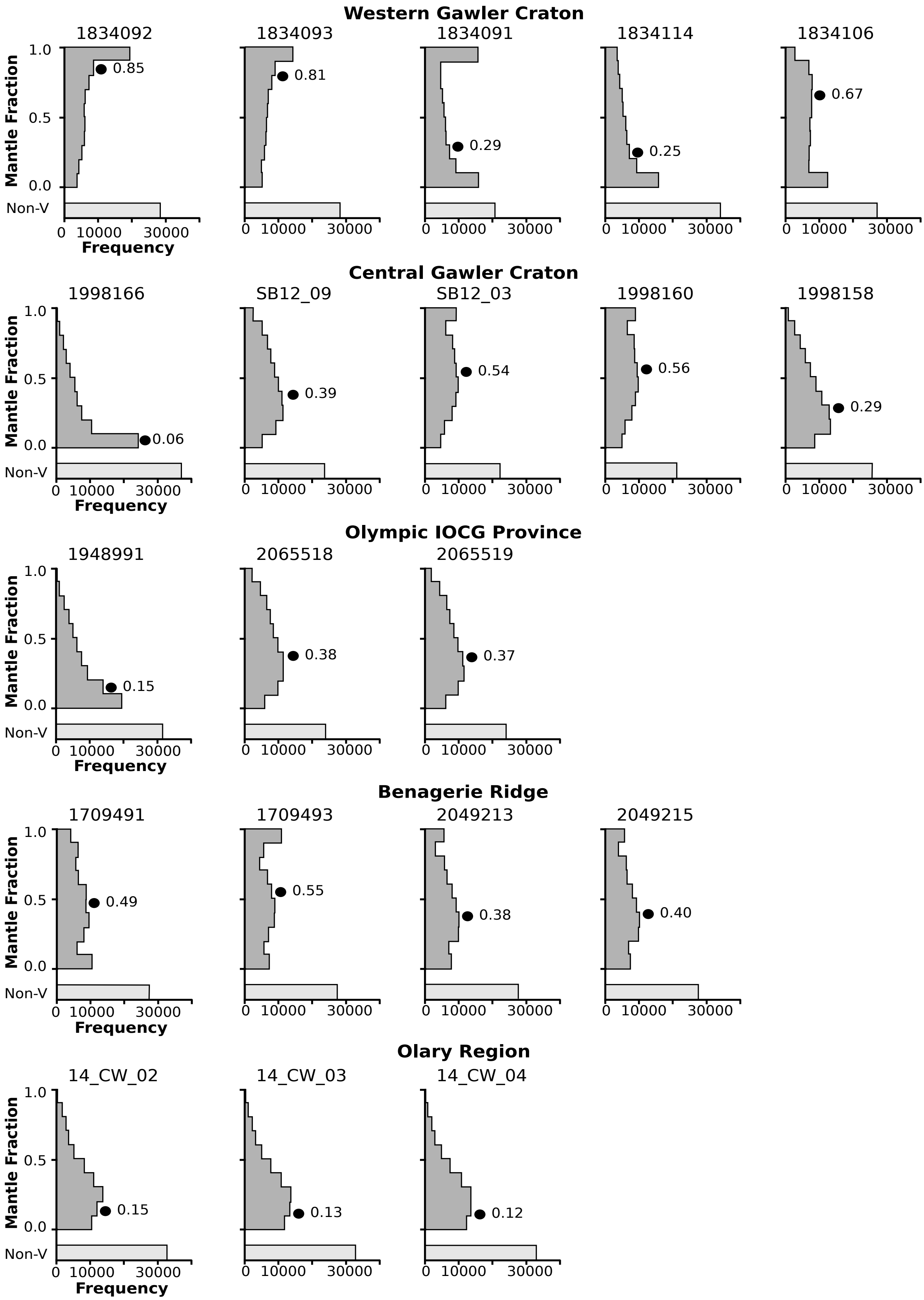

Figure 11. Mantle fraction histograms of the western Gawler Craton, central Gawler Craton, Olympic IOCG Province, Benagerie Ridge and Olary Region. Histograms are produced using a random sampling method detailed in Figure 10. Mantle fraction values calculated using the averaging method are quoted next to each black circle. Y-axis and X-axis scales and lables are the same for all plots. Sample numbers are present at the top of each histogram. Samples include all analysed in this in addition to seven from Dr. Anthony Reid. Appendix A presents the details of each sample.

5.3. IOCG Prospectivity vs Mantle Input – a one-dimensional analysis

The Olympic IOCG Province, located on the eastern flank of the Gawler Craton, is host to the Olympic Dam and Prominent Hill IOCG mines, and the Hillside, Carrapateena and Wirrda Well IOCG prospects. Hiltaba Suite and GRV samples taken from the Olympic IOCG Province show similar mantle input as those collected from the central Gawler Craton and the Curnamona Province. If mantle input is to be used as a proxy from IOCG prospectivity in Mesoproterozoic terrains of South Australia, then both the central Gawler Craton and the Curnamona Province can be considered prospective.

The Benagerie Ridge region of the Curnamona Province has been considered to be prospective for IOCG mineralisation based on similarities with the prospective Olympic IOCG Prospect (Williams and Skirrow 2000; Burtt *et al.* 2004). Two samples from the Benagerie Ridge returned $\varepsilon_{Hf}(T)$ values similar to those collected from the Olympic IOCG Province, however only the small Kalkaroo and Portia prospects have been discovered to date. The relationship between mantle input and metal endowment is unlikely the only contributing factor affecting IOCG prospectivity in the Gawler Craton and Curnamona Province. Mantle input into magmatism may not solely determine the IOCG prospectivity of an area, but instead can allow comparison of terrains, and subsequently determine if they have similar magmatic compositions to then be considered prospective. It is essential to consider other key factors required for mineralization to occur prior to considering a terrane to be prospective for IOCG mineralisation.

5.4. Chemistry and Crustal Architecture – an integrated approach to prospectivity

In order to assess the IOCG prospectivity of the Gawler Craton and Curnamona Province the role of exhumation, crustal priming and deep structures in conjunction with mantle input as considered as factors influencing the formation and preservation of IOCG mineralisation. IOCG mineralisation can form across a wide range of depths within the crust (> 12 to < 2 km). However, high-grade Cu-Au mineralisation within the Olympic IOCG province formed at or very close to the paleo-surface and commonly exhibits greenschist metamorphic facies (Jagodzinski 2005; Drummond *et al.* 2006; Belperio *et al.* 2007; Freeman and Tomkinson 2010; Porter 2010b; Williams *et al.* 2010). Prospective areas may therefore be restricted to regions that have not been exhumed from anything more than greenschist to lower amphibolite metamorphic facies at 1590 Ma. Regions that record higher metamorphic P-T conditions than lower amphibolite can be considered less prospective. This includes northern and central Mt Woods Domain (Forbes *et al.* 2011), Coober Pedy Ridge (Cutts *et al.* 2011), and southern Curnamona Province (Dutch *et al.* 2005; Rutherford *et al.* 2007). Exhumation of these areas to the current crustal levels is not favourable for preserving IOCG mineralization (Fig.12).

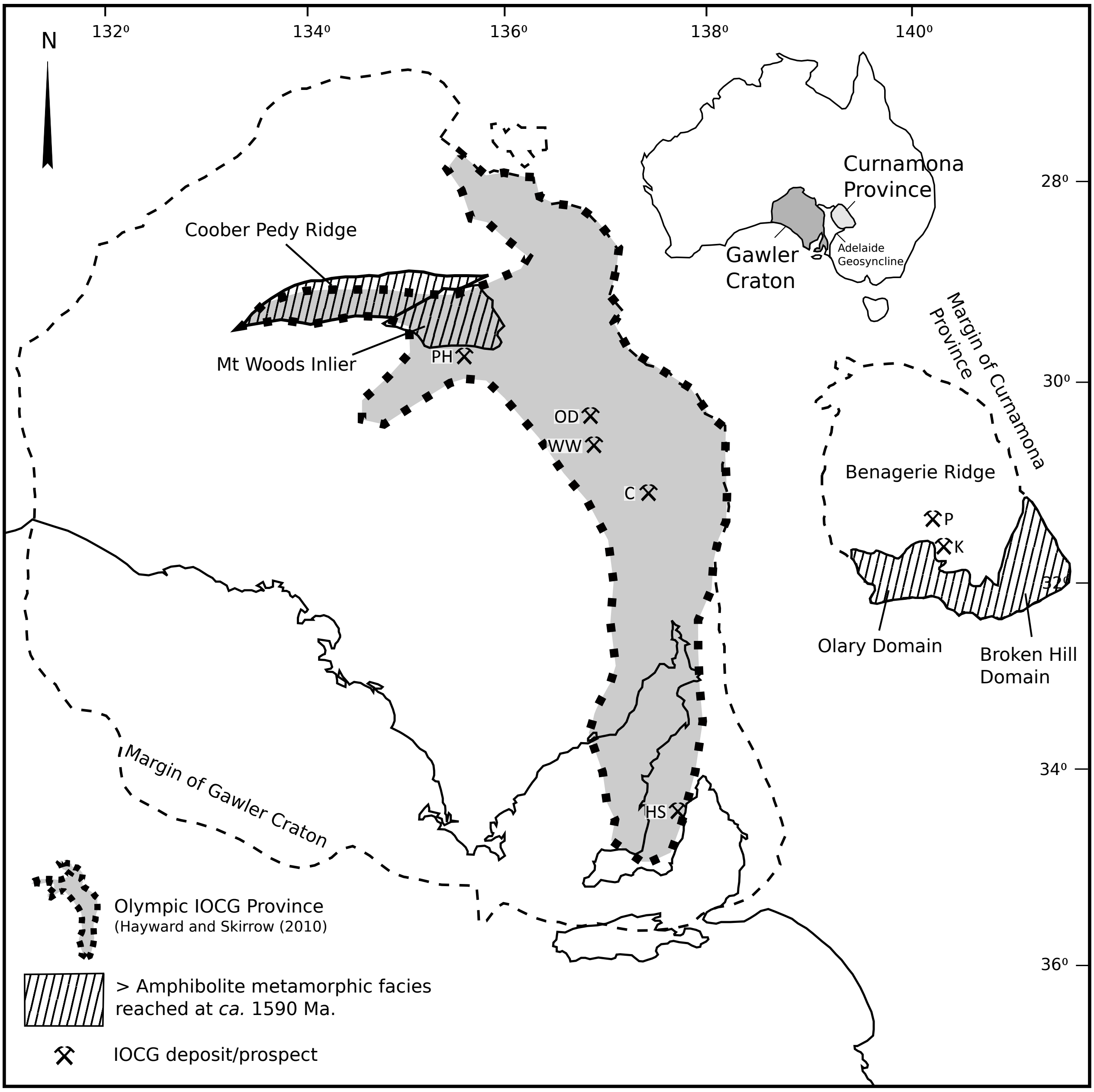

Figure 12. Regions of the Olympic IOCG Province, Gawler Craton, and the Curnamona Province exhibiting greater than amphibolite metamorphic facies conditions at *ca.* 1590 Ma. Areas exhibiting metamorphic facies greater than amphibolite facies are unlikely to have preserved Cu-Au rich mineralisation due to depth of weathering and as such are interpreted to be of low IOCG prospectivity. IOCG prospects/deposits moving west to east: PH = Prominent Hill; OD = Olympic Dam; WW = Wirda Well; C = Carrapateena; HS = Hillside; P = Portia; K = Kalkaroo. Compiled from Dutch *et al.* (2005), Hayward and Skirrow (2010), Cutts *et al.* (2011) and Forbes *et al.* (2011).

As previously discussed, the level of mantle input into *ca.* 1590 Ma magmatism is considered to be a factor in mineralization potential. IOCG deposits of eastern Gawler Craton commonly report mafic and ultra mafic dykes coeval with and within mineralised systems (Johnson and McCulloch 1995; Belperio *et al.* 2007; Hayward and Skirrow 2010). The calculated mantle input and the interpreted mantle melt composition of the central and eastern Gawler Craton and the Curnamona Province is very similar. The western Gawler Craton however shows a greater mantle influence into Hiltaba Suite magmatism than the remainder of the Gawler Craton. Bimodal magmatism of the Olympic IOCG Province and the Benagerie Ridge are comparable in terms of mantle input, interpreted mantle melt composition and rock types present and thereby interpreted prospective for the same style of IOCG mineralization. IOCG mineralization of the eastern Gawler Craton corresponds with the onset of ca. 1590 Ma magmatism of the Hiltaba Suite intrusives and the coeval GRV (Daly *et al.* 1998; Budd *et al.* 2001; Skirrow *et al.* 2002; Porter 2010b). Despite the high mantle input into magmatism in the western Gawler, prospectivity is interpreted low as a result of the significant difference seen in Hiltaba Suite magmatism and surrounding crust.

One distinct difference between the Olympic IOCG Province and the Benagerie Ridge is the effects the Kimban Orogeny had on the two regions prior to Mesoproterozoic magmatism. The effects of the Kimban Orogeny on the Gawler Craton include widespread formation of crustal-scale shear systems, granitic magmatism, and low- to high-grade metamorphism (Parker 1980; Hopper 2001; Vassallo and Wilson 2002; Betts *et al.* 2003; Payne *et al.* 2006; Hand *et al.* 2007; Payne *et al.* 2009). During this time the Benagerie Ridge was undergoing basin sedimentation of the Willyama Supergroup (Conor 1995; Conor and Preiss 2008). The role of crustal priming and its influence on magma generation may be an important factor affecting IOCG prospectivity. During the Kimban Orogeny, eastern Gawler Craton was exposed to amphibolite to granulite facies metamorphism. Dehydration of the Archean and Paleoproterozoic crust during this period is likely to have affected the subsequent Hiltaba event. Dehydrated crust would allow mantle material to reach much higher temperatures when mantle material is emplaced. These elevated temperatures would enrich the mantle by scavenging U, F and REE from the surrounding crust (Collins *et al.* 1982). Hiltaba Suite plutons are predominately metaluminous granitoids with strong enrichment in U, F and REE (Johnson and Cross 1995; Jagodzinski 2005; Budd 2006b; Zang *et al.* 2007). Mineralisation of the Olympic Dam, Prominent Hill and Carrapateena Cu-Au deposits contain elevated concentrations of U, F, Ba and REE associated with hematic breccias and Cu-Au mineralisation (Reeve *et al.* 1990; Cross *et al.* 1993; Belperio *et al.* 2007; Hayward and Skirrow 2010). The effects of the Kimban Orogeny may also be important for establishing crustal pathways. Crustal-scale structures are an important pathway and host in the formation of significant IOCG mineralisation. All significant IOCG deposits in the Olympic IOCG Province show a strong spatial correlation with steeply-plunging intersection zones of regional east-northeast and second-order northwest trending faults (Hayward and Skirrow 2010). Identification of equivalent structure in the Benagerie Ridge Region is likely an important factor to consider for IOCG prospectivity.

6. CONCLUSIONS

ε_{Hf}(T) values from magmatic zircons and compiled detrital zircon data range from +2.0 to -7.4, +0.2 to -5.3 and +2.5 to -3.8 from the central Gawler Craton, eastern Gawler Craton and the Curnamona Province respectively. Mantle input calculations return more juvenile results in the western Gawler Craton to relatively more evolved results in the central/eastern Gawler Craton and the Curnamona Province. The Benagerie Ridge region of the Curnamona Province displays similar bimodal *ca.* 1590 Ma magmatism, ε_{Hf}(T) values, mantle input characteristics, crustal preservation (exhumation) and regional IOCG alteration as the highly prospective Olympic IOCG Province. The Western Gawler however is compositionally different than the rest of the Gawler Craton and the Curnamona Province, recording more juvenile Hiltaba magmatism within more juvenile crust. Considering multiple factors influencing IOCG mineralisation, the Benagerie Ridge remains prospective.

ACKNOWLEDGEMENTS

I would like to thank Justin Payne for his excellent guidance, support, encouragement and patience throughout an eventful year. Karin Barovich is thanked for her invaluable input and assistance. Anthony Reid and Claire Wade, Department of State Development, South Australian Government, are thanked for supplying samples, Lu-Hf data and information vital for the field trip. Ben Wade and Aoife McFadden, Adelaide Microscopy, are thanked for their assistance with SEM imaging and LA-ICP-MS analyses. Will Powell, Macquarie University, is thanked for his assistance with LA-ICP-MS analyses.

REFERENCES

ALLEN S., SIMPSON C., MCPHIE J. & DALY S. 2003. Stratigraphy, distribution and geochemistry of widespread felsic volcanic units in the Mesoproterozoic Gawler Range Volcanics, South Australia*, *Australian Journal of Earth Sciences,* **50**, no. 1, 97-112.

BAROVICH K. & FODEN J. 2002 Nd isotope constraints on the origin of 1580 Ma Curnamona Province granitoid magmatism. Geological Society of Australia Abstracts. pp. 156-156. Geological Society of Australia; 1999.

BAROVICH K. & HAND M. 2008. Tectonic setting and provenance of the Paleoproterozoic Willyama Supergroup, Curnamona Province, Australia: Geochemical and Nd isotopic constraints on contrasting source terrain components, *Precambrian Research,* **166**, no. 1, 318-337.

BELPERIO A., FLINT R. & FREEMAN H. 2007. Prominent Hill: a hematite-dominated, iron oxide copper-gold system, *Economic geology,* **102**, no. 8, 1499-1510.

BETTS P. G., VALENTA R. K. & FINLAY J. 2003. Evolution of the Mount Woods Inlier, northern Gawler Craton, Southern Australia: an integrated structural and aeromagnetic analysis, *Tectonophysics,* **366**, no. 1, 83-111.

BLISSETT A., CREASER R., DALY S., FLINT R. & PARKER A. 1993. Gawler range volcanics, *The Geology of South Australia,* **1**, 107-124.

BUDD A. R., WYBORN L. A. I., BASTRAKOVA I. V. & AUSTRALIA G. 2001 The metallogenic potential of Australian Proterozoic granites. Geoscience Australia.

BUDD A. R. 2006a The Tarcoola Goldfield of the Central Gawler Gold Province, and the Hiltaba Association Granites, Gawler Craton, South Australia. Australian National University.

BUDD A. R. 2006b. A-and I-type subdivision of the Gawler Ranges-Hiltaba Volcano-Plutonic Association, *Geochimica et Cosmochimica Acta,* **70**, no. 18, p.A72.

BURTT A., CONOR C. & ROBERTSON S. 2004. Curnamona—an emerging Cu–Au province, *MESA Journal,* **33**, 9-17.

CHALMERS N. 2009 Geodynamic evolution of the St Peter Suite, Gawler Craton, South Australia: stratigraphic, geochemical and isotopic investigation. School of Geosciences. Monash University.

COLLINS W., BEAMS S., WHITE A. & CHAPPELL B. 1982. Nature and origin of A-type granites with particular reference to southeastern Australia, *Contributions to mineralogy and petrology,* **80**, no. 2, 189-200.

CONOR C. 1995. Moonta-Wallaroo region: An interpretation of the geology of the Maitland and Wallaroo 1: 100 000 sheet areas, *Mines and Energy South Australia, Open File Envelope,* **8886**.

CONOR C. C. H., RAYMOND O., BAKER T., TEALE G. S., SAY P. & LOWE G. 2010 Alteration and mineralisation in the Moonta-Wallaroo copper-gold mining field region, Olympic Domain, South Australia. *In* PORTER T. M. ed. *Hydrothermal Iron Oxide Copper-Gold & Related Deposits: A Global Perspective, v. 3 - Advances in the Understanding of IOCG Deposits,* pp. 147-170. PGC Publishing,

CONOR C. H. & PREISS W. V. 2008. Understanding the 1720–1640Ma Palaeoproterozoic Willyama Supergroup, Curnamona Province, Southeastern Australia: implications for tectonics, basin evolution and ore genesis, *Precambrian Research,* **166**, no. 1, 297-317.

COWLEY W. M., CONOR C. H. H. & ZANG W. 2003. New and revised Proterozoic stratigraphic units on northern Yorke Peninsula, *MESA J,* **29**, 46-58.

CREASER R. A. 1995. Neodymium isotopic constraints for the origin of Mesoproterozoic felsic magmatism, Gawler Craton, South Australia, *Canadian Journal of Earth Sciences,* **32**, no. 4, 460-471.

--- 1996. Petrogenesis of a Mesoproterozoic quartz latite-granitoid suite from the Roxby Downs area, South Australia, *Precambrian Research,* **79**, no. 3, 371-394.

Cross K., Daly S. & Flint R. 1993. Mineralisation associated with the GRV and Hiltaba Suite granitoids—Olympic Dam deposit, *The Geology of South Australia,* **1**, 132-138.

Cutts K., Hand M. & Kelsey D. E. 2011. Evidence for early Mesoproterozoic (ca. 1590Ma) ultrahigh-temperature metamorphism in southern Australia, *Lithos,* **124**, no. 1, 1-16.

Daly S., Fanning G. & Fairclough M. 1998. Tectonic evolution and exploration potential of the Gawler Craton, South Australia, *AGSO Journal of Australian Geology and Geophysics,* **17**, 145-168.

Drummond B., Lyons P., Goleby B. & Jones L. 2006. Constraining models of the tectonic setting of the giant Olympic Dam iron oxide–copper–gold deposit, South Australia, using deep seismic reflection data, *Tectonophysics,* **420**, no. 1–2, 91-103.

Dutch R. & Hand M. 2010. Retention of Sm–Nd isotopic ages in garnets subjected to high-grade thermal reworking: implications for diffusion rates of major and rare earth elements and the Sm–Nd closure temperature in garnet, *Contributions to Mineralogy and Petrology,* **159**, no. 1, 93-112.

Dutch R. A., Hand M. & Clark C. 2005. Cambrian reworking of the southern Australian Proterozoic Curnamona Province: constraints from regional shear-zone systems, *Journal of the Geological Society,* **162**, no. 5, 763-775.

Ehrig K., McPhie J. & Kamenetsky V. 2012. Geology and mineralogical zonation of the Olympic Dam Iron Oxide Cu-U-Au-Ag deposit, South Australia.

Fanning C., Reid A. & Teale G. 2007. A geochronological framework for the Gawler Craton, South Australia, *South Australia Geological Survey Bulletin,* **55**, p.80.

Fanning C. M. 1997 Geochronological synthesis of South Australia.: Mines Department of South Australia. Open File Envelope 8918.

Ferris G. & Schwarz M. 2004. Definition of the Tunkillia Suite, western Gawler craton, *MESA Journal,* **34**, 32-41.

Ferris G. M., Schwarz M. P. & Heithersay P. 2002 The Geological Framework, Distribution and Controls of Fe-Oxide Cu-Au Mineralisation in the Gawler Craton, South Australia: Part 1: Geological and Tectonic Framework. *In* PORTER T. M. ed. *Hydrothermal Iron Oxide Copper-Gold & Related Deposits: A Global Perspective*. PGC Publishing,

Forbes C., Betts P., Weinberg R. & Buick I. 2005. A structural metamorphic study of the Broken Hill Block, NSW, Australia, *Journal of Metamorphic Geology,* **23**, no. 8, 745-770.

Forbes C. J., Giles D., Hand M., Betts P., Suzuki K., Chalmers N. & Dutch R. 2011. Using< i> P</i>–< i> T</i> paths to interpret the tectonothermal setting of prograde metamorphism: An example from the northeastern Gawler Craton, South Australia, *Precambrian Research,* **185**, no. 1, 65-85.

Fraser G. & Neumann N. 2008. New SHRIMP U-Pb zircon ages from the Gawler craton and Curnamona province, *South Australia,* **2010**, p.256.

Fraser G., McAvaney S., Neumann N., Szpunar M. & Reid A. 2010. Discovery of early Mesoarchean crust in the eastern Gawler Craton, South Australia, *Precambrian Research,* **179**, no. 1, 1-21.

Freeman H. & Tomkinson M. 2010. Geological setting of iron oxide related mineralisation in the southern Mount Woods Domain, South Australia, *Hydrothermal iron oxide copper-gold & related deposits: A global perspective,* **3**, 171-190.

Fricke C. 2005. Source and origin of the Lower Gawler Range Volcanics (GRV), South Australia: Geochemical constraints from mafic magmas, *Unpublished Honours Thesis. Monash University, Melbourne*.

Griffin W., Belousova E., Shee S., Pearson N. & O'Reilly S. 2004. Archean crustal evolution in the northern Yilgarn Craton: U–Pb and Hf-isotope evidence from detrital zircons, *Precambrian Research,* **131**, no. 3, 231-282.

Groves D. I., Bierlein F. P., Meinert L. D. & Hitzman M. W. 2010. Iron oxide copper-gold (IOCG) deposits through Earth history: Implications for origin, lithospheric setting, and distinction from other epigenetic iron oxide deposits, *Economic Geology,* **105**, no. 3, 641-654.

Hand M., Reid A. & Jagodzinski L. 2007. Tectonic framework and evolution of the Gawler craton, Southern Australia, *Economic Geology,* **102**, no. 8, 1377-1395.

Hand M. P., Reid A. J., Szpunar M. A., Direen N., Wade B., Payne J. & Barovich K. M. 2008. Crustal architecture during the early Mesoproterozoic Hiltaba-related mineralisation event: are the Gawler Range Volcanics a foreland basin fill?, *MESA Journal,* **51**, 19-24.

Hayward N. & Skirrow R. G. 2010 Geodynamic Setting and Controls on Iron Oxide Cu-Au (±U) Ore in the Gawler Craton, South Australia. *In* PORTER T. M. ed. *Hydrothermal Iron Oxide Copper-Gold and Related Deposits: A Global Perspective,* pp. 119-146. PGC Publishing,

Hitzman M. W., Oreskes N. & Einaudi M. T. 1992. Geological characteristics and tectonic setting of Proterozoic iron oxide (Cu□ U□ Au□ REE) deposits, *Precambrian Research,* **58**, no. 1, 241-287.

Hopper D. J. 2001. Crustal evolution of paleo-to mesoproterozoic rocks in the Peake and Denison Ranges, South Australia.

Howard K. E., Hand M., Barovich K. M., Payne J. L., Cutts K. & Belousova E. A. 2011. U–Pb zircon, zircon Hf and whole-rock Sm–Nd isotopic constraints on the evolution of Paleoproterozoic rocks in the northern Gawler Craton, *Australian Journal of Earth Sciences,* **58**, no. 6, 615-638.

Hunt J., Baker T. & Thorkelson D. 2007. A review of iron oxide copper-gold deposits, with focus on the Wernecke Breccias, Yukon, Canada, as an example of a non-magmatic end member and implications for IOCG genesis and classification, *Exploration and Mining Geology,* **16**, no. 3-4, 209-232.

Jackson S. E., Pearson N. J., Griffin W. L. & Belousova E. A. 2004. The application of laser ablation-inductively coupled plasma-mass spectrometry to in situ U–Pb zircon geochronology, *Chemical Geology,* **211**, no. 1, 47-69.

Jagodzinski E. 2005. Compilation of SHRIMP U–Pb geochronological data, Olympic Domain, Gawler Craton, South Australia, 2001–2003, *Geoscience Australia Record,* **20**, no. 2005, p.197.

Johnson J. P. & Cross K. C. 1995. U-Pb geochronological constraints on the genesis of the Olympic Dam Cu-U-Au-Ag deposit, South Australia, *Economic Geology,* **90**, no. 5, 1046-1063.

Johnson J. P. & McCulloch M. T. 1995. Sources of mineralising fluids for the Olympic Dam deposit (South Australia): Sm□ Nd isotopic constraints, *Chemical Geology,* **121**, no. 1, 177-199.

Kromkhun K., Foden J., Hore S. & Baines G. 2013. Geochronology and Hf isotopes of the bimodal mafic–felsic high heat producing igneous suite from Mt Painter Province, South Australia, *Gondwana Research,* **24**, no. 3, 1067-1079.

Ludwig K. & Cooper J. 1984. Geochronology of Precambrian granites and associated U-Ti-Th mineralization, northern Olary province, South Australia, *Contributions to Mineralogy and Petrology,* **86**, no. 3, 298-308.

Ludwig K. R. 2003 User's manual for Isoplot 3.00: a geochronological toolkit for Microsoft Excel. Kenneth R. Ludwig.

Mark G., Oliver N. H. & Williams P. J. 2006. Mineralogical and chemical evolution of the Ernest Henry Fe oxide–Cu–Au ore system, Cloncurry district, northwest Queensland, Australia, *Mineralium Deposita,* **40**, no. 8, 769-801.

McFarlane C. 2006. Palaeoproterozoic evolution of the Challenger Au deposit, South Australia, from monazite geochronology, *Journal of Metamorphic Geology,* **24**, no. 1, 75-87.

Monteiro L. V., Xavier R. P., de Carvalho E. R., Hitzman M. W., Johnson C. A., de Souza Filho C. R. & Torresi I. 2008. Spatial and temporal zoning of hydrothermal alteration and mineralization in the Sossego iron oxide–copper–gold deposit, Carajás Mineral Province, Brazil: paragenesis and stable isotope constraints, *Mineralium Deposita,* **43**, no. 2, 129-159.

Page R., Stevens B. & Gibson G. 2005. Geochronology of the sequence hosting the broken hill Pb-Zn-Ag orebody, Australia, *Economic Geology,* **100**, no. 4, 633-661.

Parker A. 1980. The Kalinjala Mylonite Zone, eastern Eyre Peninsula, *Geological Survey of South Australia Quarterly Geological Notes,* **76**, 6-11.

Payne J. L., Barovich K. M. & Hand M. 2006. Provenance of metasedimentary rocks in the northern Gawler Craton, Australia: implications for Palaeoproterozoic reconstructions, *Precambrian Research,* **148**, no. 3, 275-291.

Payne J. L. 2008 Palaeo-to Mesoproterozoic Evolution of the Gawler Craton, Australia: geochronological, geochemical and isotopic constraints. School of Earth and Environmental Sciences The University of Adelaide This thesis is submitted in fulfilment of the requirements for the degree of Doctor of Philosophy in the Faculty of Science, University of Adelaide.

Payne J. L., Hand M., Barovich K. M. & Wade B. P. 2008. Temporal constraints on the timing of high-grade metamorphism in the northern Gawler Craton: implications for assembly of the Australian Proterozoic, *Australian Journal of Earth Sciences,* **55**, no. 5, 623-640.

Payne J. L., Hand M., Barovich K. M., Reid A. & Evans D. A. D. 2009 Correlations and reconstruction models for the 2500-1500 Ma evolution of the Mawson Continent. pp. 319-355.

Payne J. L., Ferris G., Barovich K. M. & Hand M. 2010. Pitfalls of classifying ancient magmatic suites with tectonic discrimination diagrams: An example from the Paleoproterozoic Tunkillia Suite, southern Australia, *Precambrian Research,* **177**, no. 3, 227-240.

Payne J. L., Pearson N. J., Grant K. J. & Halverson G. P. 2013. Reassessment of relative oxide formation rates and molecular interferences on in situ lutetium–hafnium analysis with laser ablation MC-ICP-MS, *Journal of Analytical Atomic Spectrometry,* **28**, no. 7, 1068-1079.

Porter T. M. 2000. Hydrothermal Iron Oxide Copper-Gold and Related Deposits: A Global Prospective, *PGC Publishing, Adelaide,* **1**, p.350.

--- 2002. Hydrothermal Iron Oxide Copper-Gold and Related Deposits: A Global Prespective, *PGC Publishing, Adelaide,* **2**, p.378.

--- 2010a Current Understanding of Iron Oxide Associated-Alkali Altered Mineralised Systems: Part I - An Overview. *In* PORTER T. M. ed. *Hydrothermal Iron Oxide Copper-Gold & Related Deposits: A*

Global Perspective, v. 3 - Advances in the Understanding of IOCG Deposits, pp. 5-32. PGC Publishing,

--- 2010b Current Understanding of Iron Oxide Associated-Alkali Altered Mineralised Systems: Part II - A Review. *In* PORTER T. M. ed. *Hydrothermal Iron Oxide Copper-Gold and Related Deposits: A Global Perspective,* pp. 33-105. PGC Publishing,

REEVE J., CROSS K., SMITH R. & ORESKES N. 1990. Olympic Dam copper-uranium-gold-silver deposit, *Geology of the mineral deposits of Australia and Papua New Guinea,* **2**, 1009-1035.

ROBERTSON R. S., PREISS W. V., CROOKS A. F., HILL P. W. & SHEARD M. J. 1998. Review of the Proterozoic geology and mineral potential of the Curnamona Province in South Australia, *AGSO Journal of Australian Geology and Geophysics,* **17**, no. 3, 169-182.

RUTHERFORD L., HAND M. & BAROVICH K. 2007. Timing of Proterozoic metamorphism in the southern Curnamona Province: implications for tectonic models and continental reconstructions∗, *Australian Journal of Earth Sciences,* **54**, no. 1, 65-81.

SCHAEFER B. F. 1999 Insights into Proterozoic tectonics from the southern Eyre Peninsula, South Australia. Department of Geologi/and Geophysics The University of Adelaide South Australia August 1998 Thesis submitted in fulfilment of requirements for the degree of Doctor of Philosophy in the Faculty of Science, University of Adelaide.

SEGAL I., HALICZ L. & PLATZNER I. T. 2003. Accurate isotope ratio measurements of ytterbium by multiple collection inductively coupled plasma mass spectrometry applying erbium and hafnium in an improved double external normalization procedure, *Journal of Analytical Atomic Spectrometry,* **18**, no. 10, 1217-1223.

SKIRROW R., BASTRAKOV E., DAVIDSON G., RAYMOND O. & HEITHERSAY P. 2002. The geological framework, distribution and controls of Fe-oxide Cu-Au mineralisation in the Gawler Craton, South Australia. Part II-alteration and mineralisation.

SKIRROW R. G., BASTRAKOV E. N., BAROVICH K., FRASER G. L., CREASER R. A., FANNING C. M., RAYMOND O. L. & DAVIDSON G. J. 2007. Timing of iron oxide Cu-Au-(U) hydrothermal activity and Nd isotope constraints on metal sources in the Gawler craton, South Australia, *Economic Geology,* **102**, no. 8, 1441-1470.

SLÁMA J., KOŠLER J., CONDON D. J., CROWLEY J. L., GERDES A., HANCHAR J. M., HORSTWOOD M. S., MORRIS G. A., NASDALA L. & NORBERG N. 2008. Plešovice zircon—a new natural reference material for U–Pb and Hf isotopic microanalysis, *Chemical Geology,* **249**, no. 1, 1-35.

STEWART K. 1994 High temperature felsic volcanism and the role of mantle magmas in Proterozoic crustal growth: the Gawler Range Volcanic Province. University of Adelaide, Department of Geology and Geophysics.

STEWART K. & FODEN J. 2003. Mesoproterozoic granites of South Australia: South Australian Department of Primary Industries and Resources, *Report Book,* **15**.

SWAIN G., WOODHOUSE A., HAND M., BAROVICH K., SCHWARZ M. & FANNING C. 2005. Provenance and tectonic development of the late Archaean Gawler Craton, Australia; U–Pb zircon, geochemical and Sm–Nd isotopic implications, *Precambrian Research,* **141**, no. 3, 106-136.

SWAIN G., BAROVICH K., HAND M., FERRIS G. & SCHWARZ M. 2008. Petrogenesis of the St Peter Suite, southern Australia: arc magmatism and Proterozoic crustal growth of the South Australian Craton, *Precambrian Research,* **166**, no. 1, 283-296.

TEASDALE J. 1997. Methods for understanding poorly exposed terranes: the interpretive geology and tectonothermal evolution of the western Gawler Craton.

TURNER S., FODEN J., SANDIFORD M. & BRUCE D. 1993. Sm-Nd isotopic evidence for the provenance of sediments from the Adelaide Fold Belt and southeastern Australia with implications for episodic crustal addition, *Geochimica et Cosmochimica Acta,* **57**, no. 8, 1837-1856.

VASSALLO J. & WILSON C. 2002. Palaeoproterozoic regional-scale non-coaxial deformation: an example from eastern Eyre Peninsula, South Australia, *Journal of Structural Geology,* **24**, no. 1, 1-24.

VERVOORT J. D., PATCHETT P. J., SÖDERLUND U. & BAKER M. 2004. Isotopic composition of Yb and the determination of Lu concentrations and Lu/Hf ratios by isotope dilution using MC-ICPMS, *Geochemistry, Geophysics, Geosystems,* **5**, no. 11.

WADE C. 2011. Definition of the Mesoproterozoic Ninnerie Supersuite, Curnamona Province, South Australia, *MESA Journal,* **62**, 35-52.

WADE C. E., REID A. J., WINGATE M. T. D., JAGODZINSKI E. A. & BAROVICH K. 2012. Geochemistry and geochronology of the c. 1585Ma Benagerie Volcanic Suite, southern Australia: Relationship to the Gawler Range Volcanics and implications for the petrogenesis of a Mesoproterozoic silicic large igneous province, *Precambrian Research,* **206-207**, 17-35.

WILLIAMS P. J. & SKIRROW R. G. 2000 Overview of iron oxide copper-gold deposits in the Curnamona Province and Cloncurry district (Eastern Mount Isa Block), Australia. *In* PORTER T. M. ed. *Hydrothermal iron oxide copper-gold and related deposits: a global perspective,* pp. 105-122. PGC Publishing,

WILLIAMS P. J., KENDRICK M. A. & XAVIER R. P. 2010 Sources of Ore Fluid Components in IOCG Deposits. *In* PORTER T. M. ed. *Hydrothermal Iron Oxide Copper-Gold and Related Deposits: A Global Perspective,* pp. 107-116. PGC Publishing,

WOODHEAD J., HERGT J., SHELLEY M., EGGINS S. & KEMP R. 2004. Zircon Hf-isotope analysis with an excimer laser, depth profiling, ablation of complex geometries, and concomitant age estimation, *Chemical Geology,* **209**, no. 1, 121-135.

WOODHEAD J. D. & HERGT J. M. 2005. A preliminary appraisal of seven natural zircon reference materials for in situ Hf isotope determination, *Geostandards and Geoanalytical Research,* **29**, no. 2, 183-195.

ZANG W., FANNING C., PURVIS A., RAYMOND O. & BOTH R. 2007. Early Mesoproterozoic bimodal plutonism in the southeastern Gawler Craton, South Australia, *Australian Journal of Earth Sciences,* **54**, no. 5, 661-674.

APPENDIX A: SAMPLE INFORMATION AND LOCATIONS

			Location (GDA94)					
Sample	Drill hole	Depth (m)	Easting	Northing	Zone	Region	Unit	Lithology
1998158			660498	6397578	53	central Gawler	Gawler Range Volcanics	Eucaroo Rhyolite
1998160			603745	6413019	53	central Gawler	Gawler Range Volcanics	Moonaree Dacite
SB12_09			494944	6577359	53	central Gawler	Hiltaba Suite	Rhyolite
SB12_03			545504	6416800	53	central Gawler	Gawler Range Volcanics	Granite
1998166			514905	6739483	53	central Gawler	Hiltaba Suite	Granite
1948991	MRC007A	157.0 - 158.0	722881	6323202	53	eastern Gawler	Hiltaba Suite	Granite
2065518	RED_1	392.1 - 393.1	725465	6612213	53	eastern Gawler	Gawler Range Volcanics	Rhyolite
2065519	BLD_2	841.4 - 842.2	717393	6633329	53	eastern Gawler	Hiltaba Suite	Granite
2049213	BRD013	466.0 - 484.0	437447	6613969	54	Benagerie Ridge	Benagerie Volcanic Suite	Rhyolite
2049215	CU_1	435.6 - 439.0	444350	6601733	54	Benagerie Ridge	Ninnerie Supersuite	Microgranite
14-CW-02			386964	6456985	54	Olary	Crocker Well Suite	Granite
14-CW-03			387151	6459583	54	Olary	Crocker Well Suite	Granite
14-CW-04			387151	6459583	54	Olary	Crocker Well Suite	Granite
1834090*			355853	6548258	53	western Gawler	Hiltaba Suite	Granodiorite
1834091*			355853	6548258	53	western Gawler	Hiltaba Suite	Syenogranite
1834092*			345002	6527350	53	western Gawler	Hiltaba Suite	Granodiorite
1834093*			345002	6527350	53	western Gawler	Hiltaba Suite	Monzogranite
1834106*			351020	6483143	53	western Gawler	Hiltaba Suite	Monzogranite
1834114*			344298	6559007	53	western Gawler	Hiltaba Suite	Monzogranite
1709491*			377626	6656952	54	Benagerie Ridge	Benagerie Volcanic Suite	
1709493*			377626	6656952	54	Benagerie Ridge	Benagerie Volcanic Suite	

* analysed by Dr. Anthony Reid (unpublished)

APPENDIX B: EXTENDED METHODS

Sample Collection

Samples from the Crocker Well area (Samples 14-CW-01 to 05) were collected from insitu outcrops, where a GPS coordinate was taken using a hand held Garmin eTrex device and a brief rock description noted. Weathered material was removed from the exterior of the sample using a sledge hammer. The fresh rock was allocated a sample number, labeled and bagged for transport.
Diamond drill core collected from the DMITRE Core Library, Adelaide (BRD013, RED 1, WRD 2, LMN10 1, Cu-1, BLD 2) were viewed and the least altered and deformed target rock was designated for partial ($^{1}/_{4}$ or $^{1}/_{3}$ core) sampling. Samples were assigned a DMITRE sample number before being bagged.

Sample Preparation

Samples were trimmed of weathered surfaces and any veins, and cut into smaller fragments using a rock saw, washed and then dried at low temperature (<100°C) on a hot plate. Clean, fresh fragments of whole-rock samples were crushed to centimeter-sized fragments using a customized mechanical jaw crusher, after which a mechanized disc mill was used to gradually crush the rock into a finer gravel, both are disassembled and thoroughly cleaned with compressed air and ethanol prior to the processing of each sample. A 100g representative portion is bagged for geochemistry before the sample is sieved using 79 μm and 400 μm screens. Large fraction (>400um) material remaining after sieving is returned to the disc mill and the process is repeated until minimal >400 um fraction remains.
The 79 to 400 um fraction is panned using conventional prospecting pans, whereby the less dense material is progressively removed from a primary small pan and collected in a large pan below. Once there is only a small (<teaspoon) quantity of dense material remaining in the primary small pan, the dense concentrate is passed through a fine filter paper and dried on a low temperature (<100°C) hot plate. Once dry, magnets are used to remove the magnetic minerals from the concentrate, zircon grains are then hand picked using an optical microscope. Zircons are arranged on double sided tape adhered to a glass slide, while sample positions on the tape are noted. A …mm circular cast is placed around the zircons and an epoxy resin is gently poured within the cast to encase the zircons and left on a flat surface to set. Tape is removed from the glass base and the epoxy mount before a series of wet sandpaper (800 to 2200 grit) is used to expose the zircon and reduce them to roughly half their original thickness. A wet closh polishing disc and diamond polishing paste is used to buff the zircon face to a shine.

Imaging

Polished mounts were carbon coated at Adelaide Microscopy, University of Adelaide. Images of the grains were captured at Adelaide Microscopy using Back Scatter Electron (BSE) and Cathode Luminescence (CL) imaging on a Phillips XL-40 Scanning Electron Microscope (SEM) fitted with a Gatan CL detector. BSE imaging used a 20 kV beam of spot size 5 and a working distance of 15 mm. CL imaging used a 12 kV beam of spot size 6 and a working distance of 15 mm. The images were manipulated with contrast and brightness controls to highlight zonation within the grains before being compiled using Inkscape into a map.

Zircon U-Pb Geochronology

U-Pb isotopic analysis done at Adelaide Microscopy used a New Wave 213nm Nd-YAG laser in a He ablation atmosphere, coupled to an Agilent 7500cs ICP-MS. Standard GJ-1 and inhouse standards Temora 2, 91500 and OG-1 were analysed before 15 sample analyses took place followed by analyses of standards GJ-1 and Temora 2. The Order of this was: 3x GJ-1, 2x 91500, 2x OG-1, 2x Temora 3, 2x GJ-1, 15 samples, 2x GJ-1 and 2x Temora 2. A 40 s gas blank was followed by an 80 s ablation analysis. Prior to each ablation the laser was fired for 10 s with the shutter closed to allow beam stabilisation. The beam diameter at the sample surface was 30 um or 40 um.

U-Pb isotopic analysis done at Macquarie University

Isotopes measured were ^{204}Pb, ^{206}Pb, ^{207}Pb, ^{208}Pb, ^{232}Th and ^{238}U with 10, 15, 30, 10, 10 and 15 ms dwell times respectively. ^{235}U was calculated using a ^{238}U/^{235}U ratio of 137.88. ^{204}Pb was monitored to assess potential influence on sample analysis but was not used for a common-Pb correction due to an interference of ^{204}Hg on this mass (Payne *et al.* 2006, Payne *et al.* 2008, Payne *et al.* 2010).

Zircon age calculations were made using Glitter software (vers. 4.0). Glitter is a real-time correction program developed at Macquarie University (Jackson *et al.* 2004). U-Pb fractionation was corrected using the zircon standard GJ-1 (normalisation data: ^{207}Pb /^{206}Pb = 608.3 Ma, ^{206}Pb /^{238}U = 600.7Ma and ^{207}Pb /^{235}U = 602.2 Ma, Jackson et al., 2004). Age data accuracy was confirmed by analysis and comparison of in house standards Temora 2 (~416 Ma), OG-1 (~3465 Ma) and 91500 (~1062 Ma).

Reduced monazite and zircon data was then exported into excel where subsequent conventional concordia and weighted average plots were generated using Isoplot v4.11 (Ludwig, 2003). Ages quoted throughout the study are ^{207}Pb/^{206}Pb ages as the data contains ages older than *c.* 1000 Ma and all errors stated in data tables and along side concordia diagrams are at the 1σ level. Concordancy was calculated using the ratio of ^{206}Pb/^{238}U /^{207}Pb/^{206}Pb.

Hafnium Isotope Analyses

Hafnium isotope analyses were carried out using a New Wave UP-193 Excimer laser (193 nm), attached to a Thermo-Scientific Neptune multicollector ICP-MS. Only zircon grains with less than 5% discordancy were targeted for Hf isotope analysis. Hf analyses were placed adjacent to the U-Pb spots in zircons that were large enough to allow the analysis of the same CL-textural domain within a single zircon grain. However, due to the grain size limitations imposed by some zircons, and in order to maintain the compatibility between the U-Pb ages and Hf analyses, for these zircons the laser beam was focused over the U-Pb spots with a beam diameter of 50 μm, 5 Hz repetition rate, 4 ns pulse length, and laser energy of 8–10 J/cm2. Zircons were ablated in a helium atmosphere that was mixed with argon and nitrogen (to enhance sensitivity and minimize oxide formation) upstream of the ablation cell. Typical ablation times were between 30 and 100 s. A detailed description of the mass bias corrections and rare earth element (REE) oxide molecular interference corrections for the analytical method is given in Payne et al. (2013). Initial 176Hf/177Hf ratio at the age of the zircon spot was calculated using the decay constant of 1.867 * 10–11 y–1 (Söderlund et al., 2004). Calculated depleted-mantle model ages (TDM) based on the measured 176Lu/177Hf ratios represent minimum crustal residence ages and are therefore typically more reliable for less-evolved analyses. For this reason, a two-stage model age was calculated using the measured 176Lu/177Hf value of each spot at the age of the zircon (TDM, first stage), a 176Lu/177Hf of 0.015 (Griffin et al., 2002) for the average continental crust (T C , DM second stage), and depleted-mantle 176Lu/177Hf and 176Hf/177Hf values of 0.0384 and 0.283251 (Nowell et al., 1998). The second-stage model age (T C) is used in the discussion. Epsilon Hf (εHf) values were calculated with reference to the chondrite reservoir (CHUR) assuming present-day chondritic 176Hf/177Hf and 176Lu/177Hf values of 0.282785 ± 0.000011 and 0.0336 ± 0.0001 respectively (Bouvier et al., 2008).

A combination of the Plešovice and Mudtank zircon standards were used to monitor the accuracy of the technique during the analysis.

APPENDIX C: U-PB GEOCHRONOLOGY DATA

Analysis No.	$^{207}Pb/^{206}Pb$ ratio	1σ	$^{207}Pb/^{235}U$ ratio	1σ	$^{206}Pb/^{238}U$ ratio	1σ	$^{207}Pb/^{235}U$ Age (Ma)	1σ	$^{206}Pb/^{238}U$ Age (Ma)	1σ (Ma)	$^{207}Pb/^{206}Pb$ Age (Ma)	1σ (Ma)	% Conc.
1998158_01	0.09872	0.00174	0.22289	0.00277	3.0338	0.0527	1416.2	13.3	1297.1	14.6	1600.1	32.6	81.1
1998158_02	0.09859	0.00133	0.27146	0.00308	3.6901	0.0507	1569.2	11.0	1548.2	15.6	1597.6	24.9	96.9
1998158_03	0.09821	0.00132	0.29695	0.00337	4.0213	0.0554	1638.5	11.2	1676.2	16.8	1590.5	25.0	105.4
1998158_04	0.09864	0.00136	0.26484	0.00303	3.6020	0.0507	1550.0	11.2	1514.6	15.4	1598.5	25.6	94.8
1998158_05	0.09668	0.00175	0.21541	0.00270	2.8717	0.0511	1374.5	13.4	1257.6	14.3	1561.1	33.5	80.6
1998158_06	0.09907	0.00138	0.24457	0.00280	3.3409	0.0473	1490.7	11.1	1410.4	14.5	1606.7	25.7	87.8
1998158_07	0.09762	0.00145	0.22483	0.00263	3.0263	0.0454	1414.3	11.5	1307.3	13.8	1579.1	27.6	82.8
1998158_08	0.09967	0.00152	0.21942	0.00258	3.0155	0.0462	1411.6	11.7	1278.8	13.7	1618.0	28.1	79.0
1998158_09	0.09827	0.00140	0.24641	0.00284	3.3389	0.0484	1490.2	11.3	1419.9	14.7	1591.6	26.4	89.2
1998158_10	0.09841	0.00142	0.25423	0.00294	3.4498	0.0507	1515.8	11.6	1460.3	15.1	1594.2	26.8	91.6
1998158_11	0.09719	0.00143	0.24985	0.00290	3.3485	0.0501	1492.4	11.7	1437.7	15.0	1570.9	27.3	91.5
1998158_12	0.09888	0.00147	0.24229	0.00282	3.3036	0.0498	1481.9	11.8	1398.6	14.7	1603.2	27.5	87.2
1998158_13	0.09679	0.00149	0.25407	0.00299	3.3909	0.0528	1502.3	12.2	1459.4	15.4	1563.2	28.6	93.4
1998158_14	0.09822	0.00154	0.26002	0.00308	3.5214	0.0558	1532.0	12.5	1490.0	15.8	1590.5	29.0	93.7
1998158_15	0.10166	0.00155	0.20917	0.00245	2.9320	0.0455	1390.2	11.7	1224.4	13.1	1654.7	28.0	74.0
1998158_16	0.10641	0.00169	0.22982	0.00273	3.3721	0.0541	1497.9	12.6	1333.6	14.3	1738.9	28.7	76.7
1998158_17	0.09748	0.00165	0.24854	0.00302	3.3404	0.0568	1490.5	13.3	1430.9	15.6	1576.4	31.4	90.8
1998158_18	0.09793	0.00162	0.27259	0.00329	3.6807	0.0616	1567.2	13.4	1553.9	16.7	1585.1	30.7	98.0
1998158_19	0.09701	0.00158	0.26822	0.00321	3.5876	0.0592	1546.8	13.1	1531.8	16.3	1567.4	30.3	97.7
1998158_20	0.09943	0.00164	0.22900	0.00275	3.1396	0.0523	1442.4	12.8	1329.3	14.4	1613.5	30.4	82.4
1998160_01	0.09870	0.00143	3.68607	0.05537	0.2709	0.0033	1568.4	12.0	1545.2	16.6	1599.8	26.8	96.6
1998160_02	0.09854	0.00152	3.23614	0.05130	0.2382	0.0029	1465.9	12.3	1377.4	15.2	1596.6	28.6	86.3
1998160_03	0.09970	0.00140	3.93767	0.05754	0.2865	0.0034	1621.5	11.8	1623.9	17.1	1618.5	25.8	100.3
1998160_04	0.09872	0.00147	3.80591	0.05837	0.2796	0.0034	1594.0	12.3	1589.5	17.0	1600.1	27.5	99.3
1998160_05	0.09934	0.00168	2.95042	0.05029	0.2154	0.0027	1395.0	12.9	1257.7	14.4	1611.7	31.2	78.0
1998160_06	0.09891	0.00146	3.69640	0.05619	0.2711	0.0033	1570.6	12.2	1546.2	16.5	1603.7	27.2	96.4
1998160_07	0.09741	0.00150	3.66891	0.05786	0.2732	0.0033	1564.6	12.6	1557.1	16.8	1575.0	28.5	98.9
1998160_08	0.09890	0.00155	3.64167	0.05834	0.2671	0.0033	1558.7	12.8	1525.9	16.6	1603.5	29.0	95.2
1998160_09	0.09901	0.00178	2.72088	0.04884	0.1993	0.0025	1334.2	13.3	1171.7	13.7	1605.6	33.1	73.0
1998160_10	0.09954	0.00170	3.60397	0.06203	0.2626	0.0033	1550.4	13.7	1503.2	16.8	1615.6	31.5	93.0
1998160_11	0.09852	0.00156	3.58079	0.05786	0.2636	0.0032	1545.3	12.8	1508.4	16.4	1596.3	29.3	94.5
1998160_12	0.09905	0.00168	3.68365	0.06284	0.2698	0.0034	1567.8	13.6	1539.5	17.0	1606.3	31.2	95.8
1998160_13	0.09807	0.00165	3.59941	0.06094	0.2662	0.0033	1549.4	13.5	1521.6	16.7	1587.7	31.0	95.8
1998160_14	0.09885	0.00163	3.76999	0.06286	0.2766	0.0034	1586.4	13.4	1574.4	17.1	1602.5	30.4	98.2

Analysis No.	$^{207}Pb/^{206}Pb$ ratio	1σ	$^{207}Pb/^{235}U$ ratio	1σ	$^{206}Pb/^{238}U$ ratio	1σ	$^{207}Pb/^{235}U$ Age (Ma)	1σ	$^{206}Pb/^{238}U$ Age (Ma)	1σ (Ma)	$^{207}Pb/^{206}Pb$ Age (Ma)	1σ (Ma)	% Conc.
1998160_15	0.09906	0.00168	3.5938	0.0614	0.26315	0.00324	1548.2	13.6	1606.5	31.3	1505.9	16.6	93.7
1998160_16	0.09849	0.00166	3.3932	0.0576	0.24990	0.00306	1502.8	13.3	1595.7	31.1	1437.9	15.8	90.1
1998160_17	0.10147	0.00197	2.7191	0.0522	0.19437	0.00252	1333.7	14.3	1651.1	35.6	1145.0	13.6	69.3
1998160_18	0.09848	0.00176	3.1359	0.0558	0.23097	0.00288	1441.5	13.7	1595.5	32.9	1339.6	15.1	84.0
1998160_19	0.09854	0.00180	3.4359	0.0626	0.25290	0.00318	1512.7	14.3	1596.7	33.8	1453.4	16.3	91.0
1998160_20	0.09731	0.00184	3.3850	0.0636	0.25232	0.00320	1500.9	14.7	1573.1	35.1	1450.5	16.5	92.2
1998160_21	0.09835	0.00157	3.9172	0.0746	0.28904	0.00457	1617.2	15.4	1593.1	29.5	1636.7	22.9	102.7
1998160_22	0.10871	0.00286	3.0093	0.0820	0.20095	0.00345	1410.0	20.8	1777.8	47.3	1180.4	18.5	66.4
1998160_23	0.09674	0.00160	3.7223	0.0726	0.27921	0.00443	1576.2	15.6	1562.3	30.7	1587.4	22.3	101.6
1998160_24	0.10261	0.00186	3.3422	0.0695	0.23640	0.00382	1491.0	16.3	1671.8	33.2	1368.0	19.9	81.8
1998160_25	0.10113	0.00184	4.0274	0.0839	0.28900	0.00466	1639.7	17.0	1644.9	33.4	1636.6	23.3	99.5
1998160_26	0.09781	0.00181	3.7253	0.0787	0.27638	0.00448	1576.8	16.9	1582.9	34.2	1573.1	22.6	99.4
1998160_27	0.11275	0.00216	4.7067	0.1020	0.30295	0.00492	1768.4	18.2	1844.2	34.2	1705.9	24.4	92.5
1998160_28	0.09821	0.00197	3.8640	0.0865	0.28552	0.00467	1606.2	18.1	1590.5	36.9	1619.1	23.4	101.8
1998160_29	0.09941	0.00212	3.8706	0.0907	0.28260	0.00469	1607.6	18.9	1613.1	39.1	1604.4	23.6	99.5
1998160_30	0.09734	0.00204	3.9528	0.0920	0.29467	0.00488	1624.6	18.9	1573.7	38.7	1664.8	24.3	105.8
1998160_32	0.09726	0.00217	3.7685	0.0923	0.28117	0.00471	1586.1	19.7	1572.1	41.2	1597.2	23.7	101.6
1998160_33	0.09732	0.00223	3.7731	0.0943	0.28133	0.00473	1587.0	20.1	1573.3	42.2	1598.1	23.8	101.6
1998160_34	0.09799	0.00231	3.7985	0.0975	0.28129	0.00476	1592.4	20.6	1586.3	43.5	1597.9	23.9	100.7
SB12_09_02	0.09852	0.00133	2.8025	0.0422	0.20631	0.00268	1356.2	11.3	1209.1	14.3	1596.2	25.0	75.7
SB12_09_03	0.09733	0.00133	4.0844	0.0623	0.30435	0.00397	1651.2	12.4	1712.8	19.6	1573.6	25.4	108.8
SB12_09_04	0.09860	0.00130	3.4154	0.0509	0.25121	0.00325	1507.9	11.7	1444.7	16.8	1597.9	24.5	90.4
SB12_09_07	0.09911	0.00128	3.4650	0.0508	0.25356	0.00327	1519.3	11.6	1456.8	16.8	1607.4	23.8	90.6
SB12_09_08	0.09745	0.00168	3.4094	0.0620	0.25373	0.00352	1506.6	14.3	1457.7	18.1	1575.9	32.0	92.5
SB12_09_10	0.09597	0.00128	3.5994	0.0542	0.27201	0.00353	1549.4	12.0	1551.0	17.9	1547.1	24.8	100.3
SB12_09_11	0.09896	0.00166	3.8537	0.0687	0.28242	0.00388	1604.0	14.4	1603.5	19.5	1604.7	31.0	99.9
SB12_09_13	0.17211	0.00238	11.9481	0.1855	0.50348	0.00659	2600.3	14.6	2628.7	28.3	2578.3	22.9	102.0
SB12_09_14	0.09761	0.00145	3.6919	0.0603	0.27430	0.00365	1569.6	13.1	1562.6	18.5	1579.0	27.5	99.0
SB12_09_16	0.09917	0.00165	3.8053	0.0679	0.27829	0.00382	1593.9	14.3	1582.8	19.3	1608.6	30.8	98.4
SB12_09_17	0.09837	0.00143	3.6486	0.0591	0.26901	0.00356	1560.2	12.9	1535.8	18.1	1593.4	27.0	96.4
SB12_09_19	0.10656	0.00161	5.3743	0.0893	0.36580	0.00488	1880.8	14.2	2009.6	23.0	1741.4	27.2	115.4
SB12_09_20	0.09922	0.00190	2.4868	0.0495	0.18177	0.00259	1268.2	14.4	1076.6	14.2	1609.6	35.3	66.9
SB12_09_22	0.08816	0.00199	2.6648	0.0567	0.21903	0.00215	1318.8	15.7	1276.7	11.4	1386.0	42.6	92.1
SB12_09_23	0.17864	0.00272	9.4726	0.1368	0.38466	0.00302	2384.9	13.3	2098.0	14.1	2640.3	25.1	79.5

Analysis No.	$^{207}Pb/^{206}Pb$ ratio	1σ	$^{207}Pb/^{235}U$ ratio	1σ	$^{206}Pb/^{238}U$ ratio	1σ	$^{207}Pb/^{235}U$ Age (Ma)	1σ	$^{206}Pb/^{238}U$ Age (Ma)	1σ (Ma)	$^{207}Pb/^{206}Pb$ Age (Ma)	1σ (Ma)	% Conc.
SB12_09_24	0.09367	0.00176	3.20162	0.05730	0.24804	0.00211	1457.6	13.9	1428.4	10.9	1501.4	35.1	95.1
SB12_09_25	0.10127	0.00166	3.68986	0.05734	0.26423	0.00203	1569.2	12.4	1511.4	10.3	1647.5	30.1	91.7
SB12_09_26	0.08883	0.00205	2.90598	0.06361	0.23731	0.00242	1383.5	16.5	1372.7	12.6	1400.5	43.5	98.0
SB12_09_28	0.10056	0.00181	2.78252	0.04743	0.20077	0.00170	1350.9	12.7	1179.5	9.1	1634.5	33.1	72.2
SB12_09_29	0.10158	0.00261	2.45884	0.05946	0.17567	0.00186	1260.0	17.5	1043.3	10.2	1653.2	46.9	63.1
SB12_09_32	0.09378	0.00237	2.98987	0.07152	0.23131	0.00251	1405.0	18.2	1341.4	13.1	1503.8	46.9	89.2
SB12_09_33	0.09968	0.00272	4.22594	0.10933	0.30762	0.00369	1679.1	21.2	1729.0	18.2	1618.0	50.0	106.9
SB12_09_34	0.08829	0.00223	3.22420	0.07718	0.26498	0.00285	1463.0	18.6	1515.3	14.5	1388.9	47.6	109.1
1998166_01	0.09798	0.00127	3.06315	0.03823	0.22672	0.00155	1423.5	9.6	1317.3	8.1	1585.9	24.1	83.1
1998166_02	0.09913	0.00184	3.56798	0.06312	0.26105	0.00231	1542.4	14.0	1495.2	11.8	1607.7	34.2	93.0
1998166_03	0.09329	0.00241	3.28628	0.08131	0.25553	0.00281	1477.8	19.3	1467.0	14.5	1493.9	48.2	98.2
1998166_05	0.09801	0.00127	3.68679	0.04587	0.27283	0.00190	1568.5	9.9	1555.1	9.6	1586.6	24.1	98.0
1998166_06	0.09971	0.00235	3.90231	0.08785	0.28387	0.00299	1614.2	18.2	1610.8	15.0	1618.7	43.3	99.5
1998166_07	0.09890	0.00153	3.73924	0.05518	0.27423	0.00209	1579.8	11.8	1562.2	10.6	1603.5	28.6	97.4
1998166_08	0.09748	0.00131	3.61827	0.04669	0.26919	0.00190	1553.6	10.3	1536.7	9.6	1576.5	25.0	97.5
1998166_09	0.10058	0.00247	3.67934	0.08601	0.26533	0.00279	1566.9	18.7	1517.1	14.2	1634.9	44.9	92.8
1998166_10	0.09835	0.00134	3.64631	0.04770	0.26888	0.00187	1559.7	10.4	1535.1	9.5	1593.0	25.2	96.4
1998166_11	0.09817	0.00198	3.69267	0.07102	0.27278	0.00249	1569.8	15.4	1554.9	12.6	1589.7	37.2	97.8
1998166_12	0.09592	0.00161	3.60151	0.05803	0.27231	0.00219	1549.9	12.8	1552.5	11.1	1546.2	31.3	100.4
1998166_13	0.10092	0.00245	3.65233	0.08440	0.26244	0.00265	1561.0	18.4	1502.3	13.6	1641.1	44.5	91.5
1998166_15	0.09846	0.00247	3.70958	0.08888	0.27328	0.00289	1573.4	19.2	1557.5	14.6	1595.1	46.1	97.6
1998166_16	0.10492	0.00205	3.30917	0.06261	0.22867	0.00213	1483.2	14.8	1327.5	11.2	1712.9	35.6	77.5
1998166_17	0.09502	0.00219	3.82963	0.08486	0.29222	0.00310	1599.0	17.8	1652.6	15.5	1528.4	42.8	108.1
1998166_18	0.09830	0.00119	3.76644	0.04410	0.27790	0.00187	1585.6	9.4	1580.8	9.4	1592.2	22.5	99.3
1998166_19	0.09856	0.00147	3.81204	0.05483	0.28054	0.00213	1595.3	11.6	1594.1	10.7	1597.1	27.5	99.8
1998166_20	0.10100	0.00229	3.82816	0.08394	0.27476	0.00288	1598.7	17.7	1564.9	14.6	1642.7	41.5	95.3
1998166_21	0.09671	0.00233	3.93304	0.09167	0.29482	0.00325	1620.5	18.9	1665.6	16.2	1561.7	44.6	106.7
1998166_22	0.09689	0.00179	3.73530	0.06712	0.27967	0.00247	1579.0	14.4	1589.7	12.5	1565.0	34.3	101.6
1998166_23	0.09961	0.00175	3.79114	0.06490	0.27607	0.00231	1590.9	13.8	1571.6	11.7	1616.8	32.3	97.2
1998166_24	0.09598	0.00225	3.77922	0.08693	0.28555	0.00294	1588.3	18.5	1619.3	14.7	1547.3	43.5	104.7
1998166_25	0.09751	0.00154	3.60023	0.05526	0.26781	0.00201	1549.6	12.2	1529.7	10.2	1577.0	29.3	97.0
1998166_26	0.09839	0.00207	3.57739	0.07348	0.26371	0.00248	1544.5	16.3	1508.8	12.6	1593.9	38.8	94.7
1998166_27	0.09510	0.00185	3.24452	0.06240	0.24743	0.00219	1467.9	14.9	1425.2	11.3	1530.0	36.3	93.2
1998166_28	0.09970	0.00226	3.25075	0.07229	0.23644	0.00236	1469.4	17.3	1368.2	12.3	1618.5	41.7	84.5

Analysis No.	$^{207}Pb/^{206}Pb$ ratio	1σ	$^{207}Pb/^{235}U$ ratio	1σ	$^{206}Pb/^{238}U$ ratio	1σ	$^{207}Pb/^{235}U$ Age (Ma)	1σ	$^{206}Pb/^{238}U$ Age (Ma)	1σ (Ma)	$^{207}Pb/^{206}Pb$ Age (Ma)	1σ (Ma)	% Conc.
1998166_29	0.09844	0.00146	3.68939	0.05331	0.27183	0.00200	1569.1	11.5	1550.1	10.1	1594.8	27.4	97.2
1998166_30	0.09570	0.00283	3.49716	0.10150	0.26494	0.00342	1526.6	22.9	1515.1	17.4	1541.9	54.6	98.3
1948991_01	0.09769	0.00119	3.77633	0.04448	0.28039	0.00193	1587.7	9.5	1593.3	9.7	1580.5	22.7	100.8
1948991_02	0.09760	0.00181	3.02775	0.05365	0.22490	0.00195	1414.6	13.5	1307.7	10.3	1578.9	34.4	82.8
1948991_03	0.10032	0.00213	3.95206	0.07985	0.28569	0.00284	1624.4	16.4	1619.9	14.3	1630.1	39.0	99.4
1948991_04	0.09817	0.00122	3.84137	0.04600	0.28382	0.00195	1601.5	9.7	1610.6	9.8	1589.7	23.1	101.3
1948991_05	0.09866	0.00134	3.70341	0.04828	0.27229	0.00199	1572.1	10.4	1552.4	10.1	1599.0	25.2	97.1
1948991_06	0.10289	0.00167	4.06690	0.06308	0.28658	0.00233	1647.7	12.6	1624.4	11.7	1676.9	29.7	96.9
1998166_08	0.08947	0.00132	2.04123	0.02888	0.16544	0.00121	1129.4	9.6	986.9	6.7	1414.1	28.0	69.8
1998166_09	0.09813	0.00151	3.86284	0.05690	0.28556	0.00221	1606.0	11.9	1619.3	11.1	1589.0	28.5	101.9
1998166_10	0.09854	0.00167	3.74672	0.06016	0.27572	0.00224	1581.4	12.9	1569.8	11.3	1596.7	31.2	98.3
1998166_11	0.09894	0.00200	4.04667	0.07736	0.29655	0.00278	1643.6	15.6	1674.2	13.8	1604.2	37.2	104.4
1998166_12	0.10402	0.00170	3.71682	0.05774	0.25919	0.00204	1575.0	12.4	1485.7	10.4	1697.0	29.9	87.5
1998166_13	0.09838	0.00151	3.82975	0.05605	0.28245	0.00214	1599.0	11.8	1603.7	10.8	1593.7	28.4	100.6
1998166_14	0.09774	0.00122	3.54463	0.04256	0.26312	0.00175	1537.2	9.5	1505.8	9.0	1581.4	23.2	95.2
1998166_15	0.09753	0.00134	3.60361	0.04725	0.26810	0.00191	1550.3	10.4	1531.2	9.7	1577.4	25.4	97.1
1998166_16	0.09925	0.00140	3.80955	0.05119	0.27853	0.00205	1594.8	10.8	1583.9	10.4	1610.1	26.0	98.4
1998166_17	0.09953	0.00204	3.63818	0.07015	0.26547	0.00249	1557.9	15.4	1517.8	12.7	1615.4	37.7	94.0
1998166_18	0.09402	0.00130	2.43716	0.03212	0.18809	0.00130	1253.6	9.5	1111.0	7.0	1508.4	25.8	73.7
1998166_20	0.10023	0.00191	3.57578	0.06413	0.25899	0.00227	1544.2	14.2	1484.7	11.6	1628.3	34.9	91.2
1998166_21	0.09831	0.00219	3.68240	0.07694	0.27222	0.00267	1567.6	16.7	1552.1	13.5	1592.4	41.1	97.5
1998166_22	0.09826	0.00119	2.99613	0.03501	0.22125	0.00146	1406.6	8.9	1288.5	7.7	1591.3	22.6	81.0
1998166_23	0.09597	0.00144	3.62412	0.05173	0.27412	0.00206	1554.8	11.4	1561.7	10.4	1547.1	27.9	100.9
1998166_24	0.10059	0.00167	3.55679	0.05588	0.25675	0.00208	1539.9	12.5	1473.2	10.7	1635.0	30.6	90.1
1998166_25	0.09796	0.00156	3.63873	0.05476	0.26966	0.00207	1558.0	12.0	1539.1	10.5	1585.6	29.5	97.1
1998166_26	0.09825	0.00153	3.57572	0.05257	0.26424	0.00198	1544.2	11.7	1511.5	10.1	1591.1	28.8	95.0
1998166_27	0.09919	0.00216	3.57314	0.07266	0.26173	0.00239	1543.6	16.1	1498.7	12.2	1609.0	40.0	93.1
1998166_28	0.09880	0.00149	3.54343	0.05108	0.26019	0.00197	1537.0	11.4	1490.8	10.1	1601.5	27.9	93.1
2065519_01	0.09728	0.00144	3.12412	0.04598	0.23292	0.00180	1438.6	11.3	1349.8	9.4	1572.6	27.5	85.8
2065519_02	0.09793	0.00210	3.53831	0.07560	0.26196	0.00256	1535.8	16.9	1499.9	13.1	1585.1	39.6	94.6
2065519_03	0.09809	0.00180	3.60176	0.06571	0.26632	0.00234	1549.9	14.5	1522.1	11.9	1588.1	33.9	95.8
2065519_04	0.09891	0.00210	3.33473	0.07061	0.24443	0.00238	1489.2	16.5	1409.7	12.3	1603.8	39.1	87.9
2065519_05	0.09791	0.00137	3.09359	0.04279	0.22917	0.00169	1431.1	10.6	1330.2	8.9	1584.7	25.9	83.9

Analysis No.	$^{207}Pb/^{206}Pb$ ratio	1σ	$^{207}Pb/^{235}U$ ratio	1σ	$^{206}Pb/^{238}U$ ratio	1σ	$^{207}Pb/^{235}U$ Age (Ma)	1σ	$^{206}Pb/^{238}U$ Age (Ma)	1σ (Ma)	$^{207}Pb/^{206}Pb$ Age (Ma)	1σ (Ma)	% Conc.
2065519_06	0.09803	0.00262	3.04026	0.07930	0.22496	0.00252	1417.8	19.9	1308.0	13.3	1587.0	49.2	82.4
2065519_07	0.09890	0.00198	3.93130	0.07812	0.28832	0.00265	1620.1	16.1	1633.1	13.3	1603.4	36.8	101.9
2065519_08	0.09666	0.00140	3.57070	0.05097	0.26793	0.00201	1543.0	11.3	1530.3	10.2	1560.7	26.9	98.1
2065519_09	0.09705	0.00138	3.96012	0.05596	0.29596	0.00220	1626.1	11.5	1671.3	10.9	1568.1	26.5	106.6
2065519_10	0.09739	0.00154	3.92079	0.06098	0.29202	0.00230	1618.0	12.6	1651.6	11.5	1574.8	29.3	104.9
2065519_11	0.09781	0.00255	3.02560	0.07939	0.22421	0.00249	1414.1	20.0	1304.1	13.1	1582.7	48.0	82.4
2065519_12	0.09706	0.00301	2.20124	0.06861	0.16438	0.00208	1181.4	21.8	981.1	11.5	1568.4	57.0	62.6
2065519_13	0.09778	0.00150	3.60215	0.05482	0.26719	0.00206	1550.0	12.1	1526.5	10.5	1582.3	28.5	96.5
2065519_14	0.09604	0.00386	1.96068	0.07973	0.14808	0.00237	1102.1	27.3	890.2	13.3	1548.6	73.7	57.5
2065519_15	0.09782	0.00228	3.97480	0.09324	0.29464	0.00303	1629.1	19.0	1664.7	15.1	1582.9	42.9	105.2
2065518_01	0.09794	0.00162	3.35069	0.05475	0.24813	0.00282	1493.0	12.8	1428.8	14.6	1585.3	30.7	90.1
2065518_02	0.09789	0.00174	3.19109	0.05551	0.23644	0.00277	1455.0	13.5	1368.2	14.4	1584.2	32.8	86.4
2065518_03	0.09817	0.00170	3.72329	0.06341	0.27508	0.00318	1576.4	13.6	1566.5	16.1	1589.6	32.0	98.5
2065518_04	0.09866	0.00171	3.68638	0.06299	0.27098	0.00313	1568.4	13.7	1545.8	15.9	1599.0	32.0	96.7
2065518_05	0.09900	0.00184	3.72788	0.06796	0.27311	0.00326	1577.4	14.6	1556.6	16.5	1605.3	34.2	97.0
2065518_06	0.09923	0.00180	3.30285	0.05908	0.24140	0.00284	1481.7	13.9	1394.0	14.8	1609.7	33.5	86.6
2065518_07	0.09849	0.00178	3.30407	0.05887	0.24331	0.00285	1482.0	13.9	1403.9	14.8	1595.7	33.3	88.0
2065518_08	0.09711	0.00182	1.89252	0.03487	0.14135	0.00168	1078.5	12.2	852.3	9.5	1569.3	34.6	54.3
2065518_09	0.09711	0.00187	3.55941	0.06760	0.26583	0.00321	1540.5	15.1	1519.6	16.3	1569.4	35.7	96.8
2065518_10	0.09663	0.00191	2.84355	0.05523	0.21342	0.00260	1367.1	14.6	1247.0	13.8	1560.0	36.6	79.9
2065518_11	0.09870	0.00213	3.04832	0.06438	0.22399	0.00286	1419.8	16.2	1302.9	15.1	1599.8	39.8	81.4
2065518_13	0.09799	0.00195	3.65041	0.07196	0.27019	0.00329	1560.6	15.7	1541.8	16.7	1586.2	36.8	97.2
2065518_14	0.09827	0.00217	3.39430	0.07343	0.25053	0.00322	1503.1	17.0	1441.2	16.6	1591.5	40.6	90.6
2065518_15	0.09898	0.00205	3.46430	0.07093	0.25386	0.00314	1519.1	16.1	1458.4	16.1	1604.9	38.1	90.9
2065518_16	0.09761	0.00178	3.75268	0.06676	0.27885	0.00337	1582.7	14.3	1585.6	17.0	1579.0	33.7	100.4
2065518_17	0.09916	0.00163	3.19348	0.05156	0.23359	0.00269	1455.6	12.5	1353.3	14.1	1608.5	30.3	84.1
2065518_18	0.09823	0.00165	3.55866	0.05871	0.26278	0.00305	1540.4	13.1	1504.1	15.6	1590.7	31.1	94.6
2065518_19	0.09980	0.00180	3.00796	0.05294	0.21863	0.00261	1409.6	13.4	1274.6	13.8	1620.3	33.3	78.7
SB12_03_01	0.09964	0.00232	3.96274	0.08933	0.28845	0.00409	1626.6	18.3	1633.8	20.5	1617.3	42.7	101.0
SB12_03_02	0.09825	0.00176	3.80827	0.06728	0.28111	0.00347	1594.5	14.2	1596.9	17.5	1591.3	33.0	100.4
SB12_03_03	0.09813	0.00165	3.86857	0.06483	0.28593	0.00343	1607.1	13.5	1621.2	17.2	1588.8	31.2	102.0
SB12_03_04	0.09869	0.00171	3.86919	0.06618	0.28435	0.00344	1607.3	13.8	1613.2	17.2	1599.4	31.9	100.9
SB12_03_05	0.09721	0.00198	3.82522	0.07597	0.28537	0.00371	1598.1	16.0	1618.4	18.6	1571.3	37.7	103.0

Analysis No.	$^{207}Pb/^{206}Pb$ ratio	1σ	$^{207}Pb/^{235}U$ ratio	1σ	$^{206}Pb/^{238}U$ ratio	1σ	$^{207}Pb/^{235}U$ Age (Ma)	1σ	$^{206}Pb/^{238}U$ Age (Ma)	1σ (Ma)	$^{207}Pb/^{206}Pb$ Age (Ma)	1σ (Ma)	% Conc.
SB12_03_06	0.09819	0.00291	3.43631	0.09716	0.25380	0.00410	1512.7	22.2	1458.1	21.1	1590.1	54.4	91.7
SB12_03_07	0.09890	0.00183	3.75081	0.06785	0.27505	0.00338	1582.3	14.5	1566.4	17.1	1603.5	34.0	97.7
SB12_03_08	0.09936	0.00228	3.78513	0.08386	0.27627	0.00379	1589.6	17.8	1572.6	19.2	1612.2	42.2	97.5
SB12_03_09	0.09872	0.00206	3.50750	0.07074	0.25767	0.00332	1528.9	15.9	1477.9	17.0	1600.1	38.4	92.4
SB12_03_10	0.10060	0.00237	3.47750	0.07847	0.25069	0.00345	1522.1	17.8	1442.0	17.8	1635.3	43.0	88.2
SB12_03_11	0.09785	0.00197	3.73564	0.07278	0.27688	0.00347	1579.0	15.6	1575.6	17.5	1583.5	37.1	99.5
SB12_03_12	0.09875	0.00202	3.80787	0.07528	0.27967	0.00352	1594.4	15.9	1589.7	17.7	1600.6	37.7	99.3
SB12_03_13	0.09791	0.00209	3.49097	0.07174	0.25858	0.00331	1525.2	16.2	1482.6	16.9	1584.8	39.4	93.6
SB12_03_14	0.09846	0.00267	3.75695	0.09686	0.27675	0.00410	1583.6	20.7	1574.9	20.7	1595.1	49.7	98.7
SB12_03_15	0.09978	0.00300	3.48223	0.09908	0.25311	0.00401	1523.2	22.5	1454.5	20.6	1620.0	54.9	89.8
SB12_03_16	0.10001	0.00167	3.14814	0.05210	0.22832	0.00267	1444.5	12.8	1325.7	14.0	1624.3	30.8	81.6
SB12_03_17	0.09861	0.00192	3.59361	0.06832	0.26434	0.00331	1548.1	15.1	1512.0	16.9	1598.0	35.9	94.6
SB12_03_18	0.09877	0.00281	3.23722	0.08786	0.23774	0.00371	1466.1	21.1	1374.9	19.3	1600.9	52.2	85.9
SB12_03_20	0.09583	0.00163	2.61432	0.04407	0.19787	0.00232	1304.7	12.4	1163.9	12.5	1544.5	31.6	75.4
SB12_03_21	0.09782	0.00214	3.38923	0.07204	0.25130	0.00333	1501.9	16.7	1445.2	17.2	1583.1	40.4	91.3
SB12_03_22	0.09697	0.00188	3.50966	0.06685	0.26251	0.00326	1529.4	15.1	1502.7	16.7	1566.7	35.9	95.9
SB12_03_23	0.09894	0.00233	3.41710	0.07771	0.25050	0.00345	1508.3	17.9	1441.1	17.8	1604.3	43.2	89.8
SB12_03_24	0.09674	0.00187	3.73075	0.07111	0.27972	0.00346	1578.0	15.3	1589.9	17.4	1562.2	35.9	101.8
SB12_03_25	0.09777	0.00186	3.67843	0.06904	0.27288	0.00334	1566.7	15.0	1555.4	16.9	1582.1	35.1	98.3
SB12_03_26	0.09755	0.00203	3.77309	0.07687	0.28055	0.00359	1587.0	16.4	1594.1	18.1	1577.8	38.4	101.0
SB12_03_27	0.09793	0.00201	3.71213	0.07488	0.27494	0.00349	1574.0	16.1	1565.8	17.6	1585.1	37.9	98.8
SB12_03_28	0.09689	0.00195	3.72802	0.07409	0.27909	0.00349	1577.4	15.9	1586.8	17.6	1565.0	37.3	101.4
SB12_03_29	0.10830	0.00246	3.77641	0.08352	0.25292	0.00340	1587.7	17.8	1453.5	17.5	1770.9	40.9	82.1
SB12_03_31	0.09691	0.00210	3.44405	0.07355	0.25778	0.00333	1514.5	16.8	1478.5	17.1	1565.4	40.1	94.4
2049213_01	0.09834	0.00189	3.49276	0.06514	0.25761	0.00315	1525.6	14.7	1477.6	16.2	1592.9	35.4	92.8
2049213_02	0.09900	0.00181	3.60020	0.06440	0.26375	0.00316	1549.6	14.2	1509.0	16.1	1605.4	33.8	94.0
2049213_03	0.09766	0.00168	2.98453	0.05046	0.22165	0.00258	1403.7	12.9	1290.6	13.6	1579.8	31.9	81.7
2049213_04	0.09876	0.00168	3.69358	0.06175	0.27122	0.00315	1570.0	13.4	1547.0	16.0	1600.9	31.3	96.6
2049213_05	0.09980	0.00170	3.90813	0.06585	0.28398	0.00331	1615.4	13.6	1611.4	16.6	1620.5	31.5	99.4
2049213_07	0.09814	0.00267	3.14452	0.08189	0.23237	0.00349	1443.7	20.1	1346.9	18.2	1589.0	50.1	84.8
2049213_08	0.09732	0.00171	3.11359	0.05393	0.23200	0.00274	1436.1	13.3	1345.0	14.3	1573.4	32.5	85.5
2049213_09	0.09787	0.00167	3.64432	0.06171	0.27001	0.00315	1559.3	13.5	1540.9	16.0	1584.0	31.6	97.3
2049213_10	0.09842	0.00189	3.64863	0.06880	0.26882	0.00332	1560.2	15.0	1534.8	16.9	1594.4	35.4	96.3
2049213_11	0.09858	0.00250	3.23771	0.07901	0.23816	0.00342	1466.2	18.9	1377.1	17.8	1597.4	46.6	86.2

Analysis No.	$^{207}Pb/^{206}Pb$ ratio	1σ	$^{207}Pb/^{235}U$ ratio	1σ	$^{206}Pb/^{238}U$ ratio	1σ	$^{207}Pb/^{235}U$ Age (Ma)	1σ	$^{206}Pb/^{238}U$ Age (Ma)	1σ (Ma)	$^{207}Pb/^{206}Pb$ Age (Ma)	1σ (Ma)	% Conc.
2049213_13	0.09829	0.00180	3.56110	0.06446	0.26271	0.00316	1540.9	14.4	1503.7	16.2	1592.0	33.8	94.5
2049213_14	0.09852	0.00178	3.43591	0.06164	0.25289	0.00303	1512.6	14.1	1453.4	15.6	1596.3	33.4	91.0
2049213_15	0.09888	0.00175	3.55926	0.06285	0.26101	0.00310	1540.5	14.0	1495.0	15.8	1603.1	32.7	93.3
2049213_16	0.10163	0.00196	3.09558	0.05927	0.22087	0.00272	1431.6	14.7	1286.5	14.4	1654.1	35.4	77.8
2049213_17	0.32812	0.00618	19.35738	0.36169	0.42778	0.00541	3059.8	18.0	2295.7	24.4	3608.3	28.6	63.6
2049213_18	0.12080	0.00253	3.15295	0.06487	0.18927	0.00245	1445.7	15.9	1117.4	13.3	1968.0	36.9	56.8
2049213_19	0.10363	0.00236	3.19130	0.07107	0.22330	0.00301	1455.1	17.2	1299.3	15.9	1690.2	41.4	76.9
2049213_20	0.09695	0.00190	2.51216	0.04909	0.18789	0.00232	1275.6	14.2	1109.9	12.6	1566.3	36.3	70.9
2049213_21	0.09992	0.00223	3.71388	0.08167	0.26952	0.00358	1574.4	17.6	1538.4	18.2	1622.7	40.9	94.8
2049215_03	0.09516	0.00166	3.38396	0.05780	0.25796	0.00299	1500.7	13.4	1479.4	15.3	1531.3	32.5	96.6
2049215_04	0.09752	0.00162	3.22890	0.05273	0.24020	0.00273	1464.1	12.7	1387.7	14.2	1577.2	30.7	88.0
2049215_05	0.09709	0.00167	3.36703	0.05695	0.25159	0.00290	1496.8	13.2	1446.7	14.9	1568.9	31.9	92.2
2049215_06	0.09688	0.00198	3.21668	0.06385	0.24088	0.00302	1461.2	15.4	1391.3	15.7	1564.9	37.8	88.9
2049215_07	0.09801	0.00200	3.26925	0.06484	0.24198	0.00303	1473.8	15.4	1397.0	15.7	1586.7	37.6	88.0
2049215_08	0.09808	0.00180	3.46065	0.06263	0.25599	0.00303	1518.3	14.3	1469.3	15.6	1587.9	34.0	92.5
2049215_09	0.09744	0.00183	2.41966	0.04474	0.18016	0.00215	1248.5	13.3	1067.9	11.7	1575.6	34.7	67.8
2049215_10	0.09733	0.00180	3.55083	0.06505	0.26467	0.00313	1538.6	14.5	1513.7	16.0	1573.6	34.3	96.2
2049215_11	0.09782	0.00188	3.30749	0.06280	0.24529	0.00295	1482.8	14.8	1414.1	15.3	1583.1	35.5	89.3
2049215_12	0.09843	0.00205	2.84313	0.05815	0.20955	0.00262	1367.0	15.4	1226.4	14.0	1594.6	38.4	76.9
2049215_13	0.09934	0.00231	3.64093	0.08261	0.26590	0.00355	1558.5	18.1	1519.9	18.1	1611.7	42.7	94.3
2049215_16	0.09988	0.00170	3.49365	0.05894	0.25370	0.00301	1525.8	13.3	1457.5	15.5	1621.9	31.4	89.9
2049215_17	0.09914	0.00184	2.68751	0.04878	0.19662	0.00240	1325.0	13.4	1157.1	12.9	1608.0	34.2	72.0
2049215_18	0.10594	0.00174	2.43287	0.03967	0.16656	0.00193	1252.4	11.7	993.1	10.7	1730.8	29.9	57.4
2049215_19	0.09870	0.00176	3.71937	0.06500	0.27333	0.00326	1575.5	14.0	1557.7	16.5	1599.7	32.8	97.4
2049215_20	0.09923	0.00180	3.60414	0.06410	0.26343	0.00316	1550.4	14.1	1507.4	16.1	1609.7	33.5	93.6
2049215_21	0.09859	0.00171	3.51741	0.06012	0.25878	0.00303	1531.1	13.5	1483.6	15.5	1597.5	32.1	92.9
2049215_22	0.09837	0.00179	3.18982	0.05687	0.23519	0.00280	1454.7	13.8	1361.7	14.6	1593.5	33.7	85.5
2049215_23	0.09904	0.00186	3.21595	0.05878	0.23551	0.00282	1461.0	14.2	1363.3	14.7	1606.1	34.6	84.9
2049215_24	0.09779	0.00197	3.34047	0.06511	0.24777	0.00306	1490.6	15.2	1427.0	15.8	1582.3	37.2	90.2
2049215_25	0.09448	0.00176	1.61761	0.02930	0.12419	0.00146	977.1	11.4	754.6	8.4	1517.6	34.7	49.7
2049215_26	0.09980	0.00197	3.58576	0.06844	0.26059	0.00314	1546.4	15.2	1492.9	16.1	1620.4	36.3	92.1
14_CW_02_01	0.10939	0.00222	3.75344	0.07317	0.24911	0.00227	1582.8	15.6	1433.9	11.7	1789.2	36.6	80.1
14_CW_02_02	0.10040	0.00298	3.50800	0.09930	0.25374	0.00319	1529.0	22.4	1457.7	16.4	1631.4	54.3	89.4

Analysis No.	$^{207}Pb/^{206}Pb$ ratio	1σ	$^{207}Pb/^{235}U$ ratio	1σ	$^{206}Pb/^{238}U$ ratio	1σ	$^{207}Pb/^{235}U$ Age (Ma)	1σ	$^{206}Pb/^{238}U$ Age (Ma)	1σ (Ma)	$^{207}Pb/^{206}Pb$ Age (Ma)	1σ (Ma)	% Conc.
14_CW_02_03	0.11412	0.00225	3.61722	0.06827	0.22983	0.00199	1553.3	15.0	1333.6	10.5	1866.1	35.1	71.5
14_CW_02_04	0.09805	0.00108	3.45836	0.03689	0.25586	0.00161	1517.8	8.4	1468.6	8.3	1587.3	20.4	92.5
14_CW_02_05	0.10271	0.00253	3.76433	0.08873	0.26582	0.00275	1585.2	18.9	1519.6	14.0	1673.6	44.9	90.8
14_CW_02_06	0.11489	0.00123	4.00749	0.04208	0.25301	0.00159	1635.7	8.5	1454.0	8.2	1878.2	19.2	77.4
14_CW_02_07	0.09833	0.00107	3.57669	0.03808	0.26388	0.00168	1544.4	8.5	1509.6	8.6	1592.7	20.2	94.8
14_CW_02_08	0.11020	0.00266	3.81914	0.08703	0.25216	0.00258	1596.8	18.3	1449.6	13.3	1802.7	43.3	80.4
14_CW_02_09	0.10150	0.00352	2.32443	0.07556	0.16639	0.00232	1219.8	23.1	992.2	12.9	1651.7	63.0	60.1
14_CW_02_10	0.10276	0.00208	3.57104	0.06881	0.25258	0.00226	1543.1	15.3	1451.8	11.6	1674.5	37.0	86.7
14_CW_02_11	0.09719	0.00258	3.50493	0.08711	0.26255	0.00285	1528.3	19.6	1502.9	14.6	1570.9	48.9	95.7
14_CW_02_12	0.10347	0.00408	3.43687	0.12616	0.24174	0.00364	1512.9	28.9	1395.7	18.9	1687.4	71.1	82.7
14_CW_02_13	0.10337	0.00353	2.58187	0.08481	0.18127	0.00237	1295.5	24.0	1073.9	12.9	1685.5	61.7	63.7
14_CW_02_14	0.09795	0.00303	3.31919	0.09889	0.24568	0.00300	1485.6	23.3	1416.2	15.5	1585.5	56.7	89.3
14_CW_02_15	0.10895	0.00273	3.23134	0.07599	0.21582	0.00222	1464.7	18.2	1259.7	11.8	1781.9	45.1	70.7
14_CW_02_16	0.09924	0.00152	2.97755	0.04381	0.21762	0.00167	1401.9	11.2	1269.3	8.9	1609.8	28.3	78.8
14_CW_02_17	0.10489	0.00237	3.63218	0.07744	0.25118	0.00238	1556.6	17.0	1444.5	12.3	1712.4	40.9	84.4
14_CW_02_18	0.11303	0.00166	2.99991	0.04247	0.19249	0.00140	1407.6	10.8	1134.8	7.6	1848.7	26.3	61.4
14_CW_02_19	0.11749	0.00178	3.59247	0.05247	0.22174	0.00164	1547.9	11.6	1291.1	8.7	1918.3	26.9	67.3
14_CW_02_20	0.10479	0.00175	3.77823	0.06052	0.26147	0.00205	1588.1	12.9	1497.4	10.5	1710.7	30.5	87.5
14_CW_02_21	0.10538	0.00149	3.76677	0.05158	0.25926	0.00184	1585.7	11.0	1486.0	9.4	1721.0	25.7	86.3
14_CW_02_23	0.10595	0.00131	3.61874	0.04355	0.24773	0.00165	1553.7	9.6	1426.8	8.5	1730.8	22.5	82.4
14_CW_02_24	0.10065	0.00225	3.53799	0.07443	0.25489	0.00240	1535.8	16.7	1463.6	12.3	1636.1	40.9	89.5
14_CW_02_25	0.11310	0.00255	3.48846	0.07360	0.22366	0.00209	1524.6	16.7	1301.2	11.0	1849.8	40.2	70.3
14_CW_02_26	0.09788	0.00178	3.54063	0.06155	0.26231	0.00216	1536.3	13.8	1501.6	11.0	1584.1	33.6	94.8
14_CW_02_28	0.10396	0.00246	3.33834	0.07369	0.23286	0.00226	1490.1	17.3	1349.5	11.8	1695.9	42.9	79.6
14_CW_02_30	0.09836	0.00207	3.58785	0.07164	0.26444	0.00237	1546.8	15.9	1512.5	12.1	1593.2	38.8	94.9
14_CW_02_31	0.09837	0.00116	3.84180	0.06251	0.28333	0.00438	1601.6	13.1	1608.1	22.0	1593.5	21.9	100.9
14_CW_02_32	0.09850	0.00119	3.71995	0.05584	0.27392	0.00379	1575.7	12.0	1560.7	19.2	1595.9	22.4	97.8
14_CW_02_33	0.09931	0.00116	3.67319	0.05508	0.26826	0.00378	1565.6	12.0	1532.0	19.2	1611.2	21.6	95.1
14_CW_02_34	0.09810	0.00125	3.72120	0.06327	0.27521	0.00431	1575.9	13.6	1567.2	21.8	1588.3	23.7	98.7
14_CW_02_35	0.10481	0.00133	3.88474	0.06542	0.26892	0.00417	1610.5	13.6	1535.3	21.2	1710.9	23.2	89.7
14_CW_02_36	0.09918	0.00122	3.66536	0.05594	0.26806	0.00375	1563.9	12.2	1530.9	19.1	1608.8	22.7	95.2
14_CW_02_37	0.10025	0.00110	3.53345	0.05148	0.25563	0.00360	1534.7	11.5	1467.4	18.5	1628.8	20.2	90.1
14_CW_02_38	0.09814	0.00107	3.69219	0.05385	0.27288	0.00386	1569.7	11.7	1555.4	19.6	1589.0	20.2	97.9
14_CW_02_39	0.09729	0.00106	3.53508	0.05205	0.26355	0.00377	1535.1	11.7	1508.0	19.2	1572.8	20.2	95.9
14_CW_02_40	0.09900	0.00112	3.64628	0.05368	0.26713	0.00375	1559.7	11.7	1526.2	19.1	1605.4	20.9	95.1

Analysis No.	$^{207}Pb/^{206}Pb$ ratio	1σ	$^{207}Pb/^{235}U$ ratio	1σ	$^{206}Pb/^{238}U$ ratio	1σ	$^{207}Pb/^{235}U$ Age (Ma)	1σ	$^{206}Pb/^{238}U$ Age (Ma)	1σ (Ma)	$^{207}Pb/^{206}Pb$ Age (Ma)	1σ (Ma)	% Conc.
14_CW_02_41	0.10804	0.00119	3.64401	0.05345	0.24465	0.00346	1559.2	11.7	1410.8	17.9	1766.5	20.1	79.9
14_CW_02_42	0.10184	0.00122	3.65867	0.05664	0.26056	0.00375	1562.4	12.3	1492.7	19.2	1658.0	22.1	90.0
14_CW_02_43	0.10189	0.00146	3.57738	0.06265	0.25468	0.00387	1544.5	13.9	1462.6	19.9	1658.8	26.3	88.2
14_CW_02_44	0.10038	0.00116	3.76063	0.05552	0.27172	0.00378	1584.4	11.8	1549.5	19.1	1631.1	21.3	95.0
14_CW_02_45	0.09833	0.00111	3.70485	0.05482	0.27329	0.00387	1572.4	11.8	1557.5	19.6	1592.7	20.9	97.8
14_CW_03_01	0.09741	0.00127	0.25073	0.00174	3.36818	0.04271	1497.0	9.9	1442.3	9.0	1575.1	24.3	91.6
14_CW_03_02	0.10415	0.00141	0.19984	0.00141	2.87043	0.03781	1374.2	9.9	1174.5	7.6	1699.3	24.8	69.1
14_CW_03_03	0.09771	0.00113	0.25412	0.00164	3.42394	0.03830	1509.9	8.8	1459.7	8.4	1580.8	21.4	92.3
14_CW_03_04	0.09833	0.00124	0.27662	0.00188	3.75043	0.04563	1582.2	9.8	1574.3	9.5	1592.6	23.5	98.9
14_CW_03_05	0.09773	0.00113	0.25462	0.00163	3.43131	0.03836	1511.6	8.8	1462.3	8.4	1581.3	21.5	92.5
14_CW_03_06	0.09820	0.00134	0.27599	0.00193	3.73715	0.04921	1579.4	10.6	1571.1	9.8	1590.3	25.2	98.8
14_CW_03_07	0.09881	0.00132	0.27182	0.00188	3.70384	0.04793	1572.2	10.4	1550.0	9.5	1601.8	24.8	96.8
14_CW_03_08	0.09855	0.00118	0.26315	0.00170	3.57619	0.04134	1544.3	9.2	1505.9	8.7	1596.9	22.3	94.3
14_CW_03_09	0.09802	0.00152	0.25766	0.00192	3.48248	0.05185	1523.3	11.7	1477.9	9.9	1586.7	28.6	93.1
14_CW_03_10	0.09819	0.00119	0.26133	0.00170	3.53838	0.04110	1535.8	9.2	1496.6	8.7	1590.1	22.4	94.1
14_CW_03_11	0.09963	0.00185	0.25037	0.00211	3.43876	0.06136	1513.3	14.0	1440.4	10.9	1617.1	34.2	89.1
14_CW_03_12	0.11575	0.00213	0.20811	0.00169	3.32100	0.05814	1486.0	13.7	1218.7	9.0	1891.5	32.7	64.4
14_CW_03_13	0.09782	0.00236	0.25842	0.00256	3.48435	0.08039	1523.7	18.2	1481.7	13.1	1583.0	44.4	93.6
14_CW_03_14	0.09731	0.00145	0.27124	0.00196	3.63970	0.05182	1558.3	11.3	1547.1	9.9	1573.2	27.7	98.3
14_CW_03_15	0.09733	0.00139	0.26662	0.00186	3.57815	0.04876	1544.7	10.8	1523.6	9.4	1573.5	26.6	96.8
14_CW_03_16	0.09796	0.00108	0.27755	0.00178	3.74882	0.04059	1581.9	8.7	1579.0	9.0	1585.7	20.5	99.6
14_CW_03_17	0.10044	0.00144	0.28000	0.00208	3.87638	0.05436	1608.8	11.3	1591.4	10.5	1632.2	26.4	97.5
14_CW_03_18	0.09871	0.00118	0.27322	0.00181	3.71835	0.04360	1575.3	9.4	1557.1	9.2	1600.0	22.1	97.3
14_CW_03_19	0.09979	0.00116	0.25596	0.00168	3.52106	0.04026	1532.0	9.0	1469.1	8.6	1620.1	21.5	90.7
14_CW_03_20	0.09767	0.00114	0.26961	0.00178	3.63027	0.04174	1556.2	9.2	1538.8	9.0	1580.2	21.7	97.4
14_CW_04_01	0.09956	0.00124	3.55713	0.04378	0.25919	0.00177	1540.0	9.8	1485.7	9.0	1615.9	23.1	91.9
14_CW_04_02	0.09976	0.00123	3.76387	0.04555	0.27370	0.00184	1585.1	9.7	1559.6	9.3	1619.6	22.8	96.3
14_CW_04_03	0.09854	0.00118	3.90566	0.04591	0.28751	0.00191	1614.9	9.5	1629.1	9.6	1596.7	22.1	102.0
14_CW_04_04	0.09856	0.00123	3.75429	0.04611	0.27633	0.00187	1583.0	9.9	1572.9	9.5	1597.0	23.1	98.5
14_CW_04_05	0.10324	0.00208	3.78008	0.07503	0.26559	0.00238	1588.5	15.9	1518.4	12.1	1683.1	36.8	90.2
14_CW_04_06	0.09762	0.00162	3.89992	0.06390	0.28976	0.00231	1613.7	13.2	1640.3	11.6	1579.2	30.7	103.9
14_CW_04_07	0.09885	0.00175	3.73358	0.06532	0.27403	0.00227	1578.6	14.0	1561.2	11.5	1602.5	32.7	97.4
14_CW_04_08	0.09947	0.00127	3.66726	0.04622	0.26740	0.00185	1564.3	10.1	1527.6	9.4	1614.3	23.6	94.6

Analysis No.	$^{207}Pb/^{206}Pb$ ratio	1σ	$^{207}Pb/^{235}U$ ratio	1σ	$^{206}Pb/^{238}U$ ratio	1σ	$^{207}Pb/^{235}U$ Age (Ma)	1σ	$^{206}Pb/^{238}U$ Age (Ma)	1σ (Ma)	$^{207}Pb/^{206}Pb$ Age (Ma)	1σ (Ma)	% Conc.
14_CW_04_09	0.09856	0.00128	3.87319	0.04958	0.28507	0.00197	1608.1	10.3	1616.8	9.9	1597.0	24.0	101.2
14_CW_04_10	0.09920	0.00170	4.01573	0.06842	0.29364	0.00239	1637.4	13.9	1659.7	11.9	1609.1	31.7	103.1
14_CW_04_11	0.10936	0.00166	3.60022	0.05441	0.23881	0.00188	1549.6	12.0	1380.5	9.8	1788.7	27.5	77.2
14_CW_04_12	0.09891	0.00101	3.52698	0.03633	0.25866	0.00170	1533.3	8.2	1483.0	8.7	1603.7	18.9	92.5
14_CW_04_13	0.09981	0.00152	3.59320	0.05414	0.26122	0.00208	1548.0	12.0	1496.1	10.6	1620.6	28.1	92.3
14_CW_04_14	0.12627	0.00119	2.64008	0.02533	0.15167	0.00097	1311.9	7.1	910.3	5.5	2046.7	16.6	44.5
14_CW_04_15	0.09769	0.00110	3.84039	0.04338	0.28508	0.00195	1601.3	9.1	1616.9	9.8	1580.5	20.8	102.3
14_CW_04_16	0.09721	0.00105	3.94162	0.04307	0.29408	0.00199	1622.3	8.9	1661.9	9.9	1571.3	20.1	105.8
14_CW_04_17	0.12266	0.00194	2.53877	0.03992	0.15016	0.00121	1283.2	11.5	901.9	6.8	1995.3	27.9	45.2
14_CW_04_18	0.09776	0.00161	3.74722	0.06121	0.27799	0.00228	1581.5	13.1	1581.2	11.5	1581.9	30.5	100.0
14_CW_04_19	0.09930	0.00170	3.73160	0.06328	0.27239	0.00227	1578.2	13.6	1552.9	11.5	1611.0	31.5	96.4
14_CW_04_20	0.10282	0.00185	3.71919	0.06657	0.26220	0.00225	1575.5	14.3	1501.1	11.5	1675.6	33.0	89.6
14_CW_04_21	0.09852	0.00209	3.51011	0.07397	0.25834	0.00246	1529.5	16.7	1481.3	12.6	1596.3	39.1	92.8
14_CW_04_22	0.09907	0.00149	3.54839	0.05281	0.26004	0.00200	1538.1	11.8	1490.0	10.2	1606.7	27.8	92.7
14_CW_04_23	0.10007	0.00114	3.71936	0.04303	0.26962	0.00187	1575.5	9.3	1538.9	9.5	1625.3	21.0	94.7
14_CW_04_24	0.11267	0.00204	2.98718	0.05429	0.19221	0.00167	1404.4	13.8	1133.3	9.0	1842.9	32.4	61.5

APPENDIX D: LU-HF ISOTOPE DATA

Analysis No.	Interf. Corr. Meth.	Total Hf beam (V)	$^{176}Hf/^{177}Hf$	2SE	exp. factor[1]	$^{178}Hf/^{177}Hf$	2SE	$^{176}Yb/^{177}Hf$	2SE	$^{176}Lu/^{177}Hf$	2SE	Age (Ma)	1σ	$^{176}Hf/^{177}Hf$ Initial	$e_{Hf}(t)$	1s	T_{DM} Crustal (Ga)
1998158_01	Yb	12.7	0.281726	22	0.9502	1.46736	20	0.03757	94	0.000838	26	1600.1	32.6	0.281701	-2.4	0.8	2.44
1998158_02	Yb	13.1	0.281701	25	0.9515	1.46729	18	0.03908	25	0.000818	42	1597.6	24.9	0.281676	-3.3	0.9	2.49
1998158_03	Yb	8.4	0.281680	39	0.9665	1.46735	32	0.03794	13	0.000879	34	1590.5	25.0	0.281654	-4.2	1.4	2.54
1998158_04	Yb	13.3	0.281738	20	0.9453	1.46725	13	0.03193	10	0.000721	24	1598.5	25.6	0.281716	-1.9	0.7	2.41
1998158_05	Yb	12.3	0.281709	33	0.9504	1.46743	25	0.03801	215	0.000911	57	1561.1	33.5	0.281682	-3.9	1.2	2.50
1998158_06	Yb	8.5	0.281731	46	0.9538	1.46743	39	0.04025	145	0.000916	36	1606.7	25.7	0.281704	-2.1	1.6	2.43
1998158_07	Yb	8.4	0.281712	28	0.9610	1.46743	28	0.02877	202	0.000676	46	1579.1	27.6	0.281692	-3.2	1.0	2.47
1998158_09	Yb	9.1	0.281731	50	0.9388	1.46740	45	0.04606	188	0.001063	64	1591.6	26.4	0.281699	-2.6	1.8	2.45
1998158_10	Yb	14.7	0.281732	24	0.9536	1.46725	16	0.04734	392	0.000984	64	1594.2	26.8	0.281703	-2.4	0.8	2.44
1998158_11	Yb	15.6	0.281723	24	0.9389	1.46729	18	0.03089	64	0.000673	5	1570.9	27.3	0.281703	-3.0	0.9	2.45
1998158_12	Yb	13.3	0.281673	25	0.9397	1.46728	20	0.02378	66	0.000533	13	1603.2	27.5	0.281657	-3.9	0.9	2.53
1998158_13	Yb	15.6	0.281705	23	0.9352	1.46721	21	0.02114	37	0.000469	10	1563.2	28.6	0.281691	-3.6	0.8	2.48
1998158_14	Yb	14.9	0.281716	27	0.9393	1.46727	27	0.02072	38	0.000462	12	1590.5	29.0	0.281702	-2.5	0.9	2.44
1998158_17	Yb	12.9	0.281668	35	0.8957	1.46730	29	0.03707	100	0.000890	53	1576.4	31.4	0.281642	-5.0	1.2	2.58
1998158_18	Yb	8.2	0.281700	43	0.9270	1.46731	29	0.03833	88	0.000797	9	1585.1	30.7	0.281676	-3.6	1.5	2.50
1998158_19	Yb	13.3	0.281712	23	0.9492	1.46725	17	0.02658	75	0.000615	13	1567.4	30.3	0.281694	-3.3	0.8	2.47
1998158_20	Yb	13.1	0.281783	47	0.9013	1.46774	46	0.06169	790	0.001583	263	1613.5	30.4	0.281735	-0.9	1.6	2.36
1998160_01	Yb	12.9	0.281739	20	0.9482	1.46725	13	0.02681	40	0.000627	13	1599.8	26.8	0.281720	-1.7	0.7	2.40
1998160_03	Yb	14.0	0.281807	21	0.9646	1.46723	17	0.03072	10	0.000735	28	1618.5	25.8	0.281784	1.0	0.7	2.25
1998160_04	Yb	14.3	0.281754	18	0.9632	1.46728	13	0.02131	16	0.000513	6	1600.1	27.5	0.281739	-1.0	0.6	2.36
1998160_06	Yb	7.3	0.281790	36	0.9825	1.46732	20	0.03373	29	0.000864	99	1603.7	27.2	0.281764	0.0	1.3	2.30
1998160_07	Yb	13.8	0.281753	19	0.9667	1.46731	11	0.01734	51	0.000412	6	1575.0	28.5	0.281741	-1.5	0.7	2.37
1998160_08	Yb	14.0	0.281784	24	0.9667	1.46729	15	0.02193	87	0.000519	21	1603.5	29.0	0.281768	0.1	0.8	2.29
1998160_10	Yb	13.1	0.281767	21	0.9653	1.46724	15	0.03128	107	0.000707	22	1615.6	31.5	0.281745	-0.4	0.7	2.33
1998160_11	Yb	14.2	0.281728	18	0.9503	1.46722	18	0.01970	39	0.000449	4	1596.3	29.3	0.281715	-1.9	0.6	2.41
1998160_12	Yb	12.8	0.281778	26	0.9487	1.46728	29	0.02464	45	0.000584	19	1606.3	31.2	0.281760	-0.1	0.9	2.31
1998160_13	Yb	8.3	0.281786	34	0.9615	1.46729	37	0.02816	42	0.000670	14	1587.7	31.0	0.281766	-0.3	1.2	2.31
1998160_14	Yb	14.2	0.281776	23	0.9662	1.46729	15	0.03043	140	0.000712	29	1602.5	30.4	0.281754	-0.4	0.8	2.32
1998160_15	Yb	13.6	0.281752	21	0.9591	1.46725	13	0.02379	425	0.000560	4	1606.5	16.6	0.281735	-1.0	0.7	2.36
1998160_16	Yb	11.8	0.281763	24	0.9574	1.46728	14	0.04052	128	0.000997	49	1595.7	15.8	0.281733	-1.3	0.8	2.37
1998160_19	Yb	14.7	0.281764	34	0.9429	1.46728	27	0.02984	212	0.000679	54	1596.7	16.3	0.281743	-0.9	1.2	2.35
1998160_20	Yb	12.9	0.281802	41	0.9485	1.46754	42	0.03149	105	0.000828	45	1573.1	16.5	0.281778	-0.2	1.4	2.29
1998160_21	Yb	7.6	0.281750	34	0.9790	1.46737	28	0.02144	45	0.000540	8	1593.1	22.9	0.281734	-1.4	1.2	2.37
1998160_25	Yb	13.6	0.281730	21	0.9641	1.46723	17	0.02095	14	0.000502	6	1644.9	23.3	0.281714	-0.8	0.7	2.38
1998160_26	Yb	11.9	0.281774	19	0.9628	1.46721	19	0.02105	33	0.000496	8	1582.9	22.6	0.281759	-0.7	0.7	2.32

Analysis No.	Interf. Corr. Meth.	Total Hf beam (V)	$^{176}Hf/^{177}Hf$	2SE	exp. factor[1]	$^{178}Hf/^{177}Hf$	2SE	$^{176}Yb/^{177}Hf$	2SE	$^{176}Lu/^{177}Hf$	2SE	Age (Ma)	1σ	$^{176}Hf/^{177}Hf$ Initial	e$_{Hf}$(t)	1s	T$_{DM}$ Crustal (Ga)
1998160_28	Yb	13.5	0.281768	19	0.9553	1.46724	16	0.02596	41	0.000603	2	1590.5	23.4	0.281749	-0.8	0.7	2.34
1998160_29	Yb	11.1	0.281779	37	0.9309	1.46744	15	0.02471	159	0.000693	59	1613.1	23.6	0.281758	0.0	1.3	2.31
1998160_30	Yb	12.0	0.281770	21	0.9644	1.46724	13	0.02249	31	0.000537	5	1573.7	24.3	0.281754	-1.1	0.7	2.34
1998160_32	Yb	13.1	0.281765	20	0.9600	1.46717	20	0.02425	49	0.000591	20	1572.1	23.7	0.281747	-1.3	0.7	2.36
1998160_33	Yb	8.5	0.281739	36	0.9594	1.46735	33	0.02277	31	0.000563	15	1573.3	23.8	0.281723	-2.2	1.3	2.41
1998160_34	Yb	13.3	0.281766	24	0.9718	1.46733	14	0.02771	134	0.000648	23	1586.3	23.9	0.281747	-1.1	0.8	2.35
SB12_09_03	Yb	15.7	0.281730	45	0.9311	1.46706	39	0.02431	47	0.000498	3	1573.6	25.4	0.281715	-2.5	1.6	2.42
SB12_09_04	Yb	10.5	0.281773	50	0.9701	1.46709	27	0.08599	1080	0.001760	148	1597.9	24.5	0.281720	-1.7	1.7	2.40
SB12_09_08	Yb	12.0	0.281720	27	0.9833	1.46741	30	0.02892	45	0.000645	3	1575.9	32.0	0.281701	-2.9	0.9	2.45
SB12_09_10	Yb	23.2	0.281894	79	0.9834	1.46731	20	0.23334	609	0.005261	105	1547.1	24.8	0.281740	-2.2	2.8	2.39
SB12_09_11	Yb	7.2	0.281767	46	1.0023	1.46721	51	0.02177	34	0.000554	8	1604.7	31.0	0.281750	-0.5	1.6	2.33
SB12_09_14	Yb	14.5	0.281707	33	0.9838	1.46725	20	0.07473	155	0.001447	31	1579.0	27.5	0.281664	-4.1	1.2	2.53
SB12_09_16	Yb	13.9	0.281728	31	0.9531	1.46728	30	0.04772	458	0.000943	81	1608.6	30.8	0.281700	-2.2	1.1	2.44
SB12_09_17	Yb	30.5	0.281810	57	0.9617	1.46700	38	0.09217	204	0.002062	50	1593.4	27.0	0.281747	-0.9	2.0	2.34
SB12_09_25	Yb	12.2	0.281606	183	0.9720	1.46737	33	0.44648	4657	0.008353	836	1647.5	30.1	0.281345	-13.9	6.4	3.17
SB12_09_33	Yb	14.6	0.281367	20	0.9580	1.46730	21	0.00528	7	0.000127	2	1618.0	50.0	0.281363	-13.9	0.7	3.15
2065519_01	Yb	16.3	0.281756	21	0.9148	1.46724	12	0.04154	97	0.001049	19	1572.6	27.5	0.281725	-2.1	0.7	2.40
2065519_02	Yb	16.8	0.281814	38	0.8911	1.46712	22	0.05991	199	0.001387	14	1585.1	39.6	0.281772	-0.2	1.3	2.29
2065519_03	Yb	14.6	0.281751	36	0.8921	1.46736	46	0.04470	121	0.001337	33	1588.1	33.9	0.281711	-2.3	1.3	2.42
2065519_04	Yb	13.8	0.281788	24	0.9273	1.46725	10	0.07263	457	0.001644	91	1603.8	39.1	0.281738	-1.0	0.8	2.36
2065519_05	Yb	6.7	0.281765	45	1.5465	1.46751	17	0.06799	595	0.001742	199	1584.7	25.9	0.281712	-2.3	1.6	2.42
2065519_07	Yb	17.9	0.281760	37	0.9087	1.46735	15	0.07764	217	0.001805	49	1603.4	36.8	0.281705	-2.1	1.3	2.43
2065519_08	Yb	10.7	0.281757	42	0.9115	1.46731	26	0.05846	345	0.001499	56	1560.7	26.9	0.281713	-2.8	1.5	2.44
2065519_09	Yb	17.2	0.281740	21	0.9344	1.46725	13	0.05902	42	0.001559	6	1568.1	26.5	0.281694	-3.3	0.7	2.47
2065519_10	Yb	14.6	0.281742	21	0.9028	1.46724	15	0.03318	62	0.000852	10	1574.8	29.3	0.281716	-2.4	0.7	2.42
2065519_11	Yb	6.3	0.281780	81	0.8837	1.46740	34	0.08011	391	0.002420	82	1582.7	48.0	0.281708	-2.5	2.8	2.43
2065519_13	Yb	13.2	0.281744	28	0.9294	1.46724	15	0.06880	160	0.001722	54	1582.3	28.5	0.281692	-3.1	1.0	2.47
2065519_15	Yb	13.8	0.281731	36	0.8828	1.46728	34	0.06427	288	0.001460	54	1582.9	42.9	0.281687	-3.2	1.3	2.48
2065518_01	Yb	15.0	0.281744	28	0.9439	1.46729	22	0.04439	43	0.001215	12	1585.3	30.7	0.281707	-2.5	1.0	2.43
2065518_02	Yb	16.2	0.281730	34	0.9397	1.46721	32	0.05462	190	0.001435	30	1584.2	32.8	0.281687	-3.2	1.2	2.48
2065518_03	Yb	13.5	0.281737	29	0.9245	1.46722	30	0.02952	61	0.000818	3	1589.6	32.0	0.281713	-2.2	1.0	2.42
2065518_04	Yb	6.9	0.281753	48	0.9211	1.46734	22	0.03681	161	0.001308	57	1599.0	32.0	0.281713	-1.9	1.7	2.41
2065518_05	Yb	15.0	0.281725	21	0.9135	1.46723	21	0.02619	75	0.000741	19	1605.3	34.2	0.281702	-2.2	0.7	2.43

Analysis No.	Interf. Corr. Meth.	Total Hf beam (V)	$^{176}Hf/^{177}Hf$	2SE	exp. factor[1]	$^{178}Hf/^{177}Hf$	2SE	$^{176}Yb/^{177}Hf$	2SE	$^{176}Lu/^{177}Hf$	2SE	Age (Ma)	1σ	$^{176}Hf/^{177}Hf$ Initial	$e_{Hf}(t)$	1s	T_{DM} Crustal (Ga)
2065518_06	Yb	18.0	0.281771	19	0.9470	1.46724	14	0.04723	82	0.001263	31	1609.7	33.5	0.281733	-1.0	0.7	2.36
2065518_07	Yb	11.1	0.281727	24	0.9940	1.46725	23	0.03105	73	0.000894	13	1595.7	33.3	0.281700	-2.5	0.8	2.44
2065518_09	Yb	14.5	0.281743	32	0.9659	1.46726	34	0.03718	82	0.000979	18	1569.4	35.7	0.281714	-2.6	1.1	2.43
2065518_13	Yb	18.8	0.281759	27	0.9001	1.46723	20	0.05757	253	0.001460	67	1586.2	36.8	0.281715	-2.2	0.9	2.42
2065518_14	Yb	17.9	0.281736	34	0.8972	1.46746	33	0.02899	60	0.000755	11	1591.5	40.6	0.281713	-2.1	1.2	2.42
2065518_15	Yb	12.8	0.281730	48	0.8470	1.46734	44	0.04090	53	0.001280	12	1604.9	38.1	0.281691	-2.6	1.7	2.46
2065518_16	Yb	10.0	0.281750	35	0.9133	1.46730	26	0.03922	152	0.001049	46	1579.0	33.7	0.281719	-2.2	1.2	2.41
2065518_18	Yb	16.7	0.281746	18	0.9067	1.46722	17	0.03737	72	0.000981	11	1590.7	31.1	0.281717	-2.0	0.6	2.41
SB12_03_01	Yb	4.4	0.281704	57	1.0574	1.46739	40	0.04423	219	0.001428	68	1617.3	42.7	0.281660	-3.4	2.0	2.51
SB12_03_02	Yb	10.9	0.281802	22	1.1093	1.46727	15	0.02196	58	0.000512	7	1591.3	33.0	0.281787	0.5	0.8	2.26
SB12_03_03	Yb	6.0	0.281831	35	1.4348	1.46721	14	0.03956	39	0.000931	9	1588.8	31.2	0.281803	1.0	1.2	2.23
SB12_03_04	Yb	7.2	0.281739	34	1.3276	1.46724	13	0.03021	132	0.000685	21	1599.4	31.9	0.281718	-1.8	1.2	2.40
SB12_03_05	Yb	8.0	0.281749	31	1.3659	1.46729	14	0.02311	57	0.000542	5	1571.3	37.7	0.281733	-1.9	1.1	2.39
SB12_03_06	Yb	7.9	0.281699	34	1.3780	1.46731	13	0.02031	70	0.000479	12	1590.1	54.4	0.281684	-3.2	1.2	2.48
SB12_03_07	Yb	7.3	0.281785	30	1.3751	1.46731	17	0.02527	44	0.000600	8	1603.5	34.0	0.281767	0.1	1.0	2.29
SB12_03_08	Yb	4.6	0.281720	45	1.3469	1.46736	29	0.02532	75	0.000775	35	1612.2	42.2	0.281696	-2.2	1.6	2.44
SB12_03_09	Yb	7.6	0.281720	27	1.3607	1.46725	15	0.02122	41	0.000506	4	1600.1	38.4	0.281704	-2.2	0.9	2.43
SB12_03_11	Yb	11.1	0.281769	21	1.0501	1.46723	15	0.02014	63	0.000482	9	1583.5	37.1	0.281755	-0.8	0.7	2.33
SB12_03_12	Yb	2.9	0.281851	62	1.5243	1.46731	22	0.02869	40	0.000916	19	1600.6	37.7	0.281824	2.0	2.2	2.17
SB12_03_13	Yb	6.0	0.281767	34	1.5463	1.46732	13	0.02254	37	0.000535	2	1584.8	39.4	0.281751	-0.9	1.2	2.34
SB12_03_14	Yb	6.6	0.281780	29	1.3902	1.46724	13	0.02247	118	0.000535	23	1595.1	49.7	0.281763	-0.3	1.0	2.31
SB12_03_17	Yb	12.1	0.281768	23	1.0635	1.46728	12	0.02309	40	0.000554	3	1598.0	35.9	0.281751	-0.6	0.8	2.33
SB12_03_21	Yb	7.0	0.281763	28	1.4104	1.46730	10	0.02375	67	0.000570	15	1583.1	40.4	0.281746	-1.1	1.0	2.35
SB12_03_22	Yb	7.0	0.281748	35	1.3604	1.46731	31	0.02300	38	0.000643	6	1566.7	35.9	0.281729	-2.1	1.2	2.40
SB12_03_24	Yb	3.8	0.281803	47	1.4922	1.46731	25	0.02507	41	0.000690	24	1562.2	35.9	0.281783	-0.3	1.7	2.29
SB12_03_25	Yb	8.3	0.281751	27	1.1646	1.46724	14	0.02174	49	0.000525	8	1582.1	35.1	0.281735	-1.6	0.9	2.38
SB12_03_26	Yb	6.0	0.281761	33	1.4267	1.46727	12	0.01925	31	0.000469	4	1577.8	38.4	0.281747	-1.2	1.1	2.35
SB12_03_27	Yb	5.7	0.281815	38	1.5244	1.46728	23	0.02662	192	0.000623	36	1585.1	37.9	0.281796	0.7	1.3	2.24
SB12_03_28	Yb	5.1	0.281827	35	1.4951	1.46727	24	0.02586	28	0.000690	17	1565.0	37.3	0.281807	0.6	1.2	2.23
SB12_03_31	Yb	6.2	0.281776	31	1.5312	1.46723	14	0.02135	108	0.000505	18	1565.4	40.1	0.281761	-1.0	1.1	2.33
1998166_02	Yb	17.5	0.281652	18	0.9389	1.46725	14	0.02774	110	0.000672	20	1607.7	34.2	0.281632	-4.6	0.6	2.58
1998166_05	Yb	15.3	0.281631	18	0.9259	1.46719	14	0.02234	64	0.000562	11	1586.6	24.1	0.281614	-5.7	0.6	2.63
1998166_06	Yb	15.4	0.281599	26	0.9000	1.46727	26	0.02618	33	0.000647	6	1618.7	43.3	0.281579	-6.2	0.9	2.69
1998166_07	Yb	14.4	0.281658	16	0.9139	1.46725	10	0.01959	22	0.000506	2	1603.5	28.6	0.281643	-4.3	0.6	2.56

Analysis No.	Interf. Corr. Meth.	Total Hf beam (V)	$^{176}Hf/^{177}Hf$	2SE	exp. factor[1]	$^{178}Hf/^{177}Hf$	2SE	$^{176}Yb/^{177}Hf$	2SE	$^{176}Lu/^{177}Hf$	2SE	Age (Ma)	1σ	$^{176}Hf/^{177}Hf$ Initial	**$e_{Hf}(t)$**	1s	T_{DM} Crustal (Ga)
1998166_08	Yb	12.7	0.281658	20	0.9664	1.46726	11	0.01892	74	0.000495	14	1576.5	25.0	0.281643	-4.9	0.7	2.58
1998166_09	Yb	13.5	0.281629	35	0.9264	1.46736	26	0.02265	43	0.000611	9	1634.9	44.9	0.281611	-4.8	1.2	2.61
1998166_10	Yb	13.8	0.281693	27	1.0829	1.46726	12	0.06765	155	0.001626	29	1593.0	25.2	0.281644	-4.5	0.9	2.56
1998166_11	Yb	13.8	0.281693	27	1.0837	1.46725	12	0.06741	160	0.001621	30	1589.7	37.2	0.281644	-4.6	0.9	2.57
1998166_12	Yb	7.1	0.281672	41	1.3303	1.46732	37	0.03395	72	0.001021	16	1546.2	31.3	0.281642	-5.7	1.4	2.60
1998166_13	Yb	9.3	0.281661	21	1.3865	1.46723	17	0.02235	125	0.000582	25	1641.1	44.5	0.281642	-3.5	0.8	2.54
1998166_15	Yb	7.3	0.281584	42	1.1372	1.46732	23	0.01575	45	0.000438	15	1595.1	46.1	0.281570	-7.1	1.5	2.72
1998166_17	Yb	11.3	0.281634	52	1.1526	1.46724	28	0.04308	325	0.001045	68	1528.4	42.8	0.281604	-7.4	1.8	2.69
1998166_18	Yb	10.2	0.281636	27	1.1563	1.46726	14	0.03913	94	0.000984	24	1592.2	22.5	0.281606	-5.9	0.9	2.65
1998166_19	Yb	9.8	0.281670	27	1.1396	1.46730	25	0.02222	22	0.000580	12	1597.1	27.5	0.281652	-4.2	0.9	2.54
1998166_20	Yb	6.3	0.281650	39	1.1635	1.46744	25	0.03321	126	0.000890	20	1642.7	41.5	0.281622	-4.2	1.4	2.58
1998166_22	Yb	10.8	0.281625	37	1.0599	1.46745	58	0.01959	184	0.000617	57	1565.0	34.3	0.281606	-6.5	1.3	2.66
1998166_23	Yb	17.5	0.281657	21	0.9444	1.46723	14	0.02451	75	0.000626	25	1616.8	32.3	0.281638	-4.2	0.7	2.56
1998166_24	Yb	17.4	0.281667	21	0.9448	1.46718	21	0.03475	87	0.000847	25	1547.3	43.5	0.281642	-5.7	0.7	2.60
1998166_25	Yb	7.0	0.281663	39	1.1313	1.46735	23	0.03296	104	0.001112	41	1577.0	29.3	0.281629	-5.4	1.4	2.61
1998166_26	Yb	9.1	0.281665	29	1.5092	1.46731	14	0.03284	128	0.000794	19	1593.9	38.8	0.281641	-4.6	1.0	2.57
1998166_27	Yb	16.6	0.281624	21	1.0364	1.46728	17	0.02896	158	0.000701	35	1530.0	36.3	0.281603	-7.4	0.7	2.69
1998166_29	Yb	13.1	0.281626	22	1.1138	1.46723	14	0.02178	14	0.000560	6	1594.8	27.4	0.281609	-5.7	0.8	2.64
1948991_01	Yb	17.2	0.281657	16	0.9201	1.46721	12	0.02368	113	0.000598	16	1580.5	22.7	0.281639	-5.0	0.6	2.58
1948991_03	Yb	16.0	0.281656	17	0.9027	1.46730	15	0.02280	63	0.000594	21	1630.1	39.0	0.281638	-3.9	0.6	2.56
1948991_04	Yb	14.1	0.281655	21	0.9182	1.46729	14	0.02585	98	0.000674	20	1589.7	23.1	0.281635	-4.9	0.7	2.59
1948991_05	Yb	16.9	0.281650	17	0.9294	1.46722	13	0.02824	20	0.000726	9	1599.0	25.2	0.281628	-5.0	0.6	2.60
1948991_09	Yb	15.9	0.281697	22	0.9101	1.46728	15	0.03934	299	0.001086	113	1589.0	28.5	0.281664	-3.9	0.8	2.52
1948991_10	Yb	17.9	0.281674	15	0.9262	1.46726	12	0.02017	55	0.000535	18	1596.7	31.2	0.281658	-4.0	0.5	2.53
1948991_11	Yb	16.5	0.281641	16	0.9175	1.46724	15	0.03259	49	0.000838	10	1604.2	37.2	0.281615	-5.3	0.6	2.62
1948991_13	Yb	16.6	0.281656	21	0.8942	1.46730	17	0.02604	49	0.000676	15	1593.7	28.4	0.281636	-4.8	0.7	2.58
1948991_14	Yb	17.1	0.281672	20	0.9157	1.46725	14	0.03415	246	0.000885	64	1581.4	23.2	0.281645	-4.8	0.7	2.57
1948991_15	Yb	16.0	0.281670	17	0.9006	1.46729	11	0.02058	30	0.000545	8	1577.4	25.4	0.281654	-4.5	0.6	2.55
1948991_16	Yb	22.2	0.281720	29	0.9084	1.46720	24	0.05642	495	0.001338	133	1610.1	26.0	0.281679	-2.9	1.0	2.48
1948991_17	Yb	16.0	0.281668	29	0.8524	1.46727	32	0.02175	77	0.000651	22	1615.4	37.7	0.281648	-3.9	1.0	2.54
1948991_20	Yb	14.4	0.281646	20	0.8675	1.46730	17	0.02670	156	0.000710	31	1628.3	34.9	0.281624	-4.4	0.7	2.58
1948991_23	Yb	16.1	0.281686	16	0.8880	1.46725	16	0.02258	96	0.000585	13	1547.1	27.9	0.281669	-4.7	0.6	2.54
1948991_24	Yb	15.0	0.281643	21	0.8865	1.46733	16	0.02956	112	0.000763	33	1635.0	30.6	0.281619	-4.5	0.7	2.59
1948991_25	Yb	19.1	0.281673	15	0.9077	1.46717	13	0.01925	38	0.000508	10	1585.6	29.5	0.281658	-4.2	0.5	2.54
1948991_26	Yb	18.7	0.281666	20	0.9020	1.46724	16	0.02344	48	0.000612	12	1591.1	28.8	0.281647	-4.5	0.7	2.56

Analysis No.	Interf. Corr. Meth.	Total Hf beam (V)	$^{176}Hf/^{177}Hf$	2SE	exp. factor[1]	$^{178}Hf/^{177}Hf$	2SE	$^{176}Yb/^{177}Hf$	2SE	$^{176}Lu/^{177}Hf$	2SE	Age (Ma)	2σ	$^{176}Hf/^{177}Hf$ Initial	$e_{Hf}(t)$	1s	T_{DM} Crustal (Ga)
1948991_27	Yb	18.4	0.281655	25	0.8859	1.46723	17	0.04916	138	0.001245	16	1609.0	40.0	0.281617	-5.1	0.9	2.61
1948991_28	Yb	10.0	0.281677	28	0.8956	1.46721	26	0.02663	111	0.000801	44	1601.5	27.9	0.281653	-4.0	1.0	2.54
2049213_01	Yb	4.9	0.281751	44	0.8783	1.46740	19	0.04742	126	0.001574	44	1592.9	35.4	0.281703	-2.4	1.6	2.44
2049213_02	Yb	9.5	0.281768	33	0.9339	1.46741	28	0.02552	25	0.000880	9	1605.4	33.8	0.281741	-0.8	1.2	2.35
2049213_03	Yb	7.3	0.281791	33	0.8884	1.46731	18	0.02523	63	0.000846	20	1579.8	31.9	0.281766	-0.5	1.2	2.31
2049213_04	Yb	14.6	0.281796	24	0.8861	1.46728	16	0.04309	47	0.001117	7	1600.9	31.3	0.281762	-0.2	0.8	2.31
2049213_05	Yb	15.6	0.281785	20	0.8696	1.46722	15	0.02896	76	0.000771	15	1620.5	31.5	0.281761	0.3	0.7	2.30
2049213_08	Yb	19.6	0.281831	23	0.8789	1.46725	12	0.07582	325	0.002027	80	1573.4	32.5	0.281770	-0.5	0.8	2.31
2049213_09	Yb	16.3	0.281790	28	0.8540	1.46701	42	0.04026	64	0.001078	10	1584.0	31.6	0.281757	-0.7	1.0	2.33
2049213_10	Yb	14.3	0.281811	23	0.8663	1.46716	39	0.03353	71	0.000970	20	1594.4	35.4	0.281781	0.4	0.8	2.27
2049213_11	Yb	11.6	0.281752	29	0.8656	1.46727	29	0.01987	82	0.000599	25	1597.4	46.6	0.281734	-1.2	1.0	2.37
2049213_13	Yb	8.0	0.281776	29	0.8507	1.46718	23	0.02625	74	0.000908	22	1592.0	33.8	0.281749	-0.8	1.0	2.34
2049213_14	Yb	13.2	0.281772	23	0.8699	1.46721	30	0.01872	56	0.000630	21	1596.3	33.4	0.281753	-0.6	0.8	2.33
2049213_15	Yb	18.2	0.281740	14	0.8743	1.46727	10	0.01992	26	0.000522	6	1603.1	32.7	0.281724	-1.5	0.5	2.39
2049215_04	Yb	18.2	0.281776	22	0.8774	1.46729	26	0.02722	47	0.000820	10	1577.2	30.7	0.281751	-1.1	0.8	2.34
2049215_05	Yb	18.4	0.281795	43	0.8610	1.46729	63	0.03755	212	0.000984	48	1568.9	31.9	0.281765	-0.8	1.5	2.32
2049215_06	Yb	15.3	0.281795	32	0.8817	1.46722	22	0.03812	92	0.000910	27	1564.9	37.8	0.281768	-0.8	1.1	2.31
2049215_07	Yb	18.6	0.281790	18	0.8911	1.46723	13	0.04572	98	0.001157	18	1586.7	37.6	0.281756	-0.7	0.6	2.33
2049215_08	Yb	13.5	0.281770	35	0.8405	1.46737	46	0.02474	131	0.000819	31	1587.9	34.0	0.281745	-1.1	1.2	2.35
2049215_10	Yb	13.8	0.281807	24	0.8795	1.46722	28	0.02602	45	0.000891	9	1573.6	34.3	0.281780	-0.1	0.8	2.28
2049215_11	Yb	17.5	0.281754	20	0.8770	1.46741	24	0.02732	60	0.000744	31	1583.1	35.5	0.281732	-1.7	0.7	2.38
2049215_13	Yb	15.1	0.281789	27	0.8790	1.46725	18	0.03689	97	0.000892	16	1611.7	42.7	0.281761	0.1	0.9	2.30
2049215_16	Yb	7.1	0.281867	49	0.8391	1.46716	32	0.04179	267	0.001455	87	1621.9	31.4	0.281822	2.5	1.7	2.16
2049215_19	Yb	11.7	0.281774	34	0.8750	1.46747	39	0.04164	236	0.001329	72	1599.7	32.8	0.281734	-1.2	1.2	2.37
2049215_20	Yb	19.8	0.281783	17	0.8984	1.46724	13	0.03857	102	0.001075	33	1609.7	33.5	0.281751	-0.4	0.6	2.33
2049215_21	Yb	15.4	0.281774	20	0.8824	1.46729	16	0.04305	148	0.001224	64	1597.5	32.1	0.281737	-1.1	0.7	2.36
2049215_22	Yb	22.7	0.281808	30	0.9096	1.46731	15	0.06950	683	0.001479	146	1593.5	33.7	0.281763	-0.3	1.1	2.31
2049215_23	Yb	14.5	0.281774	32	0.8739	1.46737	23	0.05772	237	0.001543	91	1606.1	34.6	0.281727	-1.3	1.1	2.38
2049215_24	Yb	14.9	0.281771	29	0.8703	1.46735	26	0.03849	265	0.001071	92	1582.3	37.2	0.281739	-1.4	1.0	2.37
2049215_26	Yb	16.0	0.281754	17	0.9033	1.46723	19	0.02127	47	0.000567	12	1620.4	36.3	0.281737	-0.6	0.6	2.35
CW_02_04	Yb	18.7	0.281786	26	0.9167	1.46720	10	0.10031	304	0.002428	76	1587.3	20.4	0.281713	-2.2	0.9	2.42
CW_02_07	Yb	17.7	0.281737	29	0.8653	1.46714	23	0.05035	59	0.001333	9	1592.7	20.2	0.281696	-2.7	1.0	2.45
CW_02_11	Yb	23.2	0.281790	23	0.9285	1.46715	12	0.08433	425	0.001913	88	1570.9	48.9	0.281733	-1.9	0.8	2.39

Analysis No.	Interf. Corr. Meth.	Total Hf beam (V)	$^{176}Hf/^{177}Hf$	2SE	exp. factor[1]	$^{178}Hf/^{177}Hf$	2SE	$^{176}Yb/^{177}Hf$	2SE	$^{176}Lu/^{177}Hf$	2SE	Age (Ma)	1σ	$^{176}Hf/^{177}Hf$ Initial	**e$_{Hf}$(t)**	1s	T_{DM} Crustal (Ga)
CW_02_24	Yb	20.9	0.281747	46	0.8900	1.46712	35	0.07196	137	0.001841	62	1636.1	40.9	0.281690	-1.9	1.6	2.44
CW_02_26	Yb	22.2	0.281770	34	0.8898	1.46726	24	0.07240	138	0.002018	26	1584.1	33.6	0.281709	-2.4	1.2	2.43
CW_02_30	Yb	11.9	0.281778	55	0.8906	1.46720	30	0.09457	218	0.003268	80	1593.2	38.8	0.281679	-3.3	1.9	2.49
CW_02_31	Yb	23.2	0.281758	22	0.8721	1.46727	13	0.06194	187	0.001499	32	1593.5	21.9	0.281713	-2.1	0.8	2.42
CW_02_32	Yb	24.2	0.281764	17	0.8873	1.46723	8	0.07551	368	0.001818	72	1595.9	22.4	0.281709	-2.2	0.6	2.42
CW_02_33	Yb	16.8	0.281758	22	0.8816	1.46725	14	0.04646	139	0.001128	27	1611.2	21.6	0.281724	-1.3	0.8	2.38
CW_02_34	Yb	19.9	0.281765	28	0.8817	1.46726	12	0.07283	323	0.001724	63	1588.3	23.7	0.281713	-2.2	1.0	2.42
CW_02_36	Yb	20.5	0.281746	20	0.8796	1.46726	11	0.07641	249	0.002001	35	1608.8	22.7	0.281685	-2.7	0.7	2.47
CW_02_37	Yb	16.1	0.281743	24	0.8747	1.46723	16	0.05087	111	0.001333	21	1628.8	20.2	0.281702	-1.7	0.8	2.42
CW_02_38	Yb	22.2	0.281754	20	0.8875	1.46722	10	0.06170	121	0.001641	15	1589.0	20.2	0.281704	-2.5	0.7	2.44
CW_02_39	Yb	18.0	0.281762	27	0.8930	1.46722	13	0.07369	211	0.002036	48	1572.8	20.2	0.281701	-3.0	1.0	2.45
CW_02_40	Yb	15.2	0.281779	17	0.8800	1.46724	10	0.05988	79	0.001568	36	1605.4	20.9	0.281731	-1.2	0.6	2.37
CW_02_44	Yb	16.0	0.281761	24	0.8771	1.46726	10	0.06605	123	0.001614	22	1631.1	21.3	0.281712	-1.3	0.8	2.40
CW_02_45	Yb	19.2	0.281777	21	0.8764	1.46722	10	0.07787	149	0.001804	31	1592.7	20.9	0.281723	-1.7	0.7	2.40
CW_03_01	Yb	9.3	0.281719	31	0.4954	1.46726	15	0.05366	154	0.001454	33	1575.1	24.3	0.281675	-3.8	1.1	2.51
CW_03_03	Yb	8.8	0.281741	33	0.4676	1.46723	16	0.05734	307	0.001485	49	1580.8	21.4	0.281696	-3.0	1.2	2.46
CW_03_04	Yb	8.1	0.281752	31	0.4605	1.46717	14	0.05387	133	0.001342	11	1592.6	23.5	0.281712	-2.1	1.1	2.42
CW_03_05	Yb	10.1	0.281763	26	0.4628	1.46719	14	0.06813	145	0.001622	5	1581.3	21.5	0.281714	-2.3	0.9	2.42
CW_03_06	Yb	11.1	0.281749	27	0.5157	1.46721	11	0.04191	247	0.001116	51	1590.3	25.2	0.281715	-2.1	0.9	2.41
CW_03_07	Yb	14.7	0.281802	30	0.6229	1.46724	17	0.09014	333	0.002252	98	1601.8	24.8	0.281734	-1.1	1.1	2.37
CW_03_08	Yb	15.9	0.281736	24	0.6900	1.46727	12	0.06581	311	0.001603	50	1596.9	22.3	0.281687	-2.9	0.8	2.47
CW_03_09	Yb	14.0	0.281732	42	0.7643	1.46745	22	0.07364	257	0.001971	46	1586.7	28.6	0.281673	-3.7	1.5	2.51
CW_03_10	Yb	15.6	0.281781	25	0.8185	1.46730	11	0.07367	191	0.001799	40	1590.1	22.4	0.281727	-1.7	0.9	2.39
CW_03_11	Yb	15.8	0.281743	21	0.8887	1.46724	14	0.05372	242	0.001302	27	1617.1	34.2	0.281704	-1.9	0.7	2.42
CW_03_13	Yb	16.0	0.281776	22	0.9029	1.46717	10	0.07946	167	0.001884	9	1583.0	44.4	0.281720	-2.1	0.8	2.41
CW_03_14	Yb	15.2	0.281730	24	0.8880	1.46724	14	0.05730	82	0.001397	6	1573.2	27.7	0.281688	-3.4	0.8	2.48
CW_03_15	Yb	16.0	0.281773	24	0.9158	1.46730	12	0.07275	136	0.001789	25	1573.5	26.6	0.281720	-2.3	0.9	2.41
CW_03_16	Yb	15.2	0.281812	35	0.9206	1.46729	17	0.08963	71	0.002182	15	1585.7	20.5	0.281747	-1.1	1.2	2.35
CW_03_18	Yb	17.3	0.281753	18	0.9212	1.46721	14	0.04885	247	0.001242	61	1600.0	22.1	0.281716	-1.8	0.6	2.41
CW_03_19	Yb	18.3	0.281748	18	0.8835	1.46724	11	0.04892	164	0.001262	46	1620.1	21.5	0.281710	-1.6	0.6	2.41
CW_04_01	Yb	5.4	0.281756	38	0.7795	1.46720	13	0.07922	357	0.002112	111	1615.9	23.1	0.281691	-2.3	1.3	2.45
CW_04_02	Yb	7.2	0.281732	27	0.6640	1.46725	10	0.03391	148	0.000944	32	1619.6	22.8	0.281703	-1.8	0.9	2.42
CW_04_03	Yb	5.1	0.281693	39	1.3819	1.46717	12	0.03181	175	0.000911	35	1596.7	22.1	0.281665	-3.7	1.3	2.52
CW_04_04	Yb	3.1	0.281702	65	1.3914	1.46719	13	0.03286	100	0.001009	17	1597.0	23.1	0.281672	-3.5	2.3	2.50

Analysis No.	Interf. Corr. Meth.	Total Hf beam (V)	$^{176}Hf/^{177}Hf$	2SE	exp. factor[1]	$^{178}Hf/^{177}Hf$	2SE	$^{176}Yb/^{177}Hf$	2SE	$^{176}Lu/^{177}Hf$	2SE	Age (Ma)	2σ	$^{176}Hf/^{177}Hf$ Initial	**$e_{Hf}(t)$**	1s	T_{DM} Crustal (Ga)
CW_04_07	Yb	16.7	0.281858	42	0.8474	1.46721	17	0.10737	458	0.002895	117	1602.5	32.7	0.281770	0.2	1.5	2.29
CW_04_08	Yb	14.1	0.281734	33	0.8965	1.46725	13	0.06609	45	0.001701	13	1614.3	23.6	0.281682	-2.7	1.1	2.47
CW_04_09	Yb	18.3	0.281763	21	0.8952	1.46734	12	0.07537	75	0.001878	11	1597.0	24.0	0.281707	-2.2	0.7	2.43
CW_04_10	Yb	18.1	0.281761	19	0.8940	1.46723	11	0.06769	162	0.001715	45	1609.1	31.7	0.281708	-1.9	0.7	2.42
CW_04_12	Yb	19.6	0.281782	26	0.8974	1.46720	13	0.09613	66	0.002561	28	1603.7	18.9	0.281704	-2.2	0.9	2.43
CW_04_13	Yb	18.2	0.281753	18	0.8834	1.46722	11	0.05376	103	0.001444	34	1620.6	28.1	0.281709	-1.6	0.6	2.41
CW_04_15	Yb	20.9	0.281698	19	0.9044	1.46726	17	0.03494	315	0.000873	54	1580.5	20.8	0.281672	-3.8	0.7	2.51
CW_04_16	Yb	19.0	0.281743	18	0.9001	1.46719	13	0.07429	137	0.001872	9	1571.3	20.1	0.281687	-3.5	0.6	2.49
CW_04_18	Yb	16.4	0.281765	28	0.9164	1.46730	17	0.07754	177	0.002113	34	1581.9	30.5	0.281701	-2.8	1.0	2.45
CW_04_19	Yb	18.6	0.281763	24	0.9193	1.46734	14	0.06091	150	0.001526	19	1611.0	31.5	0.281716	-1.6	0.9	2.40
CW_04_21	Yb	15.9	0.281747	42	0.9018	1.46735	35	0.06457	320	0.001754	64	1596.3	39.1	0.281694	-2.7	1.5	2.45
CW_04_22	Yb	18.0	0.281740	21	0.9103	1.46734	12	0.03633	21	0.000987	43	1606.7	27.8	0.281710	-1.9	0.7	2.41
CW_04_23	Yb	19.3	0.281714	18	0.9099	1.46731	11	0.0382	16	0.000986	28	1625.3	21.0	0.281683	-2.4	0.6	2.46